UNDERSTANDING OXIDIZED PHOSPHATIDYLSERINE AND SPHINGOLIPID METABOLISM IN MACROPHAGES

A Thesis

Submitted in partial fulfillment of the requirements

Of the degree

Doctor of Philosophy

By

NEELAY KAILASH MEHENDALE

20163441

IISER PUNE

INDIAN INSTITUTE OF SCIENCE EDUCATION

AND RESEARCH PUNE

2021

DEDICATED TO MY FAMILY

KAILASH HARIHAR MEHENDALE

ASHA KAILASH MEHENDALE

NEERAJA KAILASH MEHENDALE

CERTIFICATE

Certified that the work incorporated in the thesis entitled "Understanding oxidized Phosphatidylserine and Sphingolipid metabolism in macrophages" submitted by Neelay Mehendale was carried out by the candidate, under my supervision. The work presented here or any part of it has not been included in any other thesis submitted previously for the award of any degree or diploma from any other University or institution.
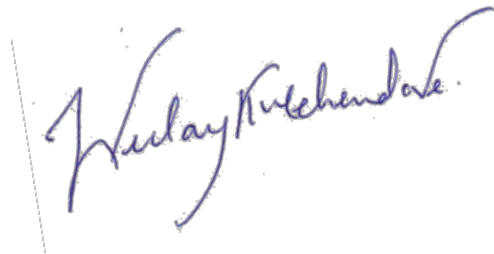
Dr. Siddhesh S. Kamat

(Supervisor)

Date: 28th June 2021

DECLARATION

I declare that this written submission represents my ideas in my own words and where others' ideas have been included, I have adequately cited and referenced the original sources. I also declare that I have adhered to all principles of academic honesty and integrity and have not misrepresented or fabricated or falsified any idea/data/fact/source in my submission. I understand that violation of the above will be cause for disciplinary action by the Institute and can also evoke penal action from the sources, which have thus been properly cited, or from whom proper permission has not been taken when needed.

Neelay Mehendale

20163441

Date: 28th June 2021

ACKNOWLEDGEMENTS

TABLE OF CONTENTS

LIST OF FIGURES

LIST OF TABLES

ABSTRACT

Understanding oxidized Phosphatidylserine and Sphingolipid metabolism in macrophages

June 2021

Neelay Mehendale, M.Sc. Biotechnology

Institute of Bioinformatics and Biotechnology, Savitribai Phule Pune University

Chair of Research Advisory Committee: Dr. Siddhesh S. Kamat

Lipids encompass more than 45,000 species and are known to partake in several biological functions. Their diversity and low abundance in biological systems presents a challenge for studying them. In my doctoral research, I have capitalized on the power of mass spectrometry to dissect the biochemistry of lipid metabolism underlying certain signaling and cell biological processes operating in macrophages – cells of the immune system.

I started off by studying the metabolism of oxidized phospholipids – oxidized phosphatidylserine in particular. Oxidative stress, through the elevation of Reactive Oxygen Species (ROS), damages cellular Phosphatidylserines (PS) and give rise to oxidized PS, which often get misread as an apoptotic signal. It was hypothesized that the cells must have a mechanism to counter this untimely apoptosis, by means of an enzyme capable of hydrolyzing oxidized PS. In an effort to find this enzyme(s), I developed methods to achieve stable and dose-dependent increase in intracellular ROS and subsequent elevation in oxidized PS, following which, a chemical-genetic screen for serine hydrolases then helped me pick out a few candidate lipases. My colleagues then proceeded to identify ABHD12 as a novel oxidized PS lipase.

To further study lipid biochemisty in macrophages, I performed lipidomic analyses of phagosomes – organelles made of internalized and membrane bound particles. The formation, maturation, and subsequent degradation of a phagosome is an important immune response essential for protection against many pathogens. Yet, the global lipid profile of phagosomes was unknown, especially as a function of their maturation in immune cells. Through mass spectrometry based lipidomics, I find that ceramides and glucosylceramides get enriched as the phagosomes proceed from an Early (EP) stage to a matured Late (LP) stage for fusion with lysosomes. This was attributed to an interplay of the activities of ceramide synthase 2, pH dependant ceramidase and glucosylceramide synthase enzymes, through proteomic and

biochemical assays. Taken together, these studies provide a comprehensive picture and possible new roles of sphingolipid metabolism during phagosomal maturation.

CHAPTER I
INTRODUCTION

Lipids form the building blocks of cells, along with proteins, nucleic acids and carbohydrates. They are fundamental components of cellular and subcellular membranes, and have roles to play in structural as well as signaling events [1]. Lipids present an enormous variety in their chemical structures, which can be used to categorize them under various classes. LIPID MAPS has defined over 45000 structures of lipids under these classes [2,3]. Among these, Fatty Acids, Glycerolipids, glycerophospholipids and sphingolipids together account for the majority of lipids.

Naturally occurring fatty acids contain even number of carbons and are classified as short chain (less than 10 carbons), medium chain (10-14 carbons), long chain (16-20 carbons) and very long chain (more than 20 carbons) fatty acids, and may be saturated or carry one or more unsaturations. These fatty acids when appended on a glycerol backbone, give rise to Mono-, Di- or Tri- Acyl glycerols (Figure 1.1). Phospholipids also have a glycerol backbone, carry acylations at the sn-1 and sn-2 positions and have a head-group attached to the sn-3 carbon through a phosphate, which determines the class of the phospholipid (Figure 1.1). Sphingolipids, on the other hand, have a sphingosine backbone with sn-2 acylation and a head-group at sn-3, which is used for classifying the sphingolipids into its subclasses (Figure 1.1).

Fatty acids are synthesized largely in the cellular cytoplasm [4] and broken down in mitochondria and peroxisomes by beta oxidation [5]. Fatty acids are converted to glycerolipids and glycerophospholipids by enzymes dedicated for their synthesis at various sites within the cell [6,7]. The metabolism of sphingolipids is centered around cermides which are usually synthesized in the endoplasmic reticulum and further converted to sphingomyelins and hexose derivatives like glucosylceramides [8]. These lipids can be often be interconverted through salvage pathways to maintain their function-specific stoichiometry.

Lipids act as signaling molecules and secondary messengers through functional interactions with receptors and other proteins [7] and are often localized in various compartments [9]. They are involved in several biological pathways, thus their activity-dependent subcellular localization is important for maintaining healthy signaling within cells. Maintaining this localization is imperative as lipids can easily diffuse through membranes and are also transported by the action of lipid transporters [9,10]. For instance, phosphatidylserines are enriched on the inner leaflet of the plasma membrane [9], while a breakdown of this membrane asymmetry, and a resultant flux of phosphatidylserine to the outer leaflet is a signal for apoptosis [11]. In another case, ceramides are synthesized in the endoplasmic reticulum [8] but found predominantly in the

trans Golgi network [12] and are known to be involved in cell proliferation, differentiation and apoptosis [13]. Aberrant signaling by ceramides has been linked to neurodegenerative disorders [13].
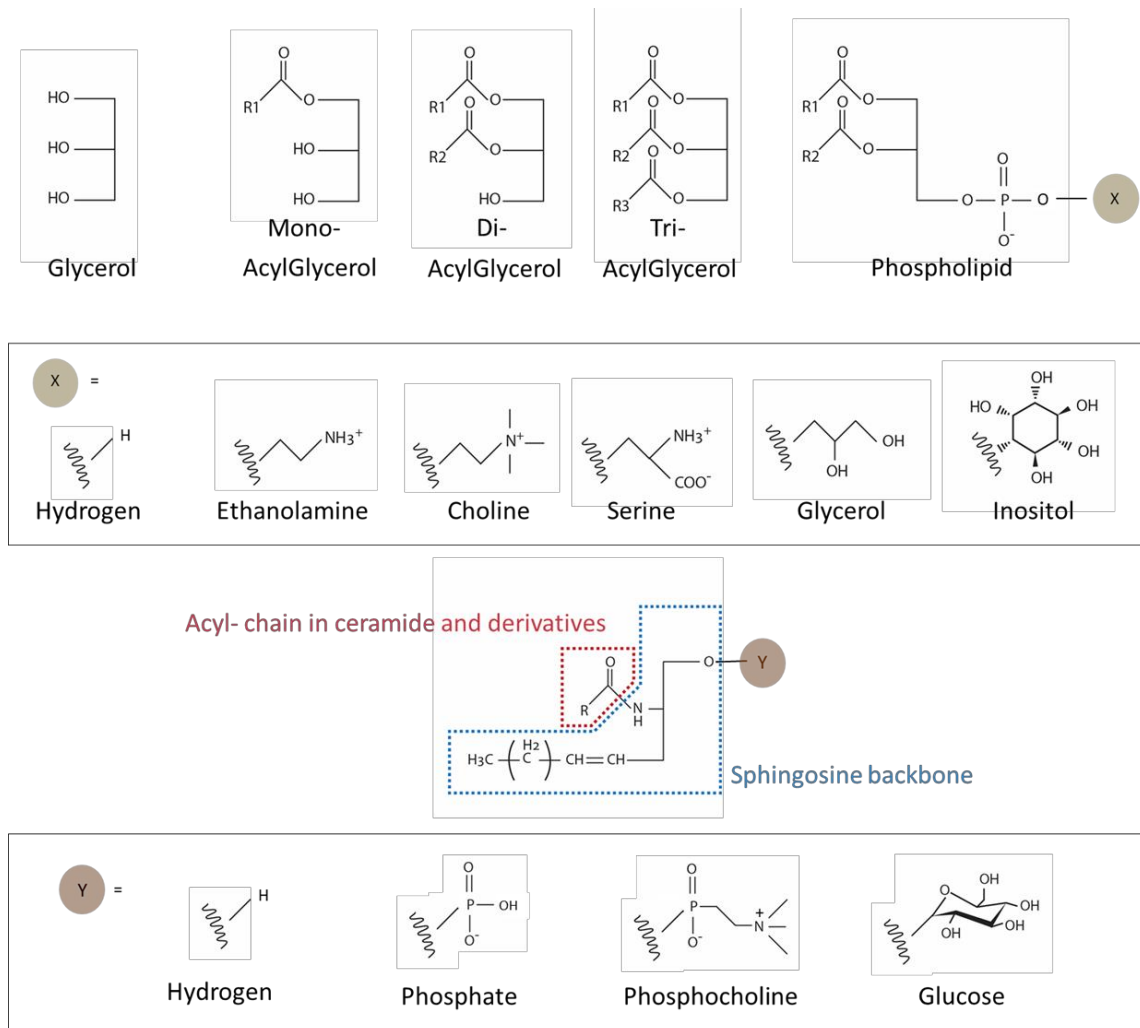
Figure 1.1. Structures of Lipids. *Glycerolipids and phospholipids have a glycerol backbone with fatty acid acylations. Phospholipids have a polar headgroup attached at sn-3 through a phosphate. Sphingolipids have a sphingosine backbone, while ceramides have an additional fatty acid acylation at the sn-2 amino group.*

Lipid homeostasis is tightly regulated by the cell to ensure cellular health. Excess or unnecessary lipids are broken down predominantly by lipases - lipid hydrolysing enzymes of the serine hydrolase family - for maintaining steady levels of accumulation [14]. All the pathways of synthesis, transport, and breakdown of lipids form a complex network that functions at a delicate equilibrium, thereby ensuring healthy cellular signaling.

Apart from enzymatic biochemistry of lipids, non-enzymatic mechanisms like oxidative damage also lead to formation of a variety of biologically active lipid products [15]. Their presence often leads to detrimental effects to normal cellular functioning. Albeit, cells have the capacity to combat these off-effects through the action of lipases that are capable of hydrolyzing oxidized lipids [16,17].

Understanding the biological relevance of lipid diversity has been a fundamental challenge owing to their low abundance. Mass spectrometry has paved the way for addressing this challenge and furthering our understanding of health and disease in the context of cellular lipid biochemistry. [18]

In my doctoral research, I aimed at understanding lipid metabolic pathways in macrophages, pertaining to oxidized phosphatidylserine during oxidative stress, and sphingolipids (ceramides and glucosylceramides in particular) in the process of phagocytosis.

Oxidative stress and lipid oxidation

Reactive oxygen species (ROS) are transient, yet highly reactive chemical intermediates containing oxygen. In biological systems, these high-energy oxygen species are produced as byproducts and/or intermediates during the metabolism of molecular oxygen. These oxygen-derived species include the superoxide radical anion, hydrogen peroxide, the hydroxyl radical and singlet oxygen. They are produced widely in biological systems as part of habitual catalytic metabolism of oxygen, through cellular processes like mitochondrial respiration, activity of enzymes or through Fenton reactions [19] (Figure 1.2A).

The concentration of ROS generated under normal physiological conditions in cells and/or tissues is tightly controlled by various enzymes and cellular anti-oxidants, which serve as a defense system to protect cells from the deleterious effects of surplus ROS. However, 'oxidative stress' arises when there is an imbalance between ROS generation and its sequestration [20].

Elevated ROS can lead to non-specific damage of DNA [21], proteins [22], and lipids (through lipid peroxidation, Figure 1.2B)[15]. Of note is that oxidative stress is an underlining contributor to a wide spectrum of human pathophysiological conditions such as neurodegenerative disorders, metabolic syndromes, autoimmune conditions, and cancer [23–25].
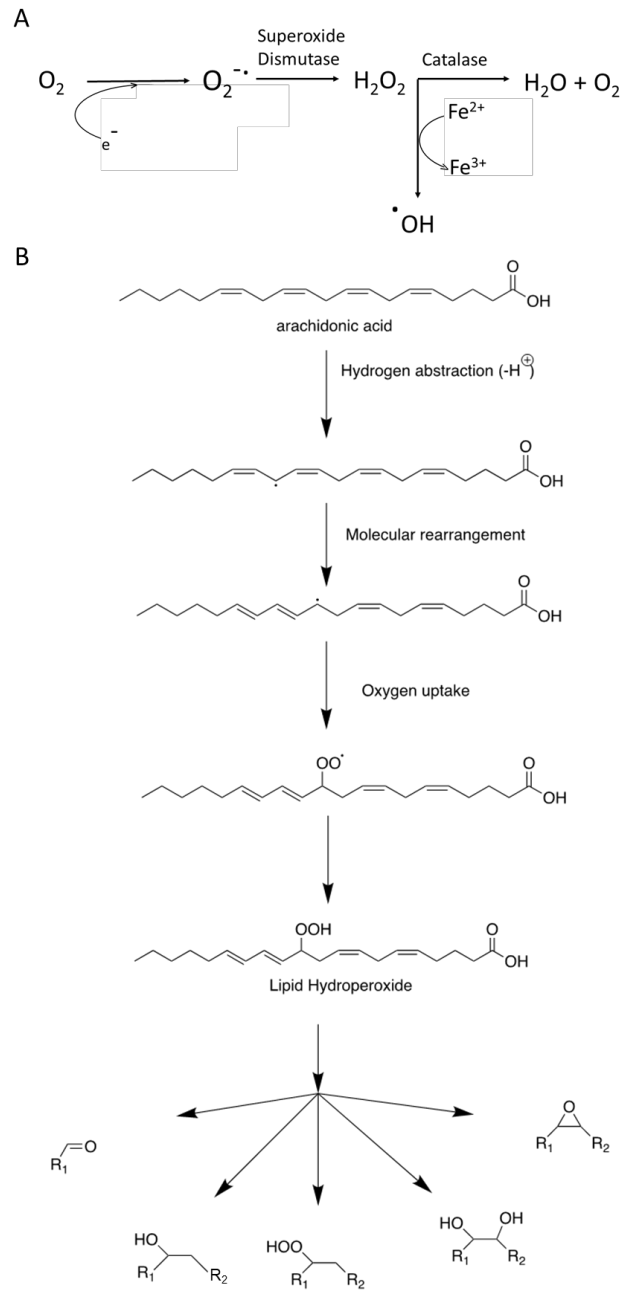
Figure 1.2. ROS are generated through mitochondrial respiration and subsequently damage membrane lipids. *(A) Superoxides are generated when oxygen accepts an electron and terminates the electron transport chain. It leads to the subsequent formation of peroxide and hydroxyl radicals. (B) The ROS species inflict damage upon lipid molecules bearing unsaturation through the process of lipid peroxidation, and finally yield several functional group derivatives of oxidatively damaged lipids.*

The lipid bilayer provides a functional barrier between subcellular compartments and between the cell and the environment, thus rendering it as the first line of defense against ROS as they traverse membranes. ROS readily oxidize the unsaturated bonds of polyunsaturated fatty acids

7

(PUFAs) like arachidonic acid (C20:4), eicosapentaenoic acid (C20:5) and docosahexenoic acid (C22:6) – among others[15]. The highly reactive hydroxyl radical, abstracts a hydrogen atom from the bisallylic position of these PUFAs, rearranges the unsaturation, and leaves behind an activated carbon radical. This is followed by peroxidation, whereby an oxygen molecule is added leading to the formation of a lipid-peroxide radical. Further, it gives rise to breakdown products that contain hydroxides, epoxides, and/ or carbonyls [15] (Figure 1.2B). PUFAs acylated to membrane phospholipids and other lipids are also susceptible to damage by ROS. Oxidative damage is indiscriminate and has detrimental effects on the physical and biochemical properties of membranes. [15,26] Oxidation of membrane lipids generates an array of biologically active products that adversely affects normal cell growth by altering membrane fluidity and elasticity, impairing cellular signaling, and eventual apoptosis [15].

Phospholipids are prone to oxidative damage, given that they are major components of most cellular membranes. Oxidized phospholipids trigger the electrophilic stress response, the unfolded protein response, affect the transcription of genes, and promote inflammation and apoptosis [26]. Oxidized phospholipids have intermediate hydrophobicity that disrupts the membrane curvature [27]. The can be recognized by several cell surface receptors and serve as ligands for CD36, SRB-1, platelet activating factor receptor, prostaglandin receptors including E2 and D2 receptors, and possibly TLRs [26]. These receptors in turn regulate inflammatory responses to oxidative stress[26].

Phosphatidylserine (PS) is actively partitioned to the inner leaflet of the plasma membrane by the enzyme flippase [9], as its presence on the outer surface recruits macrophages through interactions with scavenger receptors like CD-36 [26] ,ultimately signaling for apoptosis. Annexin V, a protein with an unclear function, is also known to bind to the head-group of PS which is considered as a marker for apoptosis, phagocytosis, and formation of plasma-membrane derived microparticles [26].

Breakdown of the membrane asymmetry of PS was earlier thought to be catalyzed by the enzyme scramblase [28] (Figure 1.3). However, Oxidized PS does not require scramblase to translocate itself to the outer leaflet, and thus acts like a non-enzymatic scramblase [29], leading to a flux of oxidized PS to the outer leaflet of the plasma membrane (Figure 1.3). Withal, it interacts with CD-36 and Annexin V with efficiency equal to that of PS [26]. Together, this not only disrupts the asymmetry of PS in the membrane but also signals for apoptosis (Figure 1.3). Interaction of oxidized PS with SRB1, also promotes clearance of apoptotic cells [26]. This

indicates that oxidized PS often gets misread as an apoptotic signal and also has a role to play in phagocytosis of apoptotic vesicles [26]. The exact chemical constitution of oxidized PS, however, has not yet been entirely characterized.
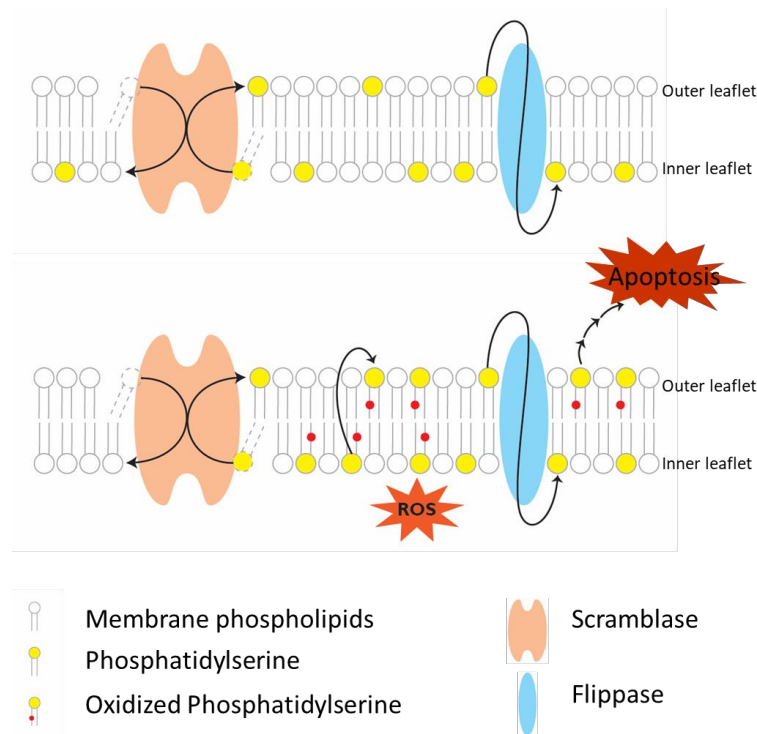
Figure 1.3. Membrane asymmetry of PS is essential for healthy cells. Under normal circumstances, PS is maintained on the inner leaflet of the plasma membrane by the action of flippases. Scramblase is known for breaking the asymmetry down upon being signaled, thus displaying PS on the outer leaflet as a signal for apoptosis. Oxidized PS on the other hand does not require scramblase for translocating itself to the outer leaflet, thus compromising the asymmetric distribution, and acting as an untimely apoptotic signal.

Our understanding of the biochemistry and metabolism of ox-PLs remains limited predominantly to that of oxidized phosphatidylcholine. Oxidative stress related diseases were observed to elevate blood levels of oxidized phosphatidylcholine in mice [30]. In other studies, oxidative stress was observed to upregulate the expression of Platelet-activating Factor Acetylhydrolase (PAF-AH or PLA2G7). This enzyme, known to hydrolyse the PAF to Lyso-PAF as means of reducing inflammatory responses, also hydrolysed oxidized phosphatidylcholines [16,17,31]. This system acts as a defence mechanism against impaired signaling brought about by oxidized phosphatidylcholines.

I hypothesized that cells must have a mechanism to tackle oxidized PS driven untimely apoptotic cascades. However, enzymes with a capacity to hydrolyze oxidized PS were as of date unknown. Thus as part of my doctoral research, I set up a system to study the composition of oxidized PS in cells under oxidative stress and performed a chemical genetic screen to fish out lipases able to reduce the resultant elevation of oxidized PS. This research has been elaborated on in chapter 2. We then proceeded to attribute oxidized PS lipase activity to ABHD12, a lipase of the serine hydrolase family, through genetic and biochemical assays.

For further understanding lipid pathways operating in macrophages, I studied the process of phagosomal maturation during phagocytosis as my next model system, and studied the lipidomic changes accompanying it.

Lipidomics of phagosomes

The cell membrane serves as a platform for several cell biological and biochemical processes. While it serves as the hub for cellular signaling, it also acts as a structural scaffold for events involving membrane modulations [1].

Movement of materials across the cell membrane and within the cell between organelles is vital for maintaining cellular homeostasis [32]. In addition to transport of ions and small molecules across the membrane, the cell needs to ingest and excrete larger molecules as well [33]. This intake is brought about by a process called endocytosis, whereas the reverse is carried out by a process called exocytosis. Endocytosis is the process of cellular ingestion, mediated by membrane invaginations. It was first discovered in 1883 by observing motile cells in transparent starfish larva surround and engulf small splinters that been inserted [34]. The process was termed 'phagocytosis' or cell-eating from the Greek words 'Phagos' (to eat) and 'Cyte' (cell). Subsequently a 'phagocyte' a type of immune cell was found to engulf, digest and clear bacterial particles. The process of cell-drinking was discovered a few decades later by observing observing the uptake of surrounding media into large vesicles, and was termed as 'pinocytosis' from the Greek word 'Pinean' (to drink)[34,35].

Phagocytosis is largely conserved, employed by protozoa for feeding, and by higher organisms for homeostasis and immunity [36]. Phagocytosis begins by casting the internalized particles as membrane bound vesicles called phagosomes [36]. They then undergo a strategic chain of events which is broadly referred to as 'phagosomal maturation', also a well conserved intermediate

process in phagocytosis [37]. Phagosomal maturation drives phagosomes towards the formation of phago-lysosomes, through fusion with lysosomes, to access the lysosome's hydrolytic machinery for digesting and breaking the internalized particles down [37] (Figure 1.4).
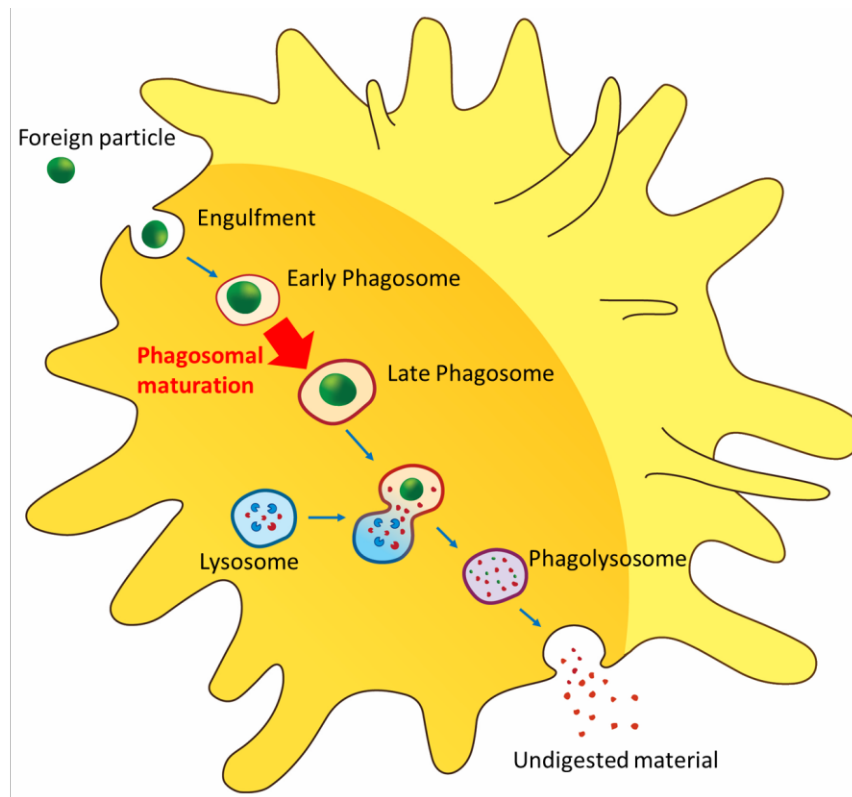
Figure 1.4. The process of phagocytosis in macrophage in brief. *The phagocyte engulfs a foreign particle and casts it as a membrane bound organelle called a phagosome. This early phagosome undergoes a sequence of well-choreographed events to mature into a late phagosome and subsequently fuse with lysosomes to digest the engulfed particles.*

The process of phagocytosis and phagosomal maturation involve extensive membrane remodeling in terms of its proteomic and lipidomic constitution. The proteomic changes accompanying the conversion of Early Phagosomes (EPs) into Late Phagosomes (LPs) have been better understood than the underlying lipidomic changes in their membranes [36].

Global lipidomic changes during phagosomal maturation, however, have not been studied. With this, as part of my doctoral research, I aimed at analysing the lipidomic content of phagosomal membranes and tracking their changes from EPs to LPs.

Through these lipidomic studies I found that ceramides get enriched on maturing phagosomes. Ceramides, like cholesterol, have been known to form lipid rafts that serve as structural

platforms [38]. Ceramides are also known to make membranes rigid and stabilize negative curvatures [38].

Thus to explore the role of ceramides along phagosomal maturation, I studied the biochemistry of ceramide synthase 2 (CerS2) on EPs and LPs. Robust CerS2 activity, and a pharmacological blockade thereof, showed that phagosomal maturation depends on ceramide enrichment for being unhindered. These studies have been elaborated on in chapter 3.

Upon further investigation, I found that the flux of ceramide is controlled not only by ceramide synthase 2, but also by the activity of pH dependant ceramidases. These findings were instrumental in mapping the biochemistry of sphingolipids on maturing phagosomes. This prompted me to cast my net wider to include glucosylceramides in my lipidomic studies of EPs and LPs. Glucosylceramides have been associated with cell proliferation, cell differention and also with Gaucher's disease, a lipid storage disorder [39–41], however their exact function(s) has not yet been entirely understood. Interestingly, glucosylceramides, like ceramides, were seen to be enriched on LPs. I attributed the enrichment of glucosylceramides on LPs to the activity of Glucosylceramide synthase through biochemical assays. Together, the studies described in chapters 3 and 4 helped put forth a comprehensive map of sphingolipid metabolism underlying phagosomal maturation.

CHAPTER II
OXIDIZED PHOSPHATIDYLSERINE
AND ITS METABOLISM IN MACROPHAGES

Introduction

Oxidative stress is defined as an imbalance between cellular oxidants and anti-oxidants in the favor of oxidants, leading to the disruption of homeostasis in cellular redox signaling, and is implicated in several human pathophysiological conditions and diseases, such as neurodegenerative diseases, autoimmune disorders, metabolic syndrome and cancers [42–46]. Under these stress conditions, there is an excess of ROS, namely superoxide, hydrogen peroxide and hydroxyl radicals, which cannot be detoxified by innate cellular mechanisms responsible to cope with them [47,48]. Unchecked, these ROS species cause damage and destruction to cellular components like DNA, proteins and even lipids (Figure 1.2),which eventually causes cell death via apoptosis or necrosis [48]. Lipids in the membrane provide the cell with its first line of defense against ROS by providing an initial physical barrier to the diffusion of these ROS into cells and subcellular compartments, and therefore constitute primary targets for oxidative damage [48,49].

Lipids are integral components of cellular membranes and energy storage in mammalian cells, where they occur in the form of phospholipids and neutral lipids, respectively [49,50]. When ROS is generated due to oxidative stress close to the membranes, the constituent lipids, in particular those bearing polyunsaturated fatty acid (PUFA) chains are oxidized [15,51]. The resulting lipid oxidation products can disrupt the local structure and integrity of the membrane, and in turn impair cellular functions by modulating the activity of a wide array of cellular proteins like enzymes, receptors and ion channels [52,53]. Such non-enzymatically oxidized lipid products also act as signaling molecules through covalently or non-covalently binding to specific proteins or receptors in mammalian cells [52,53]. Research groups in the past have focused on the oxidation of a single PUFA (e.g. arachidonic acid) [15,51], but there is little literature that describes the global lipid profile, "lipidome", under oxidative stress conditions [52,53]. Also not much is understood of the enzymatic pathways that regulate and metabolize these oxidized lipid products *in vivo*.

Phosphatidylserine (PS), a phospholipid that is localized to the inner leaflet of the membrane bilayer, has several important roles in mammalian biology [54]. Important amongst these, is its role in ROS signaling and cellular apoptotic pathways [55]. Given the asymmetry of PS in the membrane bilayer, the externalization of PS biologically reflects a cell in stress, and likely undergoing apoptosis, and this "flipped" PS is recognized by scavenger receptors on macrophages as an "eat me" signal, and such cells are eventually cleared by the innate immune

system [56–58]. Several studies suggest that under oxidative stress, surplus ROS within cells non-enzymatically reacts with the *sn*-2 esterified PUFAs of PS, to produce oxidized PS [51]. It is this oxidized PS, which is postulated to flip its membrane orientation by as of yet unknown mechanisms, and act as an apoptotic signal [56,58]. While several studies describe the production, and role of oxidized PS in mammalian biology, virtually nothing is known physiologically of the metabolism of oxidized PS. From a biological stand point, this metabolism would be important to know, as several cell types require an inherent high oxygen tension, and as a consequence have elevated ROS, that must be producing oxidized PS at a constant flux (e.g. neurons, macrophages, cancer cells). Yet there exist innate mechanisms within such cells, most likely enzymes (e.g. lipases),which can efficiently metabolize the oxidized PS produced at a constant flux, and prevent apoptosis.

Through collaborations with Dr. Ravikumar Govindan and Dr. Harinath Chakrapani (Chemistry Department, IISER-Pune), I developed a method for producing ROS in mammalian cells, established mass spectrometry based methods to study oxidized PS in cells, and with both of these in conjunction, performed a chemical genetic screen to find lipases(s) capable of metabolizing oxidized PS. More colleagues then proceeded to demonstrate the serine hydrolase ABHD12 (α/βhydrolase domain (ABHD) containing protein 12) to possess oxidized PS lipase activity, through proteomic, biochemical and *in vivo* studies.

Materials and methods

Materials. All chemicals, buffers, and reagents were purchased from Sigma-Aldrich (now Merck), all lipids and lipid standards were purchased from Avanti Polar Lipids Inc., and all primary and secondary antibodies were purchased from Abcam, unless otherwise mentioned. The mouse or human inflammatory cytokine single analyte ELISA kits from R&D Systems were used for cytokine measurements.

Mammalian cell culture and treatment. All mammalian cell lines (HEK293T, RAW264.7, A549, THP1, MCF7, HeLa) were purchased from ATCC, and cultured in RPMI 1640 medium (Thermofisher Scientific) supplemented with 10% Fetal Bovine Serum (FBS) (Invitrogen) and 1x penicillin-streptomycin (MP Biomedicals) at 37ºC with 5% CO_2. All cell lines were stained with DAPI to ensure they were devoid of any mycoplasma contamination, before performing any cellular assays. All cell viability studies for MGR1 and MGR2 treatments were done using a Bio-Rad TC20 Automated Cell Counter with trypan blue reagent (Bio-Rad) as per

manufacturers instructions. Briefly, cells were treated with varying concentrations of MGR1 (0 – 40 μM) and MGR2 (0 – 40 μM) for 4 h, and which point, the cells were detached by trypsinization and live cells estimated as per manufacturers protocol. For lipid measurements, 2 x 10^6 cells were washed with sterile Dulbecco's Phosphate Buffer Saline (DPBS) (HiMedia) (3X) and treated with MGR1 (2 μM) or MGR2 (2 μM) or DMSO for 4 h at 37°C and 5% CO_2 in 5 mL of aforementioned media (10 cm tissue culture dish).

Imaging oxidative stress using DCF dye. All cellular DCF assays were performed on mammalian cell lines (HEK293T, RAW264.7, A549, HeLa) using the 2',7'-dichlorodihydrofluorescein diacetate (DCF) dye (10 μM, 10 mins, Thermofisher Scientific). For imaging MGR1 mediated elevation in oxidative stress, the cells were treated with MGR1 (5 μM) or MGR2 (5 μM) or DMSO for 1 h, washed with sterile DPBS (3X), following which, DCF dye (10 μM) was added to the cells and fluorescence was visualized under a confocal microscope as per manufacturers instructions. To confirm that the fluorescence was indeed seen as an effect of elevated ROS, the cells (RAW264.7, HEK293T) were pre-treated with the antioxidants, pterostilbene5 (10 μM) or N-acetyl-cysteine6 (NAC, 1 mM) for 4 h, following which MGR1 (5 μM) was added, and the ROS production was assessed by cellular fluorescence microscopy using DCF dye (10 μM).

Lipid fragmentation analysis. All lipid fragmentation studies were performed by LC-MS/MS analysis on an Agilent 6540 Ultra High Definition Accurate Mass QTOF. The LC separation was achieved using a Gemini 5U C-18 column (Phenomenex, 5 μm, 50 x 4.6 mm) coupled to a Gemini guard column (Phenomenex, 4 x 3 mm, Phenomenex security cartridge). All PS, and oxidized PS lipids were assessed in the negative ionization mode using: buffer A: 95:5 (vol/vol) H_2O: methanol + 0.1% ammonium hydroxide; and buffer B: 60:35:5 (vol/vol) isopropanol: methanol: H_2O + 0.1% ammonium hydroxide [59].A typical LC-run consisted of 55 mins, with the following solvent run sequence post injection: 0.3 ml/min 0% buffer B for 5 mins, 0.5 ml/min 0% buffer B for 5 mins, 0.5 ml/min linear gradient of buffer B from 0 – 100% over 25 mins, 0.5 ml/min of 100% buffer B for 10 mins, and re-equilibration with 0.5 ml/min of 0% buffer B for 10 mins. The (M–H)⁻ of the synthetic lipid standards and the m/z values of the endogenous lipids were assessed by LC-MS/MS analysis in this study. The lipid extraction protocol for the endogenous lipids is described in the section below. The MS1 and MS2 spectra were acquired at 1.05 spectra/s, and the collision energy of 20 and 25 for oxidized PS and PS were respectively used. The fragmentor and capillary voltage were set at 120 and 4000 volts

respectively. The drying gas temperature was 380°C, the drying gas flow rate was 11 L/min, and the nebulizer pressure was 45 psi.

Quantitative lipid measurements. The organic extraction of PS and oxidized PS species were done with slight modifications to a previously established protocol based on the Folch lipid extraction method [60,61]. Briefly, the cells were washed with sterile DPBS (x 3 times), and transferred into a glass vial using 1 ml sterile DPBS. 3 mL of 2:1 (vol/vol) chloroform ($CHCl_3$): methanol (MeOH) with the lipid internal standard mix (1 nmol of each internal standard listed in Table MS1) was added, and the mixture was vigorously vortexed. The two phases were separated by centrifugation at 2800g for 5 mins. The organic phase (bottom) was removed, 50 μL of formic acid was added to acidify the aqueous homogenate (to enhance extraction of phospholipids), and $CHCl_3$ was added to make up 4 mL volume. The mixture was vortexed, and separated using centrifugation described above. Both the organic extracts were pooled, and dried under a stream of N_2 gas. The dried organic phase containing the PS and oxidized PS lipids was re-solubilized in 120 μL of 2:1 (vol/vol) $CHCl_3$: MeOH, and 20 μL was used for the targeted LC-MS analysis. All the lipid species analyzed in this study were quantified using the multiple reaction monitoring (MRM) method (see Table MS1) on an AbSciex QTrap 4500 LC-MS/MS with a Shimadzu Exion-LC series quaternary pump. All data was collected using the Acquisition mode of the Analyst software, and analyzed using the Quantitate mode of the same software. All the MS based lipid estimations were performed using an electrospray ion source, using the following MS parameters: ion source = turbo spray, collision gas = medium, curtain gas = 20L/min, ion spray voltage = 4500V, temperature = 400°C. The LC separation, buffers and method were the same as described earlier. A scheduled MRM program was used to measure oxidized PS lipids only between 25 – 29 mins, and PS lipids only between 29 – 38 mins, to get better sensitivity for the quantitative lipid measurements. A detailed list of the entire lipid species targeted in this MRM study, describing the precursor parent ion mass, the product ion targeted, and other compound specific voltages and parameters can be found in Table MS1. All endogenous phospholipid species were quantified by measuring the area under the curve, relative to the respective internal standard, and normalizing to the total cellular protein content or cell number. For oxidized PS lipid species, PS was used as an internal standard. All the data is represented as mean ± s. e. m. of between 4 – 8 biological replicates per study group (Table MS1).

Chemical genetic screen. RAW264.7 cells (1 x 10^6 cells) were cultured in 6-well plates in media described earlier. The cells were treated with 10 μM of the lipase inhibitor for 4 h, following which, the cells were washed with sterile DPBS (x 3 times), and replaced with the same media. The cells were then treated with 5 μM of MGR1 for 4 h, following which, the cells were washed again with sterile DPBS (x 3 times), and lipids extracted as described earlier to perform quantitative lipid measurements. As a control for the lipase inhibitor group, DMSO was used as a control. As a control for the MGR1 treatments, 5 μM MGR2 and DMSO were used as controls. Each treatment group contained three biological replicates.

Statistical analysis. All statistical analyses were performed using the Prism 7 for Mac OS X (GraphPad) software. All data are shown as mean ± s. e. m. The Student's two-tailed t-test was used to ascertain statistically significant differences between the different study group, where a p-value < 0.05 was considered statistically significant for this study.

Synthesis and chemical characterization of MGR1 and MGR2 were performed by Dr. Ravikumar Govindan. Furthermore, based on the results of the chemical genetic screen, more colleagues performed gel-based ABPP analyses, genetic studies, substrate assays, western blot analyses and proteomic analyses and revealed ABHD12 to exhibit oxidized PS lipase activity. These methods and results have been published in 'Nature Chemical Biology, 2019 ;15(2):169-178.'

Results

Elevation of intracellular ROS

Dr. Ravikumar Govindan generated a chemical probe, MGR1 – intracellular ROS generating probe - containing a modified juglone scaffold,5-hydroxy-1,4,4a,9a-tetrahydro-1,4-ethanoanthracene-9,10-dione (JCHD) [62], with an esterase-activated handle (Figure 2.1A) – and an inactive structural analog MGR2 (Figure 2.1A). While MGR1 and MGR2 both are acted upon by esterases *in vitro*, only MGR1 (through release of free JCHD) and not MGR2 (through release of 1-naphthol) led to robust increase in ROS – as was confirmed by luminol (Figure 2.1B, Credits: Dr. Ravikumar Govindan) and DHE assays (data not shown).
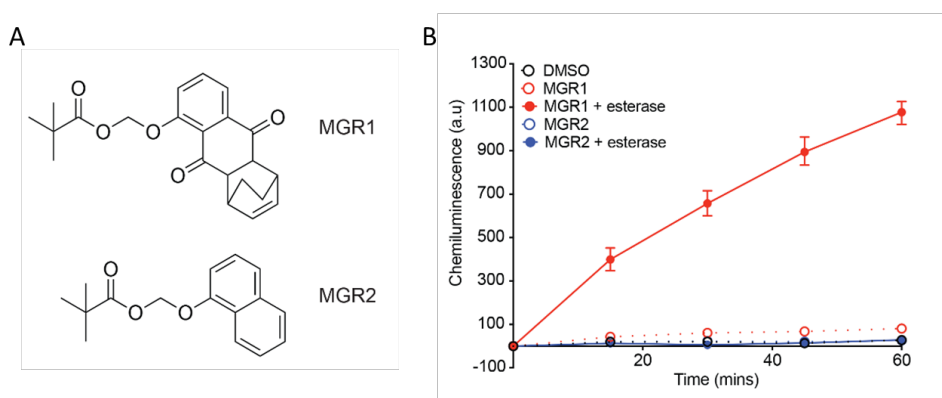
Figure 2.1. Characterization of a ROS-generating probe (MGR1), and an inactive control probe (MGR2). *(A) Chemical structures of the active dihydroquinone ROS generator MGR1 and the inactive 1-naphthol control compound MGR2. (B) Luminol-based chemiluminescence assay showing robust in vitro superoxide production by MGR1 but not MGR2, in the presence of esterase. The assay was performed at 37 °C, and each time point represents the mean ± s.e.m. in arbitrary units (a.u.) of chemiluminescence intensity from three independent experiments. Figure Credits: Dr. Ravikumar Govindan*

Following this, I tested whether MGR1 and MGR2 were active in different mammalian cells, and if the generation of surplus ROS by MGR1 affected the cellular viability of different mammalian cells (HEK293T, A549, RAW264.7, THP1, HeLa and MCF7). In these mammalian cells, after 4 hrs of MGR1 treatment, I found concentration dependent cell death

with IC$_{50}$ values between 4-7μM, while MGR2 was well tolerated – with negligible cell death even at 40 μM (Figure 2.2)
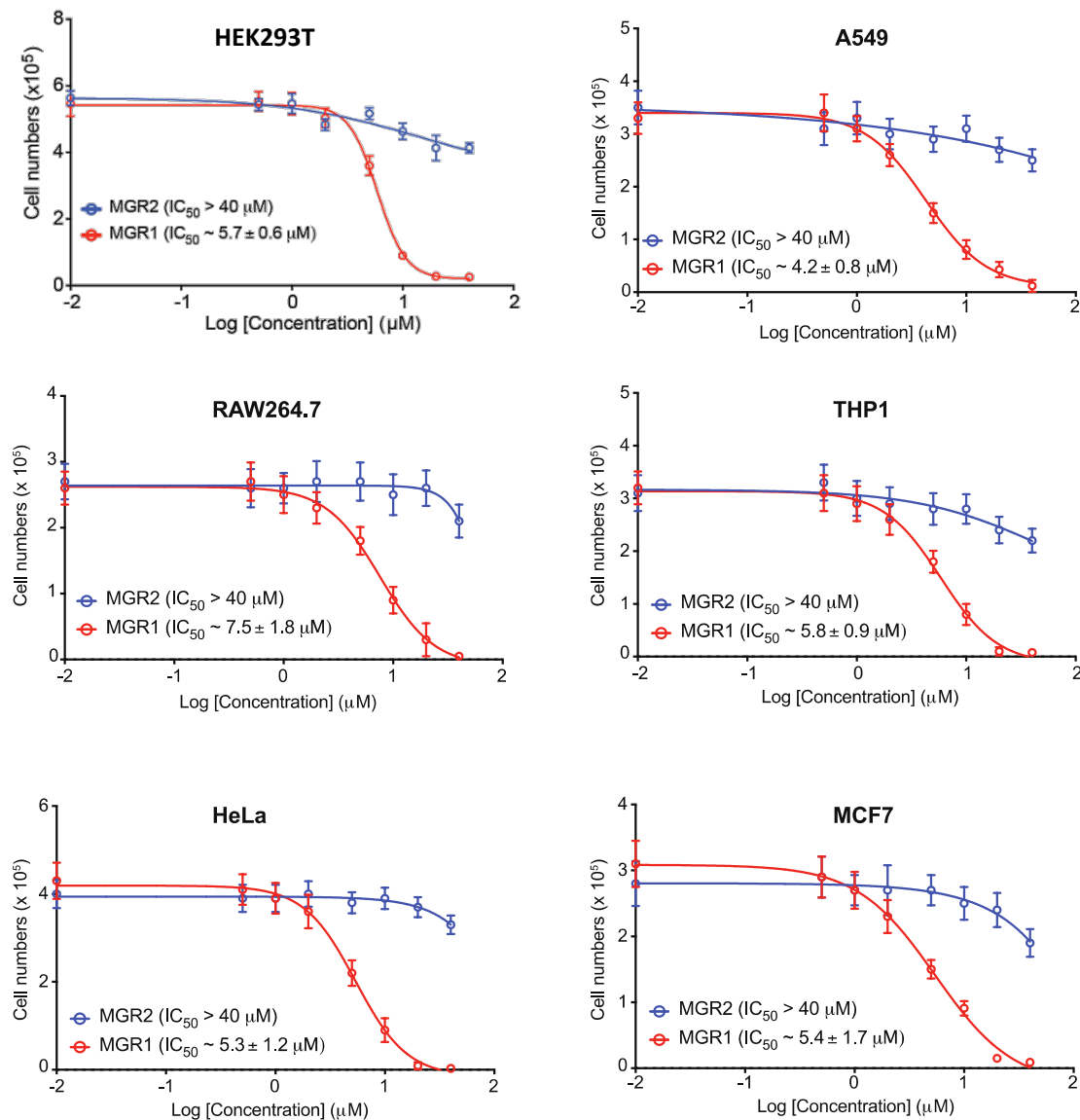
Figure 2.2. Concentration dependent cell viability of different mammalian cell lines following MGR1 or MGR2 treatment. *Different mammalian cell lines (HEK293T, A549, RAW264.7, THP1, HeLa and MCF7) were treated with varying concentrations of MGR1 or MGR2 (range: 0 – 40 μM) for 4 h. After treatment the number of live cells was estimated using a trypan blue assay (BioRad) as per manufacturers instructions. The half maximal inhibition constant (IC$_{50}$) values for MGR1 and MGR2 for each cell line are reported on the corresponding graph. Each data point represents mean ± s. e. m. for 4 biological replicates. Data shows higher concentrations of MGR1 (> 5 μM), but not MGR2, causes cell death in the current treatment paradigm.*

The proposed mechanism of action of MGR1 and MGR2 was that they both readily cross the cell membrane into the cell and are acted upon by cellular esterases, thereby releasing the the ROS generator JCHD and its structural control 1-naphthol respectively (Figure 2.3).
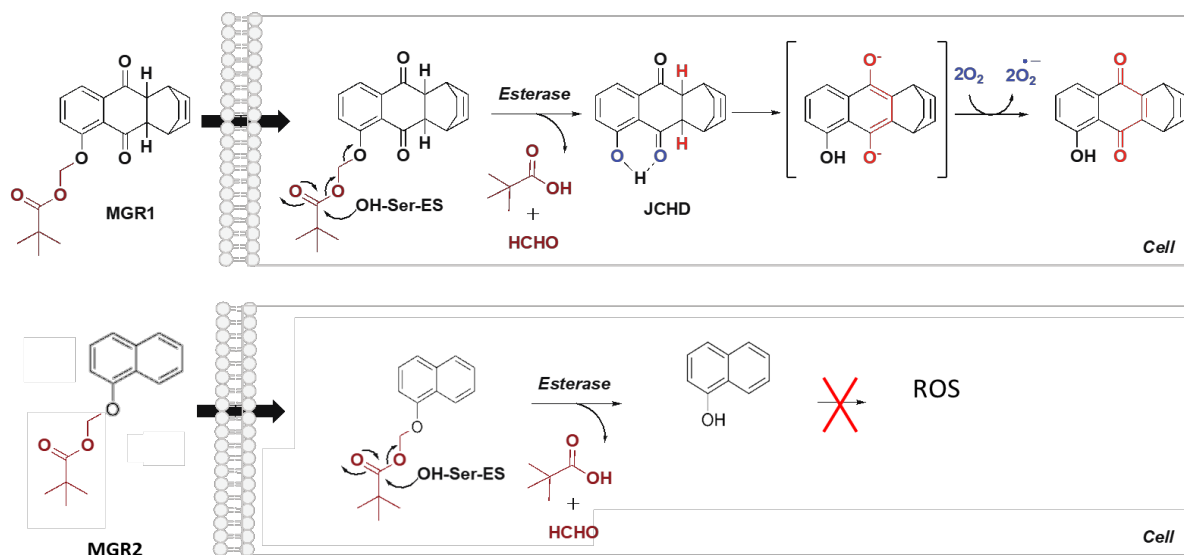
Figure 2.3. Proposed mechanism for the esterase activated ROS generation by MGR1. *In the postulated mechanism, MGR1 enters the mammalian cells, where it is acted upon by cellular esterases (serine hydrolases)* [63]*, which cleave the metabolically labile esterase cleavable linker producing the active ROS generator, JCHD* [62–64]*. MGR2 does lead to elevation of ROS as the action of esterases upon it releases inactive 1-naphthol.*

Next, to confirm that the cell death due to MGR1 treatment in mammalian cells was due to ROS production, I used the established, commercially available 2',7'-dichlorodihydrofluorescein diacetate (DCF) cellular ROS detection dye (2 – 25 μM of MGR1 or MGR2 for 1 h, followed by 10 μM of DCF, 10 mins). I found by cellular fluorescence, that MGR1, but not MGR2, produced significant ROS in HEK293T cells (Figure 2.4).

To establish a treatment paradigm for subsequent cellular studies, I required a concentration of MGR1 that would produce elevated ROS, however not enough to cause cell death. Based on the previous results, I chose 4 h of 2 μM MGR1 or MGR2 as treatment time and concentration respectively for these probes for subsequent cellular studies.
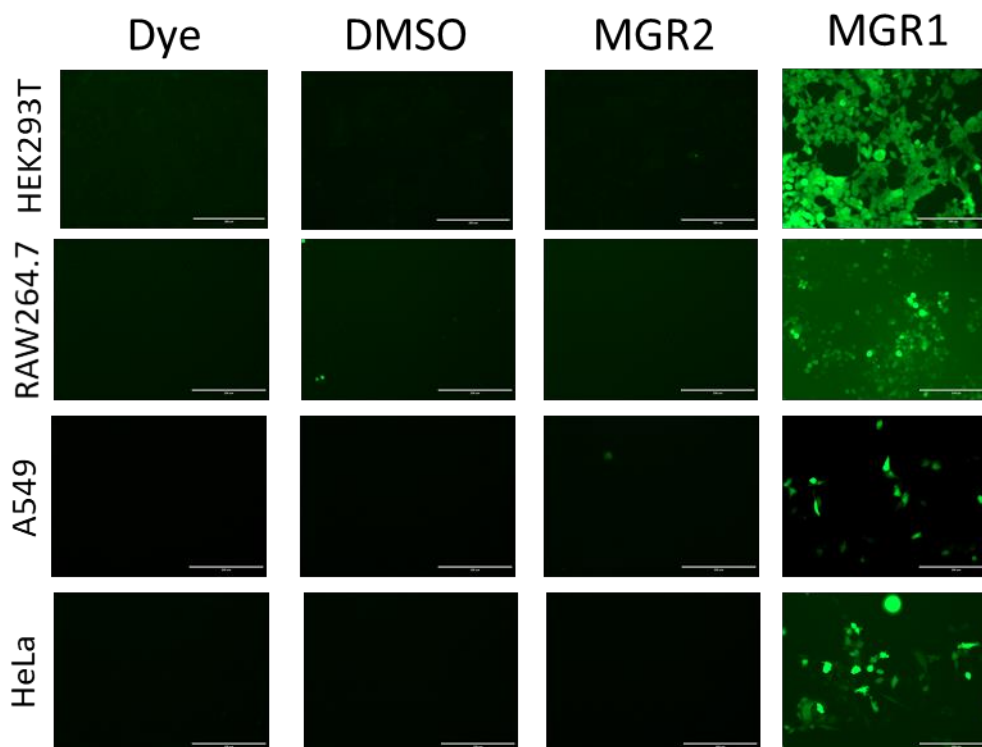
Figure 2.4. Cellular ROS levels following MGR1 or MGR2 treatment in different mammalian cell lines. *Different mammalian cell lines (HEK293T, RAW264.7, A549 and HeLa) were treated with MGR1 (5 µM) or MGR2 (5 µM) or DMSO for 1 h, following which DCF dye (10 µM) was added to the cells and fluorescence was visualized under a confocal microscope as per manufacturers instructions. The bar on the image represents 200-µm. As seen from the cellular fluorescence microscopy images, MGR1 treatment, but not MGR2 or other control (DMSO, dye only) treatment, produces elevated levels of ROS within cells (as seen by increased cellular fluorescence). This experiment was done in triplicate in all cell lines with reproducible results.*

Furthermore, to ascertain that the cell death and oxidative protein damage were was ROS dependent, I pre-treated different mammalian cells for 4 hrs with the anti-oxidants, Pterostilbene (PTS, 10 µM) [65] or *N*-acetyl-cysteine (NAC, 1 mM) [66], following which I treated the cells with 25 µM MGR1, and assessed ROS production by the DCF cellular ROS detection assay. I found that both PTS and NAC substantially reduced the cellular ROS levels after MGR1 treatment by quenching excess ROS produced by MGR1 (Figure 2.5A), thereby confirming the action of MGR1 was largely ROS mediated. The cell viability profiles also support this idea that both antioxidants PTS, and NAC completely rescue the cell death

phenotype caused by MGR1, further confirming that the cell death by MGR1 is indeed due to surplus ROS. (Figure 2.5B)
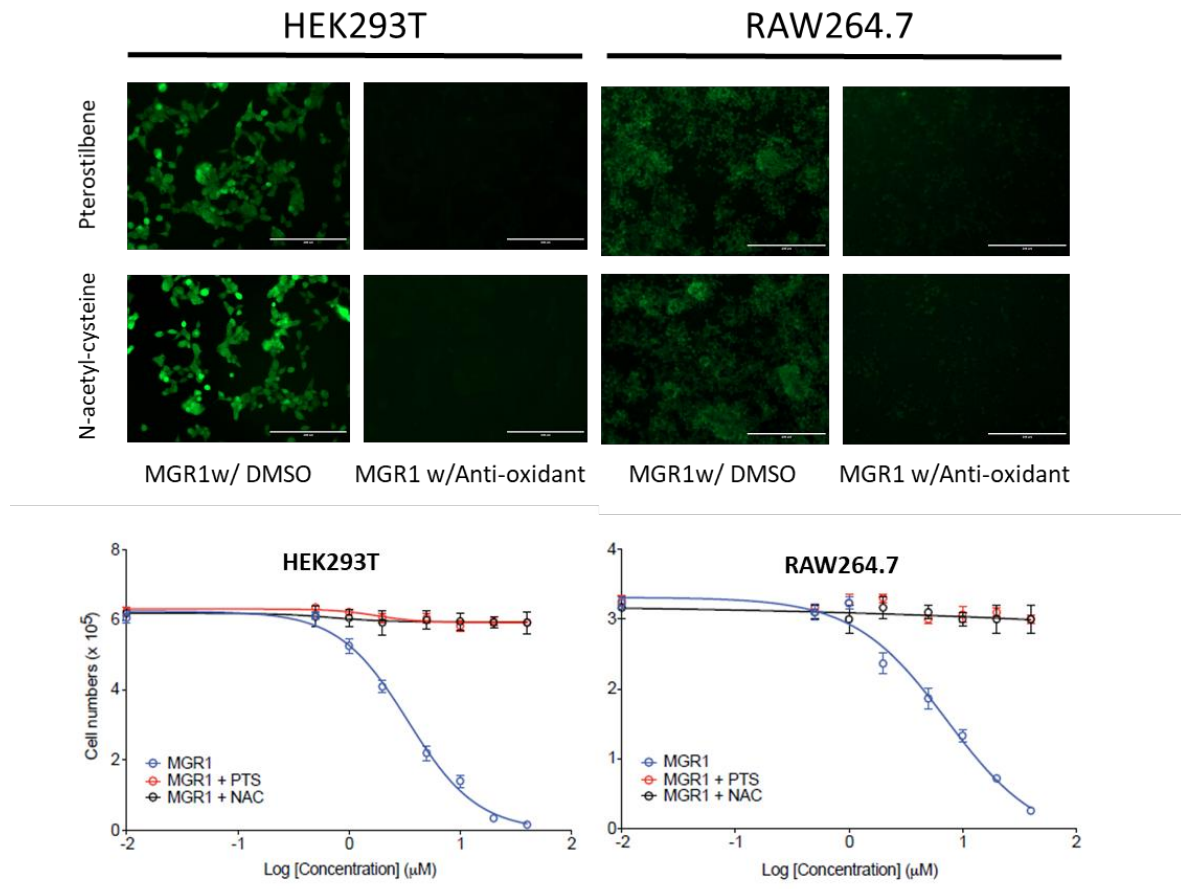
Figure 2.5. Antioxidants quench MGR1 induced ROS production in mammalian cells and rescue cells from cell death. *(A)Mammalian cells (RAW264.7, HEK293T) were pre-treated with the antioxidants, pterostilbene [65] (10 μM) or N-acetyl-cysteine [66] (NAC, 1 mM) for 4 h, following which MGR1 (5 μM) was added, and the ROS production was assessed by cellular fluorescence microscopy using DCF dye (10 μM) treatment as per manufacturers instructions. The bar on the image represents 200-μm. The antioxidants, pterostilbene and NAC quench heightened ROS produced by MGR1, and as a result do not produce a fluorescence signal. This experiment was done in triplicates with reproducible results. (B)Mammalian cells (RAW264.7, HEK293T) were pre-treated with the antioxidants, Pterostilbene6 (PTS, 10 μM) or N-acetyl-cysteine7 (NAC, 1 mM) for 4 h, following which varying MGR1 (0 – 40 μM, 4 h) was added, and the cell viability was estimated using a Trypan Blue assay (BioRad) as per manufacturers instructions. From the cell viability profiles, it is clear that both antioxidants PTS, and NAC completely rescue the cell death phenotype caused by MGR1, confirming that the cell death by MGR1 is indeed due to elevated ROS.*

Lastly, I compared the ROS levels produced by MGR1 with other known xenobiotics or ROS donors. As seen from cellular fluorescence, MGR1 treatment led to the highest elevation in levels of ROS as compared to JCHD, oxidized JCHD, Cisplatin, Artemisinin, Paraquat (1 mM), Menadione and H_2O_2 (1 mM). (Figure 2.6)
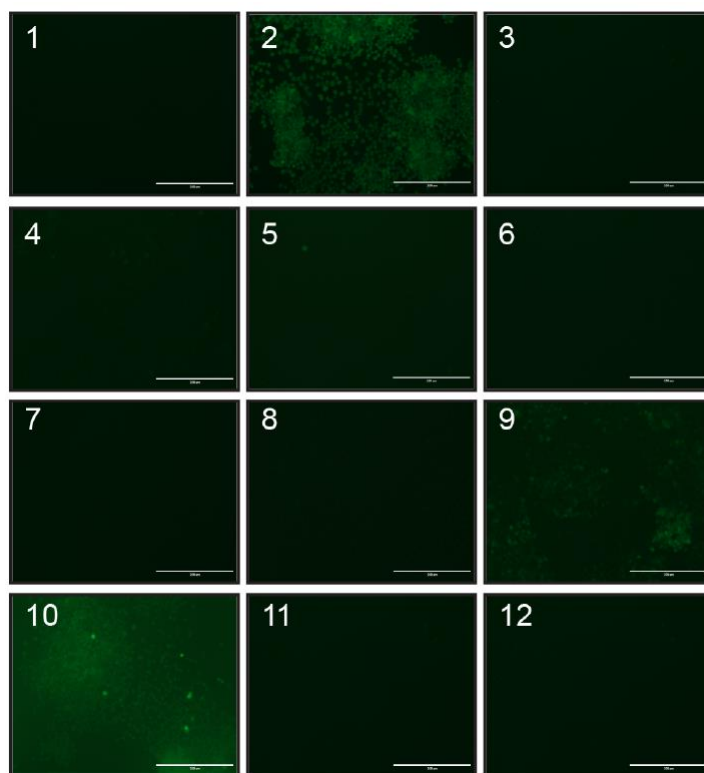
Figure 2.6. Cellular ROS levels following MGR1 or MGR2 treatment in different mammalian cell lines*. Different mammalian cell lines (A549, HeLa and RAW264.7) were treated with MGR1 or MGR2 or DMSO or xenobiotics or known ROS donors for 1 h, following which DCF dye (10 μM) was added to the cells and fluorescence was visualized under a microscope as per manufacturers instructions. The bar on the image represents 200-μm. As seen from the cellular fluorescence microscopy images, MGR1 treatment, but not MGR2 or other control (DMSO, dye only) treatment, produces elevated levels of ROS within cells (as seen by increased cellular fluorescence). This experiment was done in triplicate in all cell lines with reproducible results. The numbers denote treatment with (1) DMSO, (2) MGR1, (3) MGR2, (4) JCHD, (5) oxidized JCHD, (6) Cisplatin, (7) Artemisinin, (8) Paraquat (1 mM), (9) Menadione, (10) H2O2 (1 mM), (11) DPBS, (12) dye only.*

Detection of oxidized PS in mammalian cells undergoing oxidative stress

The ultimate goal of the project was primarily to understand the regulation of oxidized PS in mammalian cells under oxidative stress given its biological importance in programmed cell death [56].

Therefore, to establish a LC-MS/MS protocol, my colleagues chemically oxidized C18:0/18:1 PS (1-stearoyl-2-oleoyl-*sn*-glycero-3-phospho-L-serine), and measured the native and oxidized C18:0/18:1 PS. These peaks were found to be at m/z= 788.5 for [M-H]⁻ and, 804.5 and 806.6 that correspond to the addition of +16 (O) and +18 (H_2O) through oxidation. A closer look at the MS/MS fragmentation patterns for both these masses, i.e.804.5 and 806.6, suggested that mass additions of +16 (m/z = 297.2) and +18.1 (m/z = 299.3), were present on the *sn-2* esterified oleic acid of C18:0/18:1 PS, most likely across the double bond of oleic acid possibly forming a stable epoxide and hydroxide across the double bond respectively (**Fig. 2a**). The +16 and +18 mass additions were termed as ox- and hy- by us for the PS species showing these modifications.

To determine, whether MGR1 was capable of generating these oxidized PS species in mammalian cells, I treated HEK293T, RAW264.7, THP1, HeLa, MCF7 and A549 cells with 2 μM MGR1 or 2 μM MGR2 or DMSO for 4 h, and extracted the phospholipids at the end of the treatment using a modified Folch lipid extraction protocol [67]. All the treatment groups showed the presence of m/z = 788.5, however, m/z = 804.5 and 806.6, were found enriched only in the MGR1 treatment group by LC-MS analysis.

I found that the MS/MS fragmentation spectra for the endogenous C18:0/18:1 PS and the oxidized PS masses exactly matched the synthetic standards. Notably, all the three masses showed peaks at the parent m/z minus 87, corresponding to the loss of neutral serine, m/z = 437.3, corresponding to 1-stearoyl-2-hydroxy-*sn*-glycero-3-phosphate, m/z = 419.3, corresponding to 1-stearoyl-2-hydroxy-*sn*-glycero-3-phosphate minus H_2O, m/z = 283.3 corresponding to stearic acid minus H, and m/z = 153.0, corresponding to glycerophosphate minus H_2O (Figure 2.7A). M/z = 297.2 and 299.3 were also detected in the MS/MS fragmentation spectra of endogenous 804.5, and 806.6 masses respectively, confirming the formation of +16 and +18.1 oxygenated adducts that correspond to epoxy phosphatidylserine (ox-PS) and hydroxyl phosphatidylserine (hy-PS). The ox-18:0/18:1 PS, and hy-18:0/18:1 PS standards have been described in Figure 2.7A.

Based on the MS/MS fragmentation spectra, a targeted multiple reaction monitoring (MRM) based LC-MS/MS method was developed to confirm and quantitate the findings across PS lipids esterified with different fatty acids (Table MS1). This method was first validated by measuring levels of ox-18:0/18:1 PS, and hy-18:0/18:1 PS in phospholipid extracts from HEK293T cells treated with MGR1 or MGR2 or DMSO (2 μM, 4 h). MGR1 treated cells had significantly elevated levels of both ox-18:0/18:1 PS and hy-18:0/18:1 PS compared to MGR2 or DMSO treated cells (Figure 2.7C). Next, different ox- and hy-PS species were measured after MGR1 and MGR2 treatments. In HEK293T cells, several ox- and hy-PS species were found to be significantly elevated upon MGR1, but not MGR2 or DMSO treatment (Figure 2.7D).

Different mammalian cells (RAW264.7, THP1, HeLa, MCF7, and A549) treated with MGR1 and MGR2 treatment also showed elevated levels of oxidized PS lipids following treatment with MGR1 and not MGR2. (Figure 2.8). We also measured PS lipids in these experiments, and found no changes in their cellular levels following MGR1 or MGR2 treatment (Table MS1). Similar results that oxidized PS levels (both ox- and hy- species) were elevated following MGR1, but not MGR2 treatment, were observed in RAW264.7, THP1, HeLa, MCF7 and A549 mammalian cell lines,with no significant change in cellular PS levels (Figure 2.8 and 2.9, Table MS1). In all these cell lines, we did not observe any secreted oxidized PS lipids, under our experimental conditions and detection methods, presumably suggesting that these oxidized PS lipids, are not secreted from cells.

From this, it was seen that upon MGR1 treatment, there was no change in the bulk levels of the phospholipids, however 1-2% of PS got oxidized by the MGR1 mediated elevation in ROS. (Figures 2.8 and 2.9)
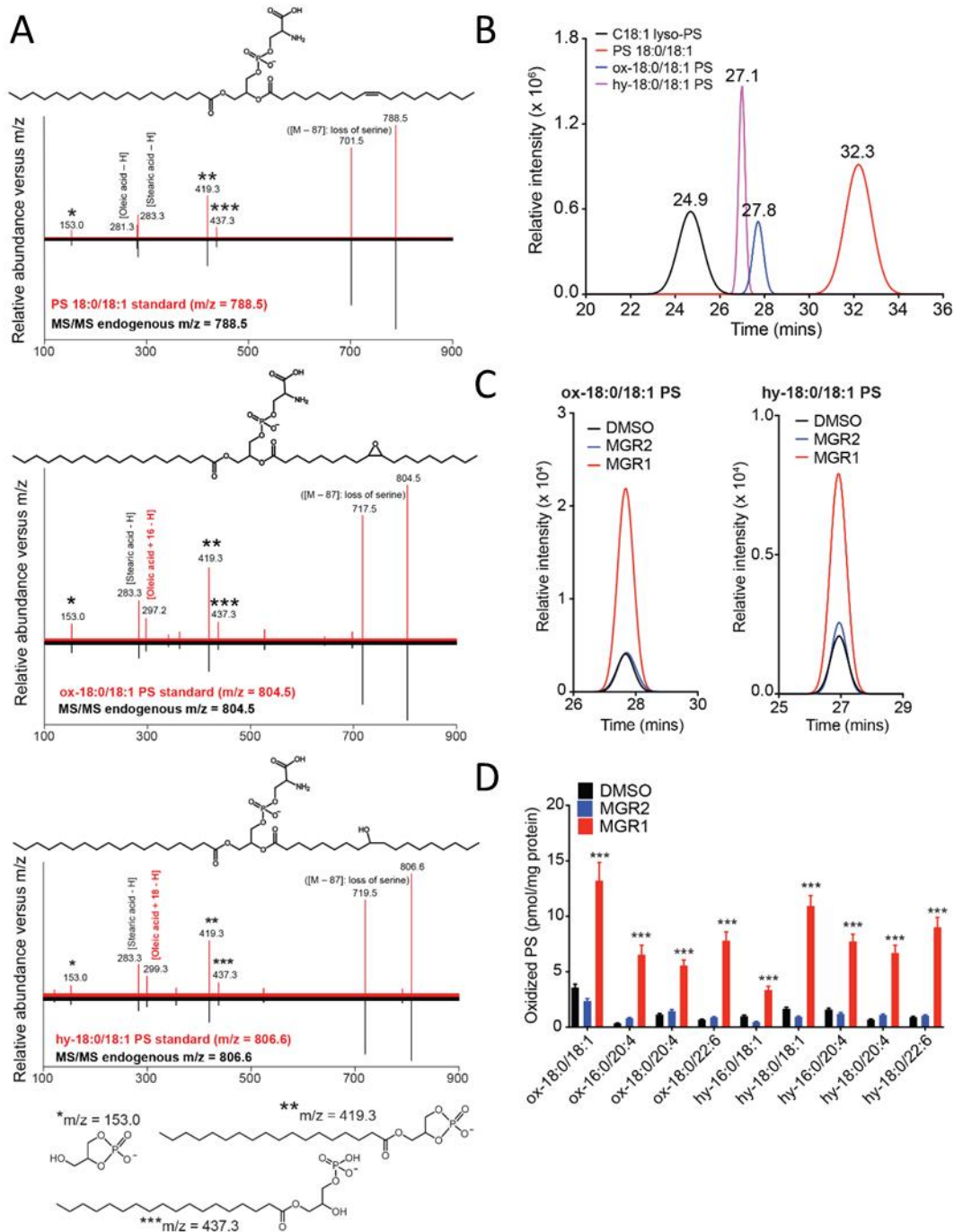
Figure 2.7. Characterization and quantification of oxidized PS produced in mammalian cells by MGR1 treatment. *(A) MS/MS fragmentation patterns for the synthetic lipids standards (red trace) for C18:0/18:1 PS, epoxy- or ox-18:0/18:1 PS and hydroxy- or hy-18:0/18:1 PS, and the corresponding endogenous phospholipid metabolites (black trace) of m/z 788.5, 804.5 and 806.6 fromHEK293T cells treated with 2 µM MGR1, 4 h. The daughter ions common to all masses from the MS/MS analysis include 153.0 (dehydro-glycerophosphate), 283.3 (stearate), 419.3 (dehydro-1-stearoyl-lysophosphatidic acid), and 437.3 (1-stearoyl-lysophosphotidic*

acid), and the parent m/z – 87 peak denoting loss of serine. The key daughter ions distinguishing the three species (denoted in red text) are 281.3 (oleate for m/z = 788.5), 297.2 (oleate + 16 amu for m/z = 804.5), and 299.3 (oleate + 18 amu for m/z = 806.6). This MS/MS fragmentation study was done in triplicate with reproducible results. (B) The LC-MS elution profile for the synthetic lipids standards for C18:1 lyso-PS, C18:0/18:1 PS, ox-18:0/18:1 PS and hy-18:0/18:1 PS, showing the increased hydrophilicity of both ox-18:0/18:1 PS and hy-18:0/18:1 PS, compared to the parent C18:0/18:1 PS lipid. The LC elution profiles were done in duplicates with reproducible results. (C) LC-MS/MS traces (MRM traces) for ox-18:0/18:1 PS (m/z = 804.5) and hy-18:0/18:1 PS (m/z = 806.6) extracted from HEK293T cells treated 4 h with MGR1 (2 μM) or MGR2 (2 μM) or DMSO, showing robust increases for both ox-18:0/18:1 PS and hy-18:0/18:1 PS, following MGR1 treatment. This experiment was done in triplicates with reproducible results. (D) Targeted LC-MS based multiple reaction monitoring (MRM) measurements of oxidized PS lipid species from HEK293T cells treated 4 h with MGR1 (2 μM) or MGR2 (2 μM) or DMSO. Data represents mean ± s. e. m. for 5 biological replicates per group. Student's t-test: *** p < 0.001 versus DMSO group. See Table MS1 for complete list of quantified lipids.
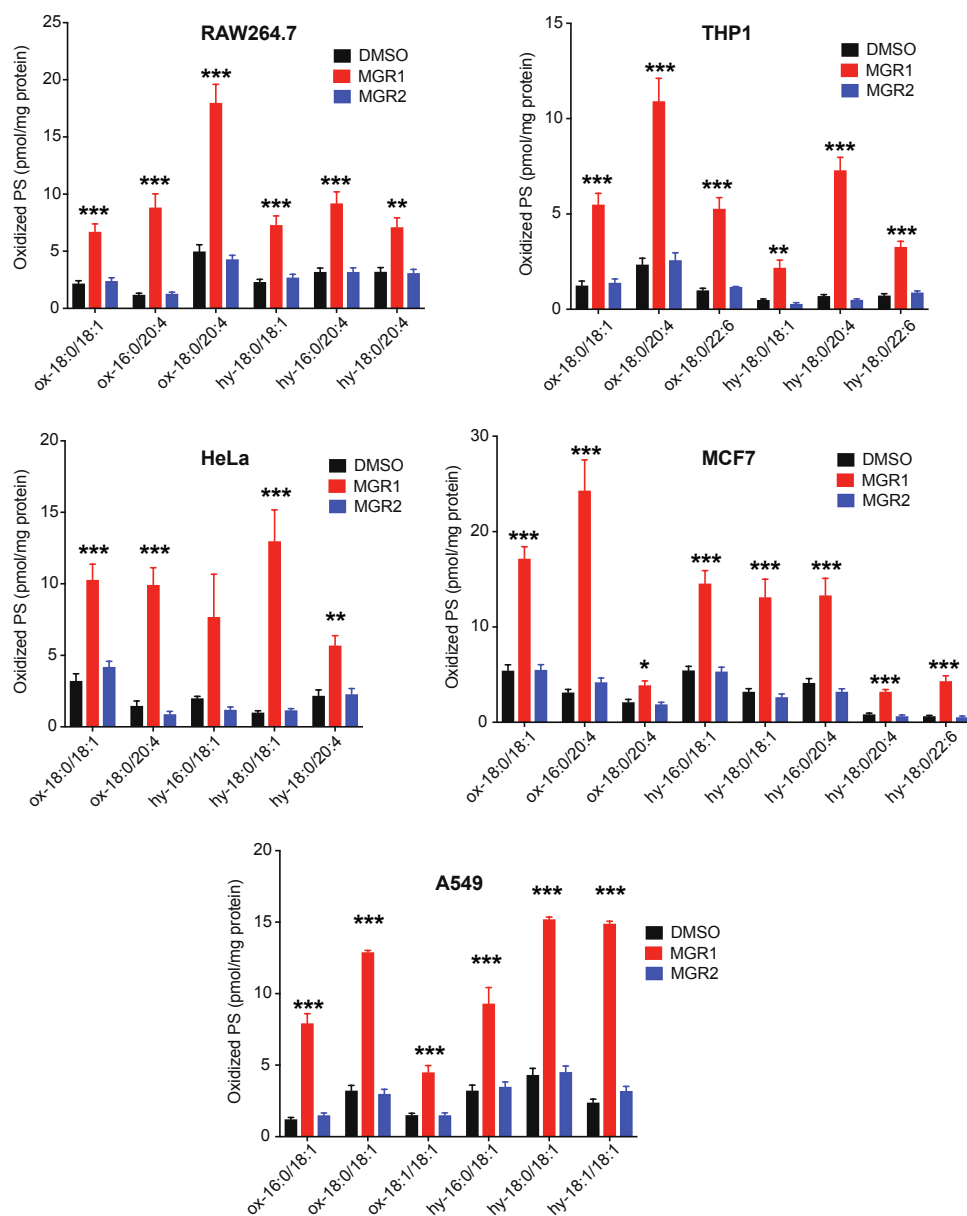
Figure 2.8. Oxidized PS content of mammalian cells treated with MGR1 or MGR2. *Different mammalian cells (RAW264.7, THP1, HeLa, MCF7, and A549) were treated with MGR1 (2 μM) or MGR2 (2 μM) or DMSO for 4 h and changes in the cellular oxidized PS lipids were measured by targeted multiple reaction monitoring (MRM) LC-MS. All lipid quantitation are reported Table MS1. Data represents mean ± s. e. m. for 5 biological replicates per group. Student's t-test: ** p < 0.01, *** p < 0.001 versus DMSO treated cells.*
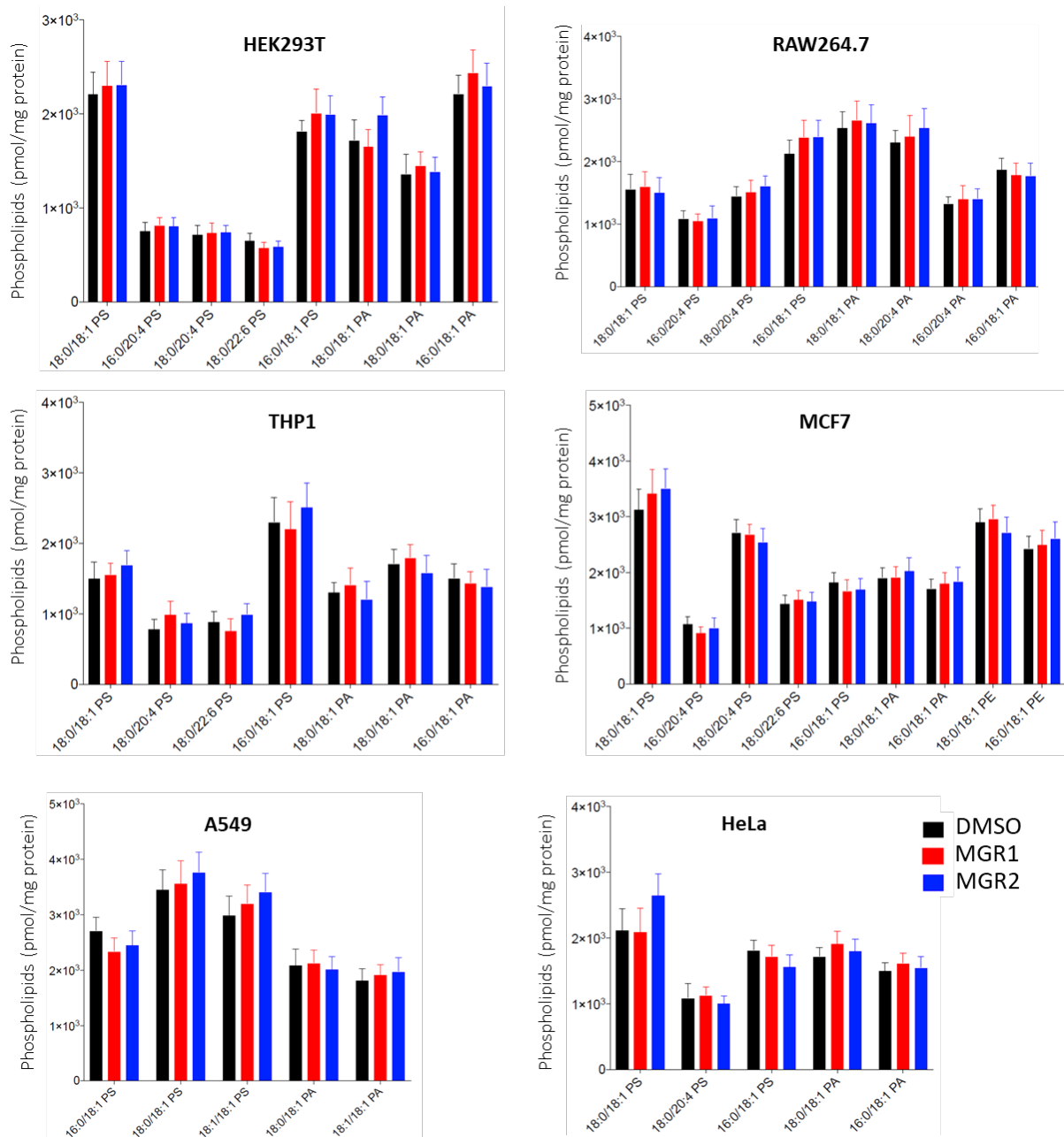
Figure 2.9. Phospholipid content of mammalian cells treated with MGR1 or MGR2.
Different mammalian cells (HEK293T, RAW264.7, THP1, HeLa, MCF7, and A549) were treated with MGR1 (2 μM) or MGR2 (2 μM) or DMSO for 4 h and changes in the cellular phospholipids were measured by targeted multiple reaction monitoring (MRM) LC-MS. The treatments do not change the bulk levels of cellular phospholipids. All lipid quantitation are reported Table MS1. Data represents mean ± s. e. m. for 5 biological replicates per group. Student's t-test: ** p < 0.01, *** p < 0.001 versus DMSO treated cells.

Chemical genetic screen to identify lipases metabolizing oxidized PS.

Having established a robust LC-MS/MS method to quantitatively measure different oxidized PS lipids in mammalian cells, we decided to develop a screen to identify enzyme(s) that metabolize these lipids. At the onset, we hypothesized that a lipase would be responsible for such an activity, and since several lipases belong to the metabolic serine hydrolase class of enzymes [68,69], we needed a cell line that expressed of many serine hydrolase enzymes and had high lipid content. Previous studies and publicly available databases [70], have shown that the RAW264.7 cell line fulfills these criteria, and was chosen as a candidate mammalian cell line for developing the screen. We collated a highly focused library of 57chemical compounds (or probes), which ranged from highly specific to very broad-spectrum lipase and/or serine hydrolase inhibitors (Table MS1) [68,69]. We treated RAW264.7 cells with inhibitor (10 μM, 4 h) followed by treatment with MGR1 (5 μM, 4 h), following which we extracted phospholipids from cells, and analyzed the oxidized PS content by targeted LC-MS/MS (Figure 2.10). As negative controls, MGR2 and DMSO were used in this screen. The rationale was that the lipase inhibitor(s) would block these enzyme(s) from metabolizing oxidized PS, which are produced as a result of MGR1 treatment, and as a consequence cause their accumulation in cells compared to screening controls, and such inhibitor(s) would be classified as "hits" in our screen (Figure 2.10).

We set a 2-fold increase cut off in oxidized PS level as a threshold for identifying hits, and found from our chemical genetic screen that most inhibitors had virtually no effect on the levels of oxidized PS, and were comparable to the DMSO control group post MGR1 treatment. However, 3 compounds, namely fluorophosphonate-alkyne (FP-alkyne), tetrahydrolipstatin (THL, also known as orlistat) and methyl arachidonyl fluorophosphonate (MAFP), showed greater than 2-fold increase in the levels of oxidized PS following MGR1 treatment compared to the DMSO control (Figure 2.10, Data given in Table 1). Both FP-alkyne and MAFP are broad-spectrum lipase (or serine hydrolase) inhibitors, and widely used chemical probes for enriching (or inhibiting) serine hydrolase enzyme activities respectively [68], further suggesting that the lipase of interest was likely a serine hydrolase enzyme(s). Since both FP-alkyne and MAFP have wide range of enzyme targets, we focused on THL, as previous studies have shown this β-lactone inhibitor potently inhibits a handful of enzymes (mostly lipases) from the serine hydrolase family [71].
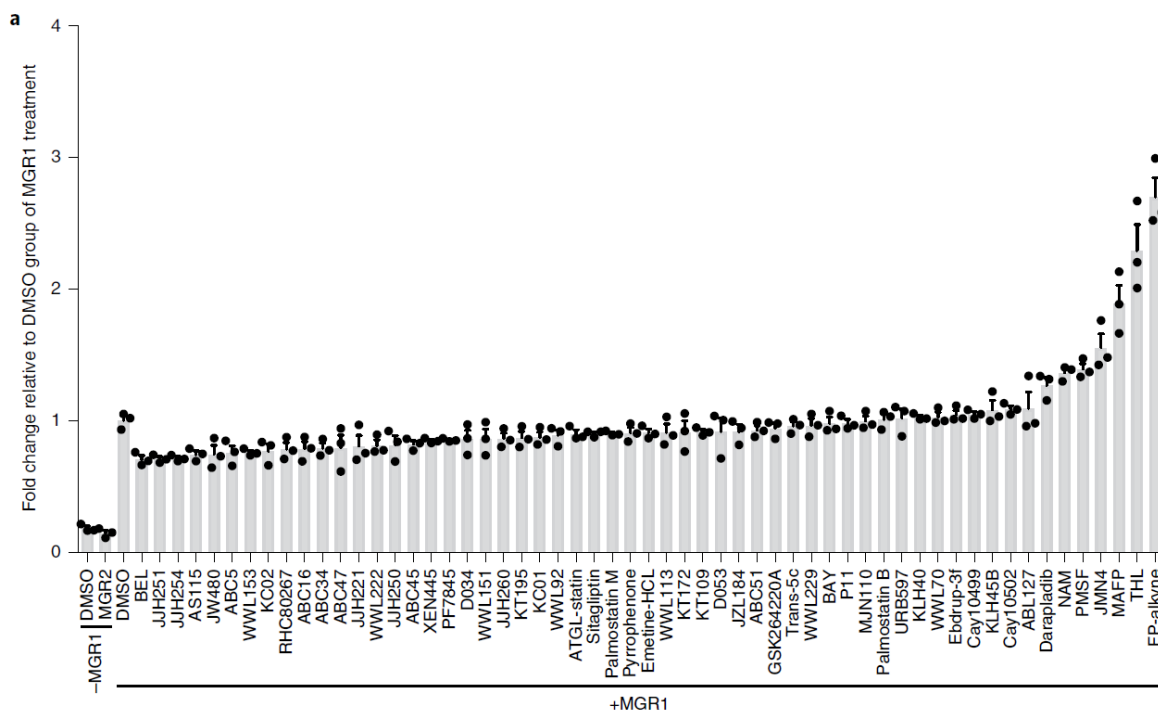
***Figure 2.10. Chemical–genetic screen to identify hit compounds for oxidized PS lipases in
mammalian cells***. *a, Relative oxidized PS levels from RAW264.7 cells from a highly focused
chemical–genetic screen of 57 known lipase inhibitors. Data represent levels relative to those
of the DMSO group of MGR1-treated controls. Each group represents mean ± s.e.m. for 3
independent experiments. A twofold increase in oxidized PS was set as a threshold to identify
hits in this screen.*

To determine possible targets of THL specifically in RAW264.7 cells, my colleagues employed
competitive activity based protein profiling (ABPP) assays, since there are no studies available
for this in RAW264.7 cells to our knowledge. Nonetheless, they over-expressed all the
enzymes that were targets of THL (ABHD6, ABHD12, ABHD16A, HSL, DAGLβ, PLA2G7,
PNPLA6, and PNPLA7) in HEK293T cells, and tested these lysates for substrate hydrolysis
activity against lyso-PS, oxidized PS and PS. It was found that ABHD12 was by-far the best
candidate, with an at least 3-fold better hydrolysis rate for oxidized PS than any other enzyme
tested in this experiment (Data not shown). As expected, ABHD12 also had good activity
against lyso-PS, but not PS (Data not shown) [59], suggesting that this enzyme can use both lyso-
PS and oxidized PS as substrates *in vitro* with near equal efficiencies.

Discussion

The oxidation of PS due to elevated ROS is linked to its transmembrane migration and presence on the exofacial membrane surface [54,72] (Figure 5.1, Chapter 5), where oxidized PS externalization generates an 'eat me' signal enabling recognition by phagocytes [52]. An elegant study has shown that apoptotic cells are indeed cleared by macrophages, through specific recognition of externalized oxidized PS by a B-type scavenger receptor [53]. Additionally, the cellular protein annexin-V binds externalized oxidized PS, and several kits for this protein–lipid interaction are available to quantitatively measure apoptotic cells. Whereas PS oxidation and its role in apoptosis are well understood, little is known regarding the enzymatic pathways that metabolize oxidized PS in vivo. In this study, we sought to identify an enzyme capable of metabolizing oxidized PS in mammalian cells. To this end, I used a chemical probe capable of robustly generating ROS in mammalian cells, thus enabling us to mimic oxidative stress (Figure 2.1). Next, I developed an LC–MS/MS method to identify and quantify oxidized PS in mammalian cells, and detected two oxidized PS species, termed ox-PS and hy-PS, in different mammalian cells in response to oxidative stress (Figure 2.7 and 2.8). I performed a chemical–genetic screen to pick out a handful of target proteins with potential oxidized PS lipase activity (Figure 2.10), from which my colleagues then identified ABHD12 as an enzyme capable of metabolizing oxidized PS in mammalian cells.

Together, we provide compelling biochemical, pharmacological and genetic evidence suggesting that ABHD12 is a major lipase capable of hydrolyzing oxidized PS. ABHD12 is of tremendous biomedical interest because it is associated with the human neurodegenerative disease PHARC, which is caused by null mutations to ABHD12 [56,59]. ABHD12 is annotated as a lyso-PS lipase in the mammalian brain and immune system [56,58,67,73,74]. Our studies together suggest a dual role for ABHD12, in which it regulates cellular oxidized PS and secreted lyso-PS, independently or simultaneously. The active site of ABHD12 is extracellularly oriented [67,74,75], which led to the belief that it can access the oxidized PS, generated by elevated cellular ROS, and translocated to the outer leaflet of the plasma membrane (Figure 5.1, chapter 5).

Finally, recent functional studies have shown that other metabolic serine hydrolases are regulators of other oxidized phospholipids in vivo [2,76]. I believe that the tools and methods described here might offer an elegant strategy for functionally annotating serine hydrolases (lipases) involved in the biochemistry of oxidized lipids. The emerging functional annotation

of orphan serine hydrolases might implicate their roles in regulating oxidized lipids from other lipid classes (for example, neutral lipids or sterols) and, in doing so, add to our understanding of the biochemistry and thereby the cellular implications of oxidized lipids under oxidative stress. In addition, developing new tools that enable visualization of oxidized PS in vivo would be beneficial in understanding the spatiotemporal distribution and regulation of these lipids in diverse biological settings. Because the protein ligands and/or receptors for oxidized PS are largely unknown, finding and understanding downstream biological signaling pathways by using emerging chemoproteomics platforms [61,77] would advance the lipid-signaling field and provide new insights into programmed cell death.

Conclusion

I report here, a successful protocol developed for generating intracellular ROS that consistently oxidized cellular phospholipids thereby giving rise to oxidized PS within cells. This was achieved by using a Juglone cyclohexadi-ene based ROS donor MGR1. While the levels of ROS were visualized using a redox-sensitive dichlorodihydrofluorescein diacetate (DCF) based dye and, oxidized PS species were detected and quantified with the help of mass spectrometry based lipidomic analyses.

Elevation of ROS, and thereby oxidized PS in RAW264.7 was found to be reproducible and was used as a foundation for performing a chemical genetic screen using a library of serine hydrolase inhibitors, to fish for lipases capable of hydrolyzing oxidized PS. I determined a few candidate lipases of which, my colleagues then proceeded to identify ABHD12 to have oxidized PS lipase activity along with its reported lysoPS lipase activity.

The strategy described here can be effectively used for studying the metabolism of other oxidized lipid species.

CHAPTER III
ROLE OF CERAMIDE SYNTHASE 2
IN PHAGOSOMAL MATURATION

Introduction

Phagocytosis, in mammals, is the process of internalization of solid particles (pathogens or cellular debris) $\geq$ 500 nm by immune cells, predominantly macrophages. Over the last century, this universally conserved process has been extensively studied and shown to be a critical component of both the innate and adaptive mammalian immune system[36] .Once internalized, these particles acquire membranes from the cellular plasma membrane and undergo a choreographed sequence of events broadly referred to as "phagosomal maturation" culminating in fusion of the phagosomes with lysosomes. During maturation, the phagosomal lumen decreases in pH from 7 to 4.5 from an early phagosome (EP) to finally fuse with lysosome (phago-lysosome) via a late phagosome (LP) intermediate on the maturation pathway [37,78,79]. During this transformation, the maturing phagosome changes profoundly in its protein and lipid composition via interactions and functional crosstalk with the endocytic pathway and inputs from the trans-Golgi-network.

Over the past two decades, several elegant proteomics studies have shown the role of specific proteins in the maturation process, and these in turn have served as unique markers for the different stages in the phagosomal maturation process[36]. For example, the GTPase Rab5 and early endosome antigen 1 (EEA1) localize to the EP, and drive the EP to mature into a LP. The GTPase Rab7 and lysosomal associated membrane protein 1 (LAMP1) are found enriched on LPs, and are critical for the formation of the phago-lysosome. Further studies in characterizing these proteins have shown that the process of phagosomal maturation is spatio-temporally regulated and highly interdependent [36]. For instance, the acquisition of Rab5 onto the EP is a prerequisite for recruiting Rab7 in order to proceed with maturation process. The localization of EPs is mostly peripheral while that of LPs is towards the peri-nuclear region of the cell, where the lysosomes reside [80]. Though the initial engulfment of a foreign particle mostly involves remodeling of actin cytoskeleton, phagosome maturation requires transport of the phagosome on the microtubule cytoskeleton. While there exist several global proteomics studies that describe the role of different proteins during phagosomal maturation, there are only a handful of studies reported that describe the lipid profiles of maturing phagosomes, and these too, only describe a specific lipid class, and the global lipid profile [81]. One such study describes the role and enrichment of different phosphoinositides at different stages of phagosomal maturation [82].

Free cholesterol was found to be enriched on the LP membrane, where it forms lipid raft domains, moreover, deregulated cholesterol metabolism leads to impairment in phagosomal maturation [83–85]. The motor protein dynein was shown to be enriched and clustered on these cholesterol richlipid microdomains on LPs, which in turn efficiently facilitates the uni-directional motion of LPs towards the lysosome [83]. As a corollary to the aforementioned work, here, my colleagues and I set out to quantitatively determine the lipid composition of EPs and LPs. We show by biochemical assays, fatty acid feeding and cellular pharmacological studies that the enzyme ceramide synthase controls the flux of ceramides during phagosomal maturation, and leads to a very pronounced increase of long-chain ceramides on LPs. This increase, we believe, is universally conserved because it is replicated in both mammalian cells (RAW264.7 macrophages) and in an early eukaryote (*Dictyostelium discoideum*). Finally, pharmacological blockade of ceramide synthase hampers the process of phagosomal maturation, suggesting an important role for this enzyme in the orchestration of phagocytosis.

Materials and methods

Materials. All chemicals, buffers, solvents and reagents were purchased from Sigma-Aldrich unless otherwise mentioned. All MS quantitation lipid standards were purchased from Avanti Polar Lipids Inc. unless otherwise mentioned.

Phagosome preparations from RAW264.7 cells. The RAW264.7 mouse macrophage cell line (ATCC)wascultured in Dulbecco's Modified Eagle's Medium (DMEM) (HiMedia) with 10% (v/v) Fetal Bovine Serum (FBS) (Thermofisher Scientific) and 1% (v/v) Penicillin-Streptomycin (MP Biomedicals) at 37°C and 5% (v/v) CO_2. 10 x 10 cm culture dishes (Eppendorf) were used for phagosomal preparations using a previously established protocol [83]. Briefly, 300 μL of 1-μm silica beads were washed with DMEM (x 3 times), pelleted by centrifugation at 500g for 5 mins after each wash, and finally resuspended in 1 mL serum free DMEM. This solution was vortexed, sonicated for 5 mins and added to 30 mL serum free DMEM pre-warmed to 37°C. 3 mL of this solution was added to a 10 cm culture dish containing RAW264.7 cells at 80% confluency. The cells were subsequently kept at 4°C for 5 mins to synchronize the uptake of beads. Post-synchronization, the bead pulse was 15 mins for EP or LP preparations. The unphagocytosed beads were removed by washing the cells with sterile Phosphate Buffer Saline (PBS) (x 3 times). For EP preparations, cells were harvested at this stage and transferred to a sterile 50 mL tube, while for LP preparations, the cells were cultured

for 4 h in DMEM with 10% (v/v) FBS at 37°C. Upon desired bead maturation, the cells were washed with sterile PBS (x 3 times), harvested by scraping, and transferred into sterile 50 mL tubes. The harvested cells are washed again sterile PBS (x 2 times), and pelleted by spinning at 500g for 5 mins after each wash. The cells were then wash with 25 mL of lysis buffer (250 mM sucrose, 3 mM imidazole, pH 7.4) followed by pelleting by centrifugation at 500g for 5 mins. Post-washing the cells were resuspended in 1 mL of lysis buffer containing protease inhibitor cocktail (Roche), 3 mM dithiothreitol (DTT) and 10 μgmL^{-1} pepstatin A. This cell suspension was lysed using a cell cracker with a 10μm clearance (Isobiotec) by 10 passages through the syringes. This cellular lysate was overlaid on a sucrose step gradient with 5 mL each of 85% (w/v) sucrose and 60% (w/v) sucrose with 3 mM imidazole. The gradient was centrifuged at 100,000g at 4°C for 1 h. The bead pellet was separated from the cellular debris and resuspended in 200 μL TNE buffer (50 mM Tris, 140 mM NaCl, 5 mM EDTA, pH 7.4) and stored at –20°C before processing for lipid extraction.

Cellular feeding and pharmacological inhibition. For the C17:1 FFA feeding experiment, the RAW264.7 cells in 10 cm culture dish at 80% confluence, were fedwith 1 mM C17:1 FFA for 4 h prior to starting the aforementioned phagosomal preparations. For CerS2 inhibition studies, 5 μM fumonisin was added after the initial bead phagocytosis, post-synchronization, and the phagosomal preparations were performed as described above.

Lipid extraction and targeted lipid profiling. The phagosomal lipid extractions were performed using a previously described protocol [61,67,86]. Briefly, the phagosomal preparations were washed with sterile Dulbecco's PBS (DPBS) (3 times), and transferred into a glass vial using 1 mL DPBS. 3 mL of 2:1 (v/v) chloroform (CHCl$_3$): methanol (MeOH) with the internal standard mix (50 pmol of each internal standard listed in Table MS1) was added, and the mixture was vortexed. The two phases were separated by centrifugation at 2800g for 5 mins. The organic phase (bottom) was removed, 50 μL of formic acid was added to acidify the aqueous homogenate, and CHCl$_3$ was added to make up 4 mL volume. The mixture was vortexed, and separated by centrifugation at 2800g for 5 mins. Both the organic extracts were pooled, and dried under a stream of N$_2$. The lipidome was solubilized in 200 μL of 2:1 (v/v) CHCl$_3$: MeOH, and 20 μL was used for the lipidomics analysis. All the lipid species analyzed in this study were quantified using the multiple reaction monitoring high resolution (MRM-HR) scanning method (Table MS1) on a Sciex X500R QTOFmass spectrometer (MS) fitted with an Exion-LC series UHPLC. All data was acquiredand analyzed using the SciexOS

software. The LC separation was achieved using a Gemini 5U C18 column (Phenomenex, 5 µm, 50 x 4.6 mm) coupled to a Gemini guard column (Phenomenex, 4 x 3 mm). The LC solvents were: positive mode: buffer A: 95:5 (v/v) H_2O: MeOH + 0.1% formic acid + 10 mM ammonium formate; and buffer B: 60:35:5 (v/v) isopropanol (IPA): MeOH: H_2O + 0.1% (v/v) formic acid + 10 mM ammonium formate; negative mode: buffer A: 95:5 (v/v) H_2O: MeOH + 0.1% (v/v) NH_4OH; and buffer B: 60:35:5 (v/v) IPA: MeOH: H_2O + 0.1% (v/v) NH_4OH. All the lipid estimations were performed using an electrospray ion source (ESI), using the following MS parameters: turbo spray ion source, medium collision gas, curtain gas = 20 $Lmin^{-1}$, ion spray voltage = 4500V(positive mode) or –5500V (negative mode), at 400ºC. A typical LC-run was 55 mins, with the following solvent run sequence post injection: 0.3 mL min^{-1} 0% B for 5 mins, 0.5 mL min^{-1} 0% B for 5 mins, 0.5 mL min^{-1} linear gradient of B from 0–100% over 25 mins, 0.5 mL min^{-1} of 100% B for 10 mins, and re-equilibration with 0.5 mL min^{-1} of 0% B for 10 mins. A detailed list of all the species targeted in this MRM-HR study, describing the precursor parent ion mass and adduct, the product ion targeted, and MS voltage parameters can be found in Table MS1. All the endogenous lipid species were quantified by measuring the area under the curve in comparison to the respective internal standard, and then normalizing to the total protein content of the phagosomal preparation. All the lipidomics data is represented as mean ± s. e. m. of 4 (or more) biological replicates per group (Table MS1).

Western blot analysis. All western blots were done using established protocols [80,83] with the following primary antibodies (rabbit): anti-CerS2 (1:1000, Sigma-Aldrich, HPA027262), or anti-EEA-1 (1:2000, Cell Signaling Technology, 2411S) or anti-LAMP1 (1:2000, Abcam, ab24170) or anti-Rab7 (1:2000, Abcam, ab137029). The goat anti-rabbit IgG (H+L) HRP conjugated (1:10,000, Abcam, ab6789) was used a secondary antibody (1 h, 25ºC), following which the protein signal was visualized using the SuperSignal West Pico Plus Chemiluminescent substrate (Thermofisher Scientific) on a Syngene G-Box Chemi-XRQ gel documentation system.

Ceramide synthase substrate assays. The substrate assay was adapted from a previously described protocol albeit with a different substrate [87]. Briefly, 50 µM behenoyl-coenzyme A (C22:0-CoA) and 20 µM sphingosine were mixed by sonication and incubated at 37ºC with shaking at 750 rpm for 5 mins, following which 10 µg of proteome was added to final volume of 100 µL in DPBS, and the mixture was incubated at 37ºC with shaking at 750 rpm for 30 mins. The reaction was quenched by addition of 250 µL of 2:1 $CHCl_3$: MeOH containing 50

pmol N-25:0-ceramide internal standard, and the mixture was vigorously vortexed. The two phases were separated by centrifugation at 2800g for 5 mins, and the organic phase (bottom) was removed. The organic extracts were dried under a stream of N_2, and solubilized in 100 μL of 2:1 (v/v) CHCl₃:MeOH. The LC-MS protocol was similar to a previously established protocol [88]. All MS analysis was performed using an ESI in the positive ion mode for ceramide formation. All MS parameters are described in Table MS1. Measuring the area under the peak, and normalizing it to the internal standard quantified the product formed for the ceramide synthase assays. The enzymatic rate was corrected by subtracting the non-enzymatic rate of hydrolysis, which was obtained by using heatdenatured proteome as a control. All the data is represented as mean ± s. e. m. of at least 3 biological replicates.

Statistical analysis. All data presented in as mean ± s.e.m. of 3 (or more) biological replicates per group for substrate assays, and as mean ± s.e.m. of at least 4 (or more) biological replicates per group for lipidomics experiments. Statistical analysis was performed using GraphPad Prism 7 (Mac OS X), and the Student's t-test (two-tailed) of this software was used to calculatestatistical significance between the different study groups. A P-value of < 0.05 was considered statistically significant in this study.

Results

Lipidomic characterization of maturing phagosomes.

To comparatively analyze the lipid profiles, herein referred to as the lipidome of EP and LP, I first extracted lipids from EPs and LPs and established a LC-MS/MS based method to exhaustively analyze >400 unique lipid species from 22 lipid classes in tandem (Figure 3.1A, Table MS1) [2,3,67,86,89]. These lipid classes broadly encompassed neutral lipids, phospholipids and their lyso-versions, sterols and their esters, and sphingolipids [2,3,49,67,86,89,90]. EPs and LPs were prepared and purified using established protocols from the mammalian RAW264.7 macrophages, and their purity was assessed to ensure these EP and LP preparations were devoid of any cellular membrane contamination (e.g. ER membrane, Golgi membrane),by previously established western blot analysis [80,83]. As reported earlier, quantitative lipidomics recapitulated a > 3-fold increase in cholesterol on LPs compared to EPs, giving further confidence in our phagosomal preparations (Figure 3.1B, Table MS1) [83,84]. Interestingly, I found that ceramides were highly enriched on LPs, and this enrichment was the most profound for very long chain

(VLC) fatty acid chain (≥ C22) containing ceramide species (Figure 3.1C, Table MS1). Additionally, there was a concomitant decrease in the level of sphingosine (Figure 3.1D, Table MS1),and VLC fatty acid bearing phosphatidylcholine (PC) and phosphatidylethanolamine (PE) phospholipids (Figure 3.1E, Table MS1). Surprisingly, two free polyunsaturated fatty acids (PUFAs) namely arachidonic acid (C20:4), and docasahexenoic acid (C22:6) were enriched on LPs, with a concomitant decrease in the concentrations of PUFA containing PC and PE lipids on LPs (Table MS1). Besides these lipids, no other major lipid class was found to change significantly between the EP and LP groups Table MS1).
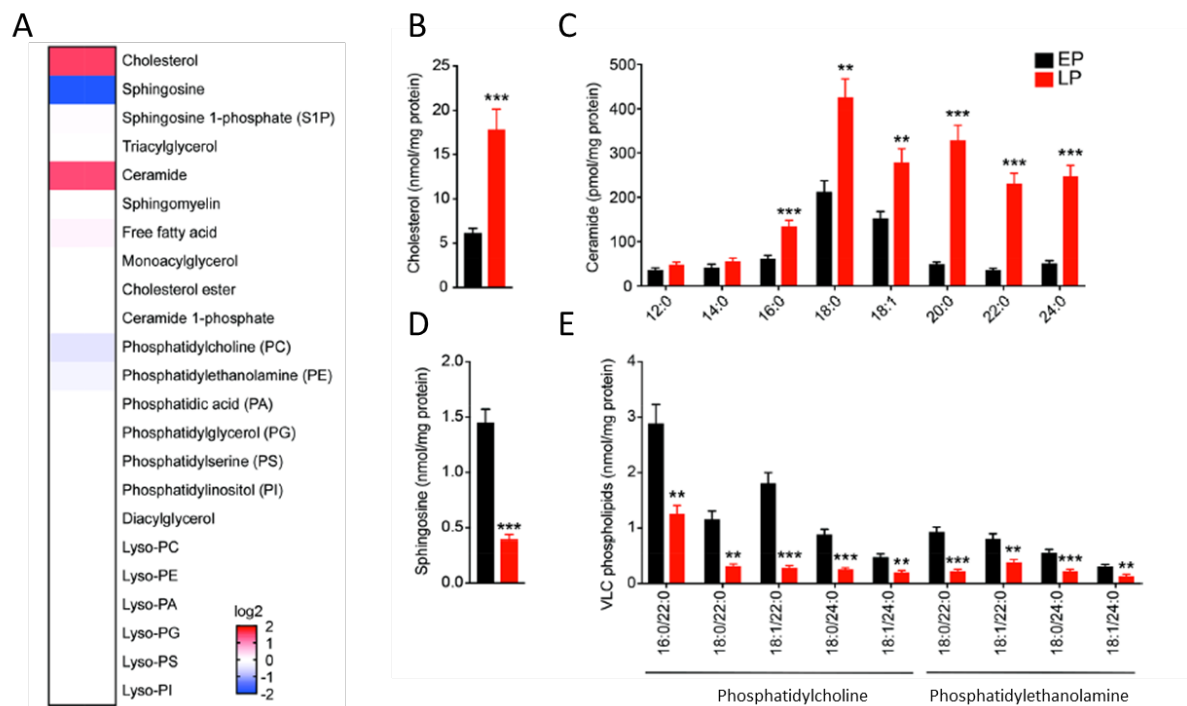
Figure 3.1. Lipidomic characterization of EPs and LPs derived from RAW264.7 mouse macrophages. *(A) Heat map plot showing the different lipid classes assessed by comparative LC-MS/MS analysis for EPs and LPs from RAW264.7 mouse macrophages. The heat map plot represents an average of fold changes (LP/EP) on a log 2 scale for different lipids from a particular lipid class. Blue and red color changes show enrichment of a particular lipid class on EP and LP respectively. Data represent six biological replicates per group. See Supporting Information Table 1 for complete data sets. Concentration of (B) cholesterol, (C) ceramides, (D) sphingosine, and (E) very long chain (VLC) containing phosphatidylcholine (PC) and phosphatidylethanolamine (PE) phospholipids from EPs and LPs. **P < 0.01, ***P < 0.001 for LP group versus EP group by Student's t test.*

As a control, to assess whether the changes in ceramides were EP and LP specific, and not a cellular event during phagosomal maturation, I measured ceramide levels in RAW264.7 macrophages at 0.5 and 4 h post feeding of beads, and compared these concentrations to "no bead" treated RAW264.7 macrophages. I found no change in the concentration of cellular ceramides in this experiment, suggesting that ceramide changes from the last experiment were indeed EP and LP specific (Figure 3.2).
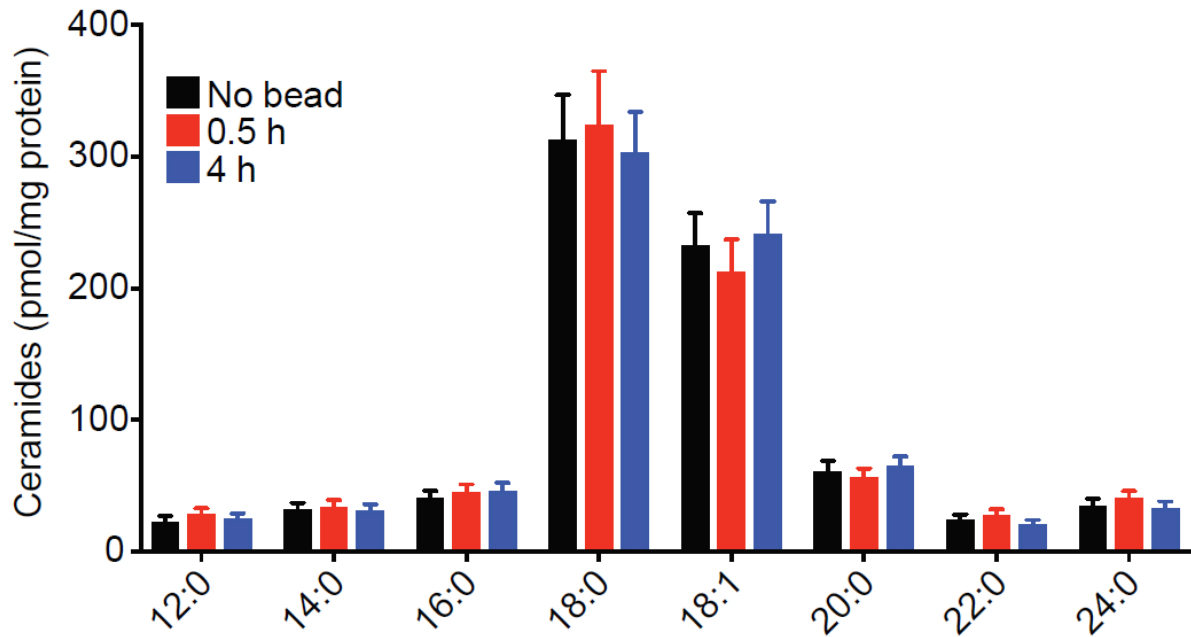
Figure 3.2. Cellular concentration of ceramides and CerS2 following bead phagocytosis from RAW264.7 cells. *As a control experiment to determine whether (A) cellular ceramides and (B) cellular CerS2 were altered in RAW264.7 cells when fed with beads, and concentrations of ceramides and CerS2 were measured by LC-MS/MS and western blot analysis respectively at 0.5 and 4 h post bead feeding (which represent time points of EP and LP maturation respectively). Based on these data, both these cellular levels are unaltered, suggesting that changes in ceramides and CerS2 are indeed EP and LP specific. The data in panel (A) represents mean ± s. e. m. for 4 biological replicates, while the data in panel (B) was performed in duplicate with reproducible results.*

Since phagocytosis is an evolutionary conserved immune process, Dr. Divya Pathak, with Dr. Roop Mallik, performed similar quantitative lipidomics experiments using *Dictyostelium discoideum,* a primitive eukaryote. The phytosterols (stigmasterol and sitosterol, as Dictyostelium discoideum does not have any cholesterol), and VLC fatty acid containing ceramides were found most enriched on LPs, while the sphingolipid precursors (sphingosine and sphinganine), and VLC fatty acid containing PCs were found enriched on EPs, reflecting the lipidomics findings in phagosomes from RAW264.7 macrophages. (Data not shown)

Given the striking increase in VLC fatty acid containing ceramides and a concomitant decrease in sphingosine and VLC containing phospholipids (PC, PE) on LPs in both RAW264.7 macrophages and *Dictyostelium discoideum* cells, we hypothesized that an enzyme capable of biosynthesizing ceramides from sphingosine and phospholipid-derived fatty acid precursors was likely causing ceramide accumulation on the phagosome membrane during their maturation. Based on the lipidomics data, we also postulated that this enzyme has a preference for biosynthesizing VLC fatty acid containing ceramides.

Role of ceramide synthase 2 in phagocytosis.

Mammals have an integral membrane enzyme, ceramide synthase (CerS), that biosynthesizes ceramides from sphingosine and fatty acyl-coenzyme A (CoA) (Figure 3.3A). There are six isoforms of ceramide synthase (CerS1-6) in mammals, with different tissue distributions and fatty acyl-CoA substrate preferences [91]. Both large-scale gene expression studies (http://biogps.org/) [70] (Figure 3.3B) and literature precedence support CerS2 being the major ceramide synthase in RAW264.7 macrophages [92] but its detection at a protein level and enzymatic activity in RAW264.7 macrophages remains lacking.

Interestingly, biochemical characterization of recombinant CerS2 has shown that this enzyme prefers VLC fatty acyl-CoA as substrates, to form VLC fatty acid containing ceramides [93]. This CerS2 substrate profile matches our lipidomic profile, where I see the highest enrichment for VLC containing ceramide species on LPs (e.g. C22:0, C24:0 ceramides) (Figure 3.1C**,** Table MS1). To test whether CerS2 was indeed the dominant ceramide synthase in RAW264.7 cells, I performed ceramide synthase activity assays on membrane lysates of RAW264.7 cells using fumonisin B1 (referred as fumonisin), a fungal natural product, which is a potent inhibitor of CerS2 [94–96]. In these assays, we found that the membrane lysates of RAW264.7 cells had robust

ceramide synthase activity that was potently inhibited by fumonisin treatment (5 µM, 30 mins) (Figure 3.3C). I also confirmed by western blot analysis that CerS2 is indeed expressed abundantly in the membrane lysates of RAW264.7 cells (Figure 3.3D).
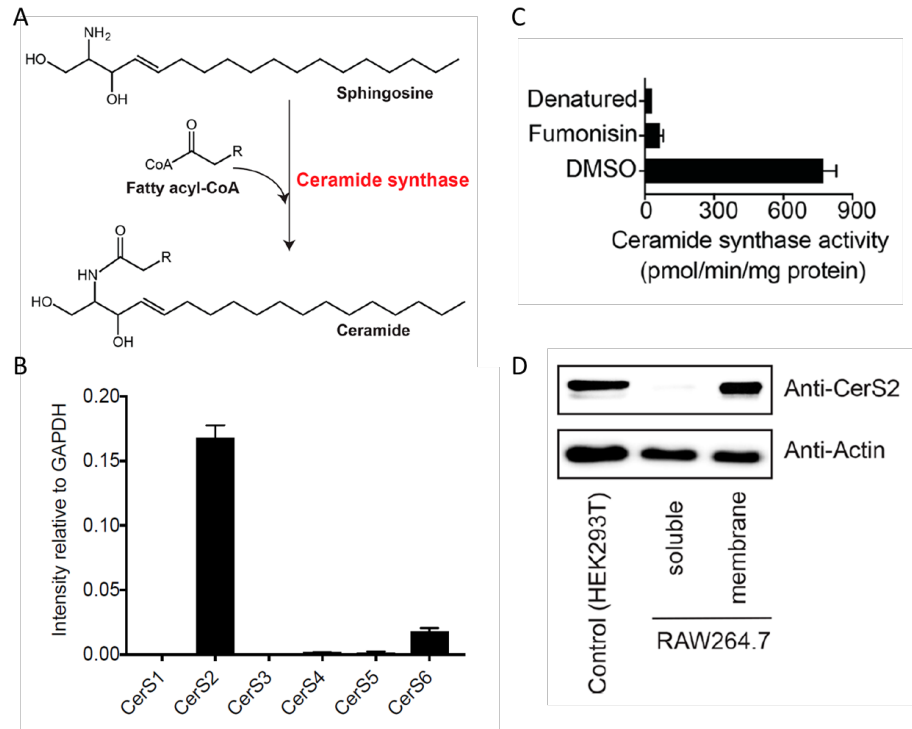
Figure 3.3. Identification of CerS2 as major ceramide synthase in RAW264.7 mouse macrophages. *(A) The reaction catalyzed by ceramide synthase. (B) Expression profile for different ceramide synthase isoforms in RAW264.7 mouse macrophages. The mRNA levels of ceramide synthase isoforms 1 – 6 in mammalian RAW264.7 cells relative to GAPDH from public large-scale gene expression studies (http://biogps.org/)* [70,92]. *The mRNA expression data suggests that CerS2 is the major ceramide synthase in RAW264.7 mouse macrophages3, with probably some contribution from CerS6. (C) Ceramide synthase in vitro activity assays on membrane lysates from RAW264.7 mouse macrophages treated with fumonisin (5 µM, 30 min) or DMSO, showing robust inhibition of ceramide synthase activity following fumonisin treatment. As a control, denatured membrane proteomes were used. Data represent mean ± SEM for three biological replicates per group. (D) Western blot analysis confirming abundant expression of CerS2 in RAW264.7 membrane lysates. As a positive control, membrane lysates from HEK293T were used. A total of 40 µg of lysate was loaded for all samples in this analysis, and actin was used as a loading control. The Western blot analysis was performed on five biological replicates with reproducible results.*

Having established CerS2 as the major ceramide synthase in RAW264.7 cells, I wanted to assess whether this enzyme is present on EPs and LPs, as maturing phagosomes acquire their membranes predominantly from cellular components that they interact with during their journey towards lysosomes (e.g. plasma membrane, ER membrane) [78].

Towards this, EPs and LPs were assessed for CerS2 content by western blot analysis. Very interestingly and contrary to our initial expectations, I found that EPs had significantly more CerS2 than LPs (~ 3-fold) (Figure 3.4A). Consistent with the enriched CerS2 on EPs, I found that the ceramide synthase activity was ~ 3 fold higher on EPs, compared to LPs (Figure 3.4B). As a control, I measured the cellular levels of CerS2 in RAW264.7cells, during this treatment, and found no changes in CerS2 cellular levels, suggesting that the change in CerS2 level was EP and LP specific (Figure 3.4C).
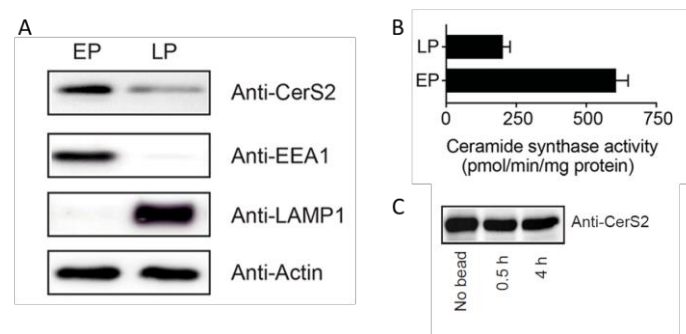
Figure 3.4. Characterization of CerS2 activity during phagosomal maturation. (A) Western blot analysis confirming the enrichment of CerS2 on EPs. As controls, EEA1 and LAMP1 were used to assess the purity of EP and LP preparations, respectively. In each case, 25 µg of lysate was loaded for all samples in this analysis, and actin was used as a loading control. The Western blot analysis was performed on eight biological replicates with reproducible results. (B) Ceramide synthase in vitro activity assay on EPs and LPs from RAW264.7 mouse macrophages, showing heightened ceramide synthase activity on EPs. (C) A control experiment to determine whether cellular CerS2 were altered in RAW264.7 cells when fed with beads, and concentrations of ceramides and CerS2 were measured by LC-MS/MS and western blot analysis respectively at 0.5 and 4 h post bead feeding (which represent time points of EP and LP maturation respectively). Based on these data, both these cellular levels are unaltered, suggesting that changes in ceramides and CerS2 are indeed EP and LP specific. The data in panel (A)and (B) represents mean ± s. e. m. for 4 biological replicates, while the data in panel (C) was performed in duplicate with reproducible results.
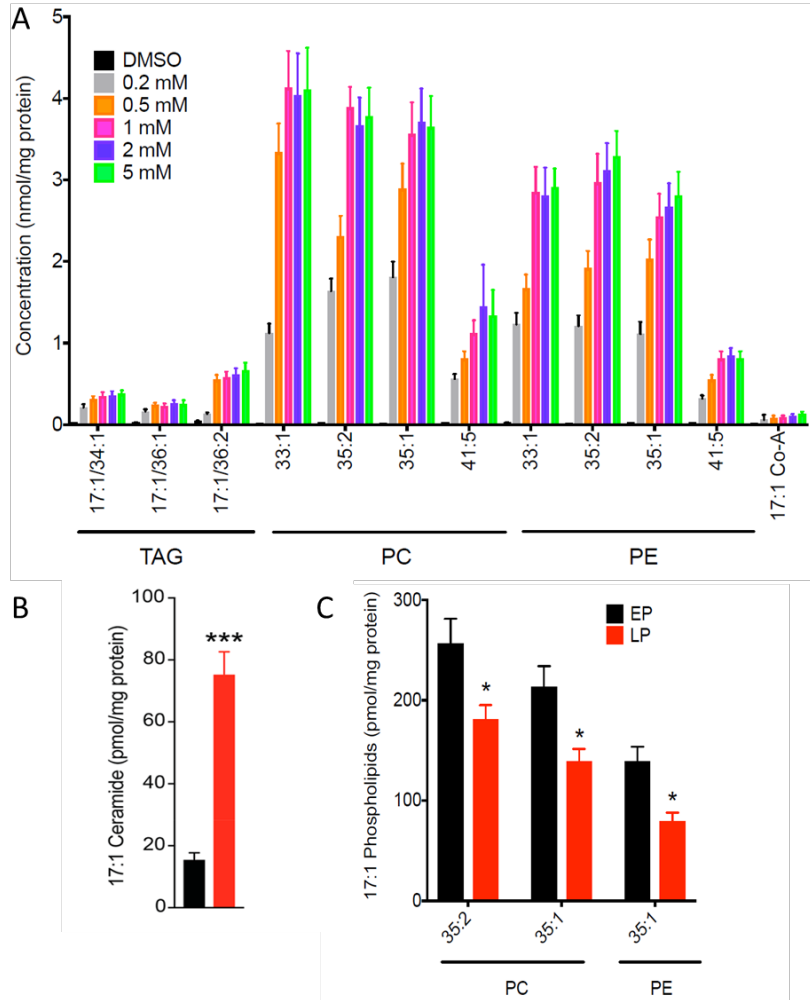
Figure 3.5. Incorporation of C17:1 FFA into cellular lipids. *(A) Concentrations of C17:1-containing storage lipids, namely triglycerides (TAG), phosphatidylcholines (PC), phosphatidylethanolamines (PE) and co-enzyme A (Co-A) from RAW264.7 mouse macrophages, following feeding varied concentrations of C17:1 FFA (0 – 5 mM, 4 h). Data shows that the C17:1 FFA is predominantly incorporated into cellular PC and PE lipids. Data represents mean ± s. e. m. for 4 biological replicates per group. Since there was no significant change beyond feeding 1 mM C17:1 FFA, hence this concentration was chosen for the feeding experiments. (B) Levels of C17:1 containing ceramide on EPs and LPs, following feeding of RAW264.7 mouse macrophages with 1 mM C17:1 FFA (4 h, 37 °C). Data represent mean ± SEM for five biological replicates. ***P < 0.001 for LP group versus EP group by Student's t test. (C) Phospholipid concentrations of EPs and LPs following C17:1 FFA feeding to RAW264.7 mouse macrophages. Quantitative lipidomics measurements of C17:1-containing PC and PE lipids showing changes in absolute levels between EPs and LPs groups. Data*

Next, I fed RAW264.7 cells with the unnatural long chain fatty acid, heptadecenoic acid (C17:1 FFA, 1 mM, 4 h), and found that the C17:1 FFA was mostly incorporated into cellular PC and PE pools in accordance with previously studies (Figure 3.5A) [97]. I then prepared EPs and LPs by feeding silica beads to cells containing C17:1- PC and PE from C17:1 FFA feeding. The lipids from the EPs and LPs derived from this experiments were enriched using previously described methods [61,67,86], and these lipids were subjected them to quantitative lipidomics, looking specifically for C17:1 containing lipids from different lipid classes (Table MS1). Consistent with previous lipidomics studies (Figure 3.1C), I found that the levels of C17:1-ceramide were significantly elevated on LPs (Figure 3.5B), and there was a concomitant decrease in levels of C17:1-containing PC and PE lipids on LPs (Table MS1, Figure 3.5C).

These results corroborate earlier lipidomics data (Figure 3.1C, E) and seem to suggest that PC and PE class of phospholipids on EPs likely serve as the fatty acid donor for the generation of fatty acyl-CoA that is eventually converted to ceramide by the *N*-acylation action of CerS2.
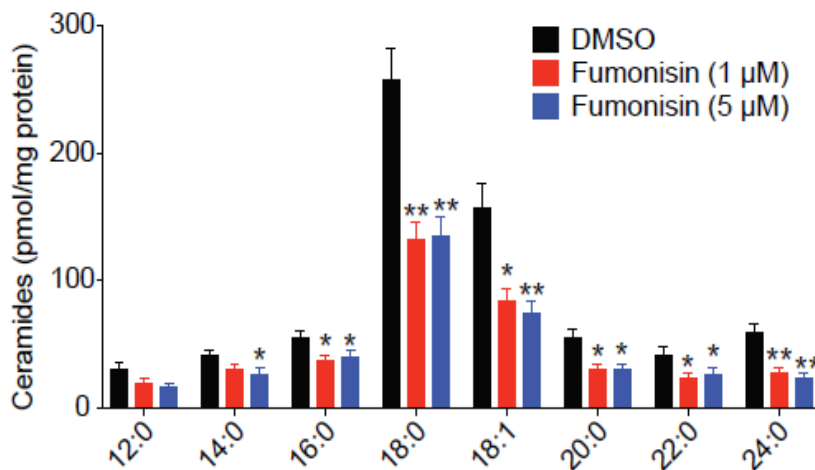
Figure 3.6. Pharmacological blockade of CerS2 by fumonisin in RAW264.7 mouse macrophages. Ceramide concentrations of RAW264.7 cells following treatment with fumonisin (1 or 5 μM) or DMSO (control) for 4 h. Data represent mean ± s. e. m. for 4 biological replicates per group. * P < 0.05 and ** P < 0.01 by Student's t-test for treatment groups versus DMSO control.

Effects of pharmacological blockadeof CerS2 on phagocytosis.

To validate whether fumonisin was pharmacologically active, and to verify the effects of inhibition of CerS2 in RAW264.7 cells, first, I treated RAW264.7 cells *in situ* with fumonisin (1 or 5 μM, 4 h). I found that following fumonisin treatment, ceramide formation was potently inhibited (Figure 3.6), without the cells getting activated or undergoing apoptosis (data not shown).

Next, I tested whether pharmacologically disrupting CerS2 had any effect on phagosomal ceramide content. Towards this, we allowed RAW264.7 cells to phagocytose silica beads for 15 mins so as to generate EPs. I then treated cells *in situ* with DMSO (LP-DMSO) or 5 μM fumonisin (LP-fumonisin) for 4 h, and harvested LPs at the end of this treatment using established protocols [80]. Lipids were extracted from each these phagosomal preparations, and subjected them to LC-MS/MS lipidomic analysis looking specifically at the concentration of phagosomal sphingolipids (Table MS1). I was able to recapitulate changes between the EP and LP-DMSO pools as seen previously, where VLC fatty acid containing ceramides and sphingosine increased and decreased respectively on phagosomes from the LP-DMSO group compared to the EP group (Figure 3.7).
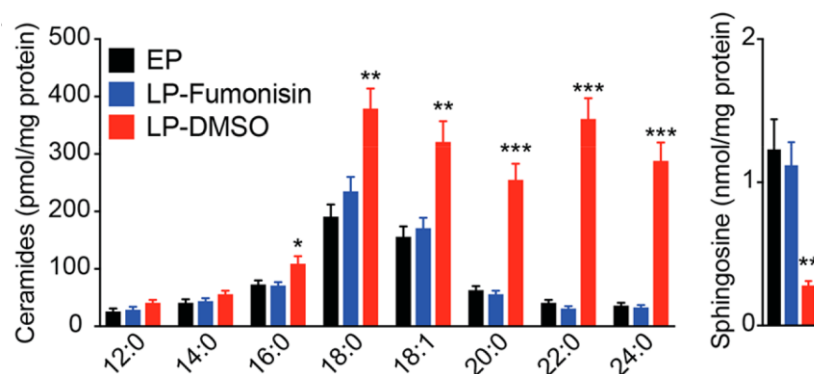
Figure 3.7. Lipidomics of Pharmacological blockade of CerS2 hampering phagosomal maturation. *Concentration of ceramides and sphingosine on LPs from RAW264.7 mouse macrophages following fumonisin treatment (LP-fumonisin, 5 μM, 4 h, 37 °C). As controls, EP and LP (LP-DMSO) were used. Data represent mean ± SEM for four biological replicates per group. **P < 0.01, ***P < 0.001 for experimental groups (LP-fumonisin and LP-DMSO) versus EP group by Student's t test.*

Thus far, no other sphingolipid changed in our study, suggesting that CerS2 is likely the major enzyme controlling the flux of sphingolipid metabolism during phagosomal maturation. Corroborating this, I found that the sphingolipid profiles for the phagosomes from the LP-fumonisin group, looked near identical to those from the EP group (Figure 3.7).

Having shown that pharmacologically inhibiting CerS2 by fumonisin treatment leads to the impairment of phagosomal ceramide synthesis, we wanted to determine whether this lipid profile change had any functional effect on phagosomal maturation. Towards this, Dr. Divya Pathak looked at the levels of CerS2, and known EP and LP markers, to determine, whether the pharmacological blockade of CerS2, indeed has any effect on phagosomal maturation. We found by western blot analysis, as seen previously, that CerS2 levels are lower on LPs (LP-DMSO group) than EPs, and the phagosomes from the LP-fumonisin group havenear EP levels of CerS2 (Figure 3.8). We also find that the EP protein marker, EEA1 is enriched on the phagosomal preparations from the EP group, and the LP-fumonisin group, but not on the LP-DMSO group (Figure 4B). Finally, we find that the LP protein markers, LAMP1 and Rab7, are enriched on the LPs (LP-DMSO group), but not on EPs. Interestingly, we find that the phagosomes from the LP-fumonisin group have significantly lesser amounts of both LAMP1 and Rab7 compared to the LP-DMSO group (Figure 3.8). Taken together, these results suggest that the pharmacological blockade of CerS2, results in partial blockade or delay in phagosomal maturation.
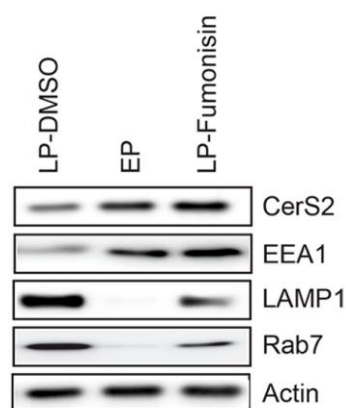
Figure 3.8. Phagosomal markers post pharmacological blockade of CerS2. *Western blot analysis confirming a defect in phagosomal maturation following inhibition of CerS2. In each case for each group, 30 µg of lysate was loaded for all samples in this analysis, and actin was also used as a loading control. The Western blot analysis was performed in triplicate with reproducible results. Credits: Dr. Divya Pathak*

Discussion

These findings taken together provide compelling evidence that mature phagosomes (LPs) are enriched with ceramides, especially VLC fatty acid containing ceramides, which are biosynthesized from sphingosine and fatty acyl-CoA by the action of CerS2, a major ceramide synthase, in mammalian macrophages (Figure 3.1, Figure 3.3).

I show that the pharmacological blockade of CerS2 results in depleting VLC fatty acid containing ceramide levels on LPs, thereby hampering phagosomal maturation, thus confirming the importance of CerS2 in the process. Interestingly and quite paradoxically, EPs have greater amounts and heightened activity of CerS2. The increased activity of CerS2 on EPs earlier appeared as an anticipatory mechanism for producing ceramides that eventually enriched on LPs. This suggests that, the regulation of ceramide on EPs/ LPs observed here seems to constitute a previously unknown biochemical pathway with respect to phagosomal maturation. Thus along with CerS2, there appears to be an involvement of other enzymes from the sphingolipid pathway partaking in the direct regulation of ceramide flux. (Further studied in the next chapter)

Additionally, from our data we speculate that the fatty acyl-CoA substrate for CerS2 is likely synthesized from PC and PE phospholipid present on EPs by unknown mechanisms (Figure 3.1C, E, Table MS1, Figure3.4, Figure 3.5 B, C).

Phagosomes accumulate cholesterol as they mature, possibly making their membranes more rigid, and making their transport within cells to lysosomes efficient [98]. *In vitro* studies from others, suggest that ceramide is critical for stabilizing lipid rafts, and making ordered rigid membrane microdomains [99]. Our current data along with studies from others suggests, that the increased ceramide on LPs is likely functioning to generate ordered lipid microdomains on maturing phagosomes, thus enabling the recruitment of appropriate proteins during the phagosome maturation process. Additionally, we believe that the membrane-associated dynein motors that drive phagosome transport towards lysosomes, may be able to generate force efficiently and in a more directed manner if the underlying sphingolipid (ceramide) rich membrane is rigid and more organized [83].

Projecting forward, the discovery of ceramide and CerS2 as a new player in phagosomal maturation suggests that an as-of-yet unknown sphingolipid metabolism pathway exists in mammalian phagosomal maturation (Figure 3.9).
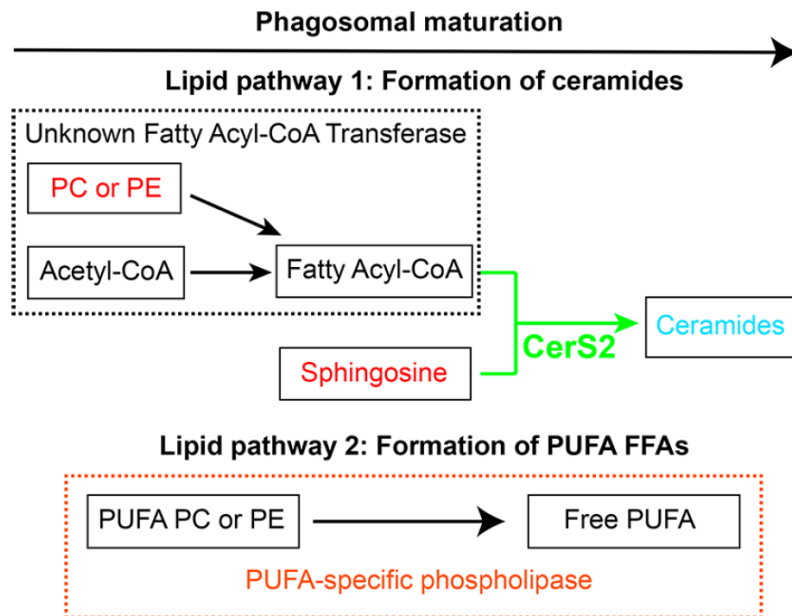
Figure 3.9. Schematic representation of putative lipid pathways in phagosomal maturation. *As phagosomes mature, their ceramide content increases due to the activity of CerS2, which is found enriched on EPs. Two other cryptic activities are postulated in this scheme based on our lipidomics results. The first, an unknown fatty acyl-CoA transferase, which converts PC and/or PE to generate fatty acyl-CoA, which is eventually converted to ceramide, by the N-acylation activity of CerS2. The second is a PUFA-specific phospholipase activity, which converts PUFA containing PC and/or PE lipids into free PUFAs that are found enriched on LPs.*

Unlike mammals, *Dictyostelium discoideum* possess only a single isoform of ceramide synthase, *crsA*, which shares ~30% sequence homology to the mammalian ceramide synthase isoforms with 100% conservation in the active site *Lag1P* motif (Figure 3.10) [87,91].

Our lipidomics studies on EPs and LPs (Figure 3.1, Table MS1) suggest that this evolutionary conserved enzyme might serve as a nodal point for heightened ceramide levels on LPs, and might in turn, be regulating phagosomal maturation even in primitive eukaryotes. We speculate that this sphingolipid pathway has another unannotated enzyme in mammals and primitive eukaryotes, a putative fatty acyl-CoA transferase that generates fatty acyl-CoA from PC and/or PE lipids (Figure 3.9). Additionally, our lipidomics data also suggests that there exists a

phospholipase, which prefers PUFA containing PC and/or PE phospholipids as substrates, and produces free PUFAs, that are found enriched on LPs (Figure 3.9, Table MS1). The discovery of these enzymes would certainly help in a greater understanding of phagosomal maturation, and provide new insights into the spatio-temporal regulation, cellular pathways crosstalk and interdependence of this very important immune response.

```
CERS1_MOUSE   127  FF-HDPPSVFYDWRSGMAVPWDIAVAYLLQGSFYCHSIYATVYMDSWRKD
CERS2_MOUSE   159  WF-YDLRKVWEGYPIQ-SIIPSQYWYYMIELSFYWSLL-FSIASDVKRKD
CERS3_MOUSE   158  WA-YDLWEVWNDYPRQ-PLLPSQYWYYILEMSFYWSLV-FSLSTDIKRKD
CERS4_MOUSE   159  WL-WSPSLCWENYPHQ-TLNLSLYWWYLLELGFYLSLL-ITLPFDVKRKD
CERS5_MOUSE   167  WF-WDTRQCWYNYPYQ-PLSRELYYYITQLAFYWSLM-FSQFIDVKRKD
CERS6_MOUSE   158  WL-WNTRHCWYNYPYQ-PLTADLHYYYILELSFYWSLM-VSQFTDIKRKD
Q54S87_DICDI  102  WSIFPTMNIWLGWPTQ-PFSTLFRTYYLIELSFYVHCT-IALFFETRRKD

CERS1_MOUSE   176  SVVMLVHHVVTLLLIASSYAFRYHNVGLLVFFLHDVSDVQLEFTKLNIYF
CERS2_MOUSE   206  FKEQIIHHVATIILLCFSWFANYVRAGTLIMALHDASDYLLESAKMFNYA
CERS3_MOUSE   205  FLAHVIHHLAAISLMSFSWCANYIRSGTLVMFIHDISDIWLESAKMFSYA
CERS4_MOUSE   206  FKEQVVHHFVAVGLIGFSYSVNLLRIGAVVLLLHDCSDYLLEGCKILNYA
CERS5_MOUSE   214  FLMMFIHHMIGIMLTTFSYVNNMVRVGALIFCLHDFADPLLEAAKMANYA
CERS6_MOUSE   205  FGIMFLHHLATIFLITFSYVNNMARVGTLVLCLHDSADALLEAAKMANYA
Q54S87_DICDI  150  FNQMLTHHVATFFLVGCSYWYRYHRIGIAILWIHNIADIFLYSAKALNYI

CERS1_MOUSE   226  K-------ARGGAYHRLHGLVANLGCLSFCFCWFWFRLYWFPLKVLYATC
CERS2_MOUSE   256  G-------WKN---------TCNNLFIVFAIVFIITRLVIMPFWILHCTM
CERS3_MOUSE   255  G-------WKQ---------TCNTLFFIFTVVFFISRFIIFPFWILYCTL
CERS4_MOUSE   256  H------FRR---------GCDALFIMFALVFFYTRLIFFPTQVIYTSV
CERS5_MOUSE   264  R-------RER---------LCTTLFVIFGAAFIVSRLAIFPLWILNTTL
CERS6_MOUSE   255  K------FQK---------MCDLLFVMFAVVFITTRLGIFPLWVLNTTL
Q54S87_DICDI  200  SKEVKNKTIQI---------ICDGLFVMFAVSFFVTRLIFFPFTLIKSSL
```

Figure 3.10. Sequence alignment of mammalian (mouse) ceramide synthase isoforms (CerS 1 – 6) with ceramide synthase from Dictyostelium discoideum (CrsA, Q54S87). *The residues highlighted in green represent the invariant catalytically important residues, while the residues underlined in red constitute the highly conserved Lag1P motif of ceramide synthase enzymes* [87,91].

Our findings open up several new questions such as the origin and mechanism of CerS2 localization on phagosomes, the effect of ceramide on lipid microdomains and resultant transport of phagosomes inside cells, and the possible synergistic requirement of cholesterol and ceramide (and other sphingolipids) for assembly of lipid rafts on a phagosome [83].

For the aforementioned study, I had not included glucosylceramides, the simplest glycosphingolipids. While the other sphingolipid classes remain unchanged, levels of glucosylceramides were seen to change during the process of maturation, the lipidomics and biochemistry of which have been described in the next chapter (chapter 4). Since they are

directly synthesized from ceramides, I performed further biochemical studies on ceramides and their metabolism which also have been described in chapter 4.

Conclusion

Global lipidomics analysis of maturaing phagosomes revealed that ceramides, along with cholesterol, get enriched on LPs. This increase of ceramide pools is brought about by the activity of CerS2, the pharmacological inhibition of which delayed phagosomal maturation. Interestingly, CerS2 accumulation and activity was observed to be higher on EPs than LPs. This seemingly counterintuitive finding has been clarified through further research on ceramide biochemistry in chapter 4.

CHAPTER IV
MAPPING SPHINGOLIPID METABOLISM
IN PHAGOSOMAL MATURATION

Introduction

Phagocytosis is an evolutionarily conserved immunological process, where solid particles $\geq$ 500 nm are engulfed by a class of cells called phagocytes [34,36,37,81]. In mammals (including humans), these phagocytes, typically macrophages or immune cells from the monocyte lineage, leverage the process of phagocytosis as a means of clearing detrimental solid particles (e.g. microbial and/or viral pathogens, or apoptotic cells) and are essential innate immune cells for fighting invading infections and/or clearing damaged cells to prevent tissue (organ) and/or systemic damage [36,81,100]. The detrimental solid particles that are engulfed and internalized by phagocytes are then enclosed tightly in membrane bound vesicles called phagosomes, and are subsequently transported to the lysosome for eventual degradation[36]. During phagocytosis, these phagosomes undergo a well-orchestrated sequence of events that are spatiotemporally regulated, whereby they "mature" from a nascent phagosome (also called early phagosome (EP)) to a late phagosome (LP) [36,37,78,79]. This LP then fuses with the lysosomal membrane to form the phagolysosome, and thus marks the end of the transport of the solid particles from the extracellular environment to the lysosome for degradation and/or detoxification [36,37]. During this maturation process, both the protein and lipid composition of the phagosomes change significantly through transient interactions with various sub-cellular components and their membranes. This process is popularly known now as the "kiss and run mechanism" [101,102], and these protein and lipid changes are thought to be critical in directing the maturing phagosome from the cellular periphery to the lysosome.

Several exhaustive shotgun proteomics studies have investigated the changes in the global protein content of phagosomes during the maturation process, and these have resulted in establishing protein markers that are hallmarks of various stages of maturation [103–106]. For example, the EP is enriched with Rab5 (a small GTPase from the Rab family) and the early endosome antigen 1 (EEA1), that together initiate the membrane formation for the engulfment of the foreign solid particle, while the LP is enriched with the GTPase Rab7 and the lysosomal associated membrane proteins 1 (LAMP1), both of which, are essential in directing the LP to the lysosome and facilitating its fusion to form the phagolysosome [105–107]. Interestingly, concomitant to the aforementioned protein changes, during maturation, the luminal pH within the phagosomes, progressively decreases from neutral ($\sim 7 - 7.5$) to acidic ($\sim 4.5 - 5$), and this drop in pH is thought to be mediated by the recruitment of vacuolar ATPases (vATPases) on LPs [79]. Contrary to the exhaustive proteomics studies, surprisingly, lipidomics studies have until recently been limited to only a single lipid class[108]. For example, it has been shown that

cholesterol is significantly enriched on LPs, and that physiologically, this accumulation of cholesterol is necessary to form stable lipid rafts that recruit dynein motors, which generate sufficient intracellular forces in facilitating the unidirectional motion of the ageing phagosomes (LPs) towards the lysosome [83].

An exhaustive comparative mass spectrometry based lipidomics analysis between EPs and LPs (described in chapter 3) revealed that along with cholesterol, certain sphingolipids also displayed differential enrichments on phagosomes across different stages of maturation [109]. Specifically, we found that ceramides, particularly those bearing very-long chain (VLC) lipids, were massively elevated on LPs, with a concomitant decrease in precursor sphingosine concentrations [109]. Upon further biochemical characterization of this sphingolipid pathway, we found that the enzyme ceramide synthase 2 (CerS2) [93,110] was responsible for orchestrating the enrichment of ceramides, specifically VLC lipid containing ceramides, on LPs. Interestingly, the pharmacological inhibition of CerS2 greatly reduced ceramide levels on LPs, and delayed the process of phagosomal maturation [109]. Given their complementary structure to cholesterol, ceramides are also thought to stabilize lipid rafts [99], and possibly make such lipid (micro)domains rigid enough for the efficient recruitment of important protein factors (e.g. GTPases, motor proteins), necessary to promote phagosomal maturation.

Ceramides are the central lynchpin in mammalian sphingolipid metabolism that flux reversibly into various modified sphingolipid species like the sphingomyelins, ceramide phosphates, and glucosylceramides by the action of dedicated biosynthetic and degradative enzymes [111–117] (Figure 4.1). Having shown the differential enrichment and importance of ceramides, particularly VLC lipid containing ceramides, during phagosomal maturation, and it's possible implications and/or involvement in the stabilization of lipid rafts, we were interested in quantitatively assessing the full complement of sphingolipids present on EPs and LPs, and mapping the possible biochemical (enzymatic) activities that might be contributing to the accumulation of different sphingolipids during various stages of phagocytosis. To address this, in this study, we show using biochemical enzymatic assays, that the ceramidase activity during phagosomal maturation also contributes significantly towards the accumulation of ceramides on LPs. Further using lipidomics measurements, we show that de novo ceramide biosynthesis contributes little to the flux of ceramides during phagocytosis, while glucosylceramides significantly increase on LPs. We validate this finding using biochemical assays, and show that heightened glucosylceramide synthase activity on LPs contributes to this sphingolipid change during phagocytosis. Our findings taken together provide a comprehensive picture of

sphingolipid metabolism during phagocytosis and establish new sphingolipid pathways that are likely to be important for phagosomal maturation and pathogen clearance.
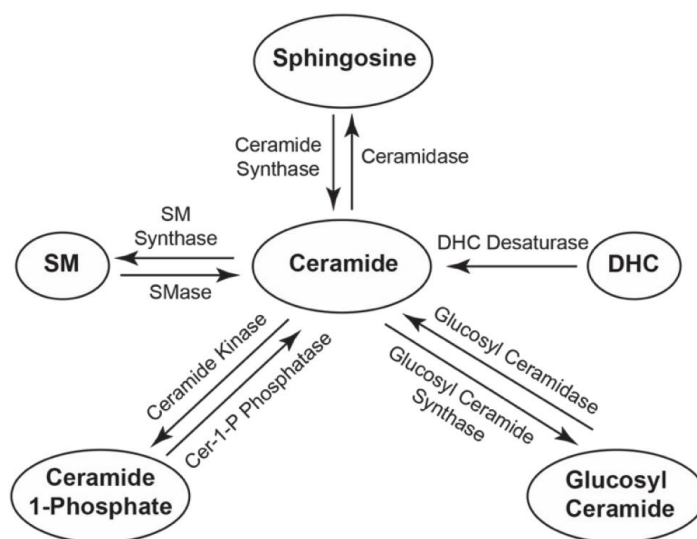
Figure 4.1. Schematic representation of the ceramide metabolism in mammalian cells. (SM = Sphingomyelin, DHC = Dihydroceramide, Cer-1-P = Ceramide 1-Phosphate)

Materials and methods

Materials. All chemicals, buffers, solvents, and reagents were purchased from Sigma-Aldrich, all tissue culture supplies were purchased from HiMedia, and all lipids and lipid standards were purchased from Avanti Polar Lipids. 1-μm silica microspheres (beads) were purchased from Polysciences (Cat. 24326-15) Preparation of phagosomes from RAW264.7 mouse macrophages. RAW264.7 macrophages were purchased from ATCC, and cultured in Dulbecco's Modified Eagle's Medium (DMEM) (HiMedia) containing 10% (v/v) Fetal Bovine Serum (FBS) (HiMedia) and 1% (v/v) Penicillin- Streptomycin (MP Biomedicals) at 37°C and 5% (v/v) CO2. For a single phagosomal preparation (biological replicate) for either EP or LP, 10 x 15 cm tissue culture plates (HiMedia) with RAW264.7 macrophages at 80% confluency were used, using standard protocols previously described earlier [83,109] .

Lipid extraction and LC-MS based targeted lipidomics. The lipid extractions from EPs or LPs were performed using a protocol reported earlier [109]. All the sphingolipid species described in this study were quantified by liquid chromatography coupled to mass spectrometry (LC-MS) using the established high-resolution multiple reaction monitoring (MRM-HR) method on a Sciex X500R QTOF mass spectrometer (MS) fitted with an Exion UHPLC system. All data

was collected and analysed using the SciexOS software. The LC separation, chromatographic solvents and MS parameters were identical to those reported by us previously [109,118,119]. A detailed list of all the sphingolipid species described by us in this MRM study, along with their precursor parent ion mass, the product ion mass and other MS parameters can be found in Table MS1. All the sphingolipid species were quantified by measuring the area under the curve relative to the respective quantitative internal standard, and then normalizing this ratio to the total protein content for the specific phagosomal preparation. All the lipidomics data for sphingolipids is represented as mean ± SEM from 3 (or more) biological replicates per experimental group or biological replicate.

Biochemical enzyme assays. To measure the specific activities of the putative enzymes involved in sphingolipid metabolism, purified EPs or LPs were washed twice with phosphate buffered saline (PBS) and re-suspended in 0.2 M sucrose solution to yield a final protein concentration of 1 mg/mL. The biochemical assays were performed at pH 4.5 and pH 7, by using sodium acetate buffer and PBS respectively. Heat denatured proteomes of EPs and LPs and substrate-only reactions (only substrate, no phagosomal proteome added) were used as controls for all biochemical enzymatic assays to account for the non-enzymatic rate of reactions. All enzymatic assays were performed in a final volume of 100 μL at 37 °C with constant shaking, using 25 μg of EP or LP proteome, and quenched at the desired time point by adding 500 μl of LC-MS grade methanol. The ceramidase assay was performed as described in literature [120] at pH 4.5 and pH 7 using C18:1 ceramide as a substrate at a final concentration of 20 μM, with an assay time of 3 hours. The concentration of sphingosine released from C18:1 ceramide in this LC-MS based ceramidase assay was obtained by measuring the area under the curve for sphingosine relative to an unnatural internal standard of sphingosine (C17:1 sphingosine, 100 pmol) used in the assay, by an established MRM-HR based LC-MS protocol previously reported by us1. The specific rate of the ceramidase activity was obtained by normalizing the concentration of sphingosine released from C18:1 ceramide to the assay time and the amount of protein used. The glucosylceramidase assay was performed as described in literature [121] at pH 4.5 and pH 7 using C17:0 glucosylceramide as a substrate at a final concentration of 20 μM, with an assay time of 2 hours. The concentration of C17:0 glucosylceramide consumed in this LC-MS based glucosylceramidase assay was obtained by measuring the area under the curve for C17:0 glucosylceramide in the enzymatic assay relative to the controls (heat denatured proteomes and substrate only reaction) used in the assay, by an established MRM-HR based LC-MS protocol described in this study (see Table MS1). The

specific rate of the glucosylceramidase activity was obtained by normalizing the consumed C17:0 glucosylceramide concentration to the assay time and the amount of protein used. The glucosylceramide synthase assay was performed as described in literature [122] at pH 4.5 and pH 7 using C18:1 ceramide and UDP-glucose as substrates at a final concentrations of 100 and 250 μM respectively, with an assay time of 2 hours. The concentration of the product i.e. C18:1 glucosylceramide formed from the substrates in this LC-MS based glucosylceramide synthase assay was obtained by measuring the area under the curve of C18:1 glucosylceramide relative to an unnatural internal standard of sphingosine (C17:0 glucosylceramide, 100 pmol) used in the assay, by an established MRM-HR based LC-MS protocol described in this study (see Table MS1). The specific rate of the glucosylceramide synthase activity was obtained by normalizing the concentration of C18:1 glucosylceramide produced from the substrates to the assay time and the amount of protein used. To prevent ceramide degradation in this glucosylceramide synthase assay, the ceramidase inhibitor Ceranib-2 was added to the buffers at a final concentration of 2 μM. Additionally, 500 mM MgCl2, 500 mM MnCl2 and 1 M EDTA were also added to the assay as cofactors (and/or adjuvants) for UDP-glucose.

Targeted proteomics. Using established protocols reported by us [118,123], 50 μg of EP or LP proteome was denatured, reductively alkylated and digested to yield peptides using MS grade trypsin (Promega). The peptides were subsequently cleaned using STAGE tip protocol [124], and subjected to LC-MS analysis on a TripleTOF 6600 mass spectrometer (Sciex) fitted with an Eksigent nanoLC 425 (Sciex). The LC separation columns, chromatographic solvents, gradients and MS parameters were identical to those reported by us previously [118,123]. For a developing targeted proteomics platform for quantitatively assessing the candidate enzymes involved in sphingolipid metabolism, we decided to use the LC-MS based MRM-HR analysis, and the target peptide sequences of candidate enzymes involved in sphingolipid metabolism were selected based on theoretical peptide predictions by using Skyline [125] and other publicly available data repositories (e.g. NCBI), taking into account several selection criteria that have been previously reported for such type of targeted LC-MS based assays [126–128]. In general, the full tryptic peptides without any missed cleavages, ranging from 8 – 25 amino acids in length were shortlisted, and post-translational or artificial static modifications were excluded, while developing the targeted LC-MS based MRM-HR assays. Peptide detectability of candidate enzymes involved in sphingolipid metabolism was searched across several databases including SRMAtlas and PeptideAtlas, and other publicly available online repositories of identified peptides that have been previously observed in LC-MS analyses [129–131]. A final list of all the

peptides for the candidate enzymes involved in sphingolipid metabolism quantitatively assessed in this study, describing the precursor parent ion mass and the product ion targeted can be found in Table MS2.

Data plotting and statistical analysis. All data in this study was plotted and statistically analysed using the Prism 9 (version 9.1.0) software for MacOS (GraphPad). All chemical structures were made using the ChemDraw 19.0 software (Perkin Elmer). The Student's two-tailed unpaired parametric t-test was used to determine the statistical significance between various experimental groups, and a p-value < 0.05 was considered significant in this study.

Results

Early phagosomes have higher ceramidase activity.

I have previously shown that the ceramide synthase activity (Figure 4.2A) is higher on EPs, but unexpectedly, ceramide concentrations are significantly lower on EPs compared to LPs [109]. This was at the time, attributed by us, to an anticipatory function of CerS2, where ceramides, (particularly VLC containing ceramides) are biosynthesized on EPs, but are eventually found on LPs. Following up on this finding, we also decided to investigate whether counter to the CerS2 (ceramide synthesis) activity, there exists any ceramidase (ceramide degradation) activity (Figure 4.2A) and if so, how does this ceramidase activity change as a function of phagosomal maturation. In mammals, there are three types of ceramidases [132,133], namely the acid ceramidase (ASAH1), the neutral ceramidase (ASAH2), and the alkaline ceramidase (ACER1-3), whose activity, as their names suggest, is pH dependent. Since previous studies on phagosomal maturation, have shown that luminal pH of EPs and LPs is neutral and acidic respectively, I decided to perform the ceramidase assays at neutral and acidic pH. For the EP, I found that the specific ceramidase activity at neutral pH (31.9 ± 2.4 pmol/mg/min) was significantly higher (~ 6-fold) than that observed at an acidic pH (5.2 ± 1.2 pmol/mg/min), while for the LP, the specific ceramidase activities at both neutral (10.0 ± 1.0 pmol/mg/min) and acidic pH (7.9 ± 1.7 pmol/mg/min) were comparable (Figure 4.2B). Given their luminal pH values based on available literature, I found that specific ceramidase activity for EP at a neutral pH was significantly higher (~ 4-fold) than that of the LP at an acidic pH (Figure 4.2B, 2C). On a similar note, I also assessed the ceramide synthase arising from CerS2 on EPs and LPs, and found consistent with our previous studies[109], that EP had significantly higher (~ 2.5-fold) ceramide synthase activity than LPs (Figure 4.2C). Interestingly, I found that the relative

to LPs, EPs had relatively higher ceramidase activity (~ 4-fold) compared to the CerS2 mediated ceramide synthase activity (~ 2.5-fold) (Figure 4.2C).
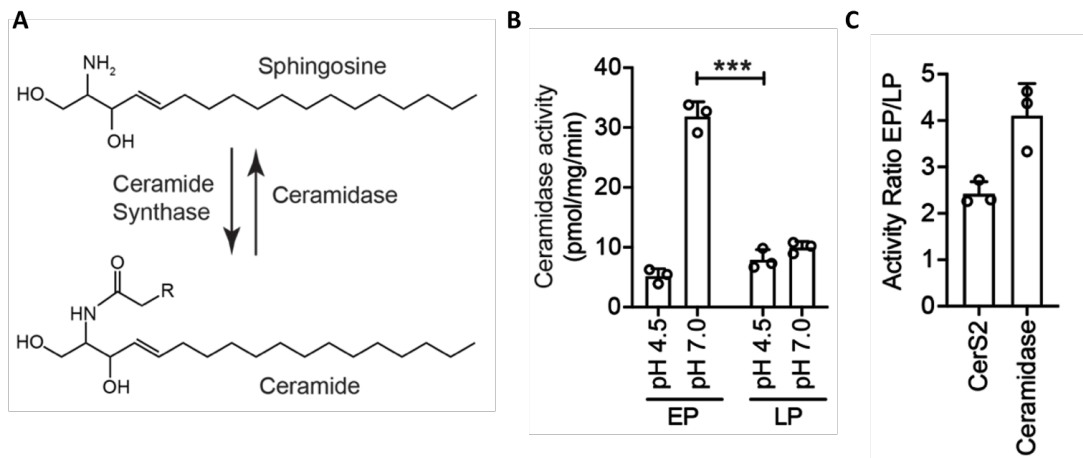
Figure 4.2. The ceramidase activity during phagosomal maturation. *(A) The biochemical reaction catalyzed by the enzymes ceramide synthase and ceramidase. (B) The specific ceramidase activity of EPs and LPs at neutral (pH 7) and acidic (pH 4.5) conditions. (C) Relative levels of ceramide synthase (from CerS2) and ceramidase activities on EP versus LP. For (B) and (C), the bar plots represent data as mean ± standard deviation from three biological replicates per experimental group. ***p < 0.001 by Student's t-test for the two groups compared.*

In a quest to find whether ASAH1 and/or ASAH2 were differentially present on EPs and LPs, I screened several commercially antibodies for both enzymes, and unfortunately, found that none of them were selective enough to robustly report on the abundance of either protein. Hence, I decided to investigate the levels of ASAH1 and ASAH2 on EP and LP by a targeted proteomics approach using tryptic peptide preparations previously reported earlier [118,123,134]. From this LC-MS based proteomics experiment, I found that consistent with its luminal pH, as expected, relative to a control protein (β-actin) [109], LPs had significantly more ASAH1, while EPs had increased levels of ASAH2 (Figure 4.3). Finally, I also screened for both the alkaline ceramidase activity at pH 10, and the enzymes associated with this activity i.e. ACER1-3, and was unable to detect either in my assays. Taken together, from all these assays, the results show that while both the EP and LP possess ceramidase activity, this enzymatic activity, particularly the neutral ceramidase activity compared to LPs, is significantly higher on EPs.
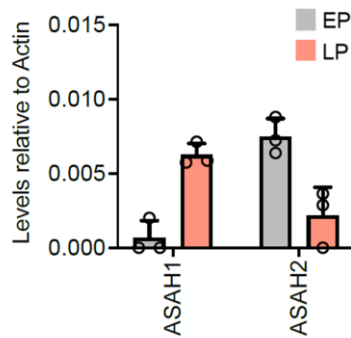
Figure 4.3. Relative protein levels of the ceramidases ASAH1 and ASAH2 on EP versus LP as determined by targeted proteomics relative to the control protein. *The bar plots represent data as mean ± standard deviation from three biological replicates per experimental group, where the grey bars represent data from EP preparations, while the red bars represent data from LP preparations.*

Dihydroceramide levels remain unchanged during phagosomal maturation. In mammals, ceramide is biosynthesized from dihydroceramide (DHC) by the action of the enzyme DHC saturase [112,135,136] (Figure 4.1), and I wanted to determine if this de novo biosynthetic pathway contributes to the increased ceramide levels that we observe on LPs. I had not measured this sphingolipid class in earlier investigations, and using reported LCMS based MRM methods, I quantified DHCs on EPs and LPs. From this LC-MS based lipidomics experiment, I found that I could reliably measure several DHC species, and that there was no notable change in their concentrations on EPs and LPs (Figure 4.4). These results therefore suggest that phagosomes likely obtain DHC from various cellular membranes that they make contacts with during the maturation process, and that de novo biosynthesis of ceramide is not a major pathway that contributes to increased ceramide concentration on LPs.
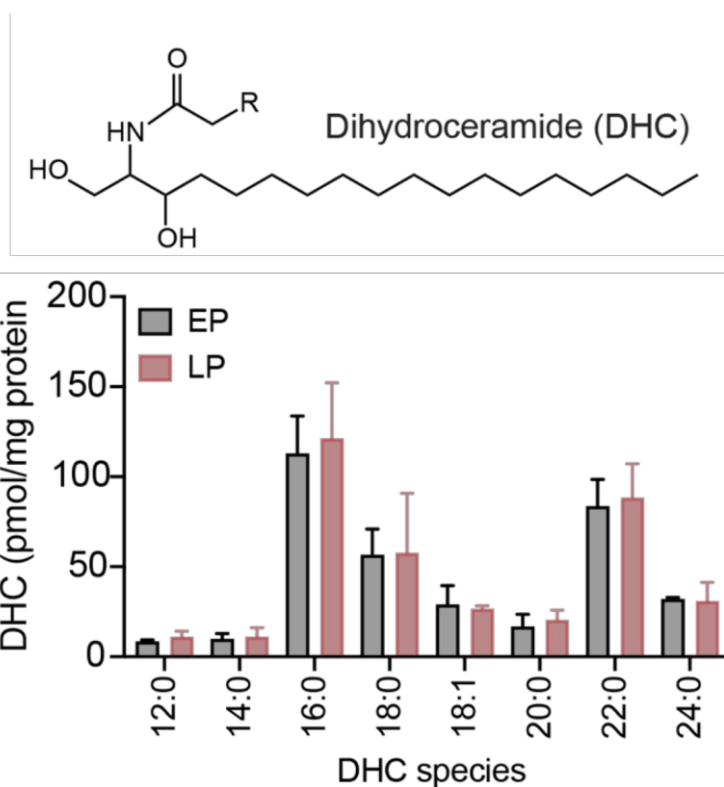
Figure 4.4. DHC levels on EPs and LPs. *The bar plots represent data as mean □ standard deviation from three biological replicates per experimental group.*

Late phagosomes have higher levels of glucosylceramides.

As described earlier, during the metabolism of sphingolipids, ceramides flux into sphingomyelins, ceramide 1-phosphate and glucosylceramides by the action of dedicated enzymes [111–117] (Figure 4.1). Previously, I have measured levels of sphingomyelins and ceramide 1-phosphates on EP and LP preparations, finding no significant differences in the concentrations of sphingomyelins or ceramide 1-phosphates between EPs and LPs [109]. However, I had not measured the levels of glucosylceramides during phagosomal maturation, and given the increased ceramides on ageing phagosomes, I was interested in measuring glucosylceramides on EPs and LPs. I first decided to generate a MS/MS fragmentation map for the commercially available unnatural C17:0 glucosylceramide (Figure 4.5), towards developing a LC-MS based MRM-HR method for quantitatively measuring glucosylceramide levels on EPs and LPs. From this high-resolution LC-MS based MS/MS fragmentation study, I found that at a collision energy of 40 V in the positive ionization mode, C17:0 glucosylceramide ([M+H+]: m/z = 714.5878) formed 4 major fragments (Figure 4.5). Based

on the mass to charge (m/z) ratio of these MS/MS fragments, I was successfully able to annotate their chemical structures based on the chemical structure of the parent C17:0 glucosylceramide (Figure 4.5). Of note, from this MS/MS fragmentation map, we found the characteristic "Fragment O" ([M+H+]: m/z = 264.2685) [137,138] (Figure 4.5), that is a signature for all ceramide species, and used the fragmentation of the parent glucosylceramide m/z to this "Fragment O" as the MRM-HR transition (Table MS1) for the absolute quantification of glucosylceramides on EPs and LPs.
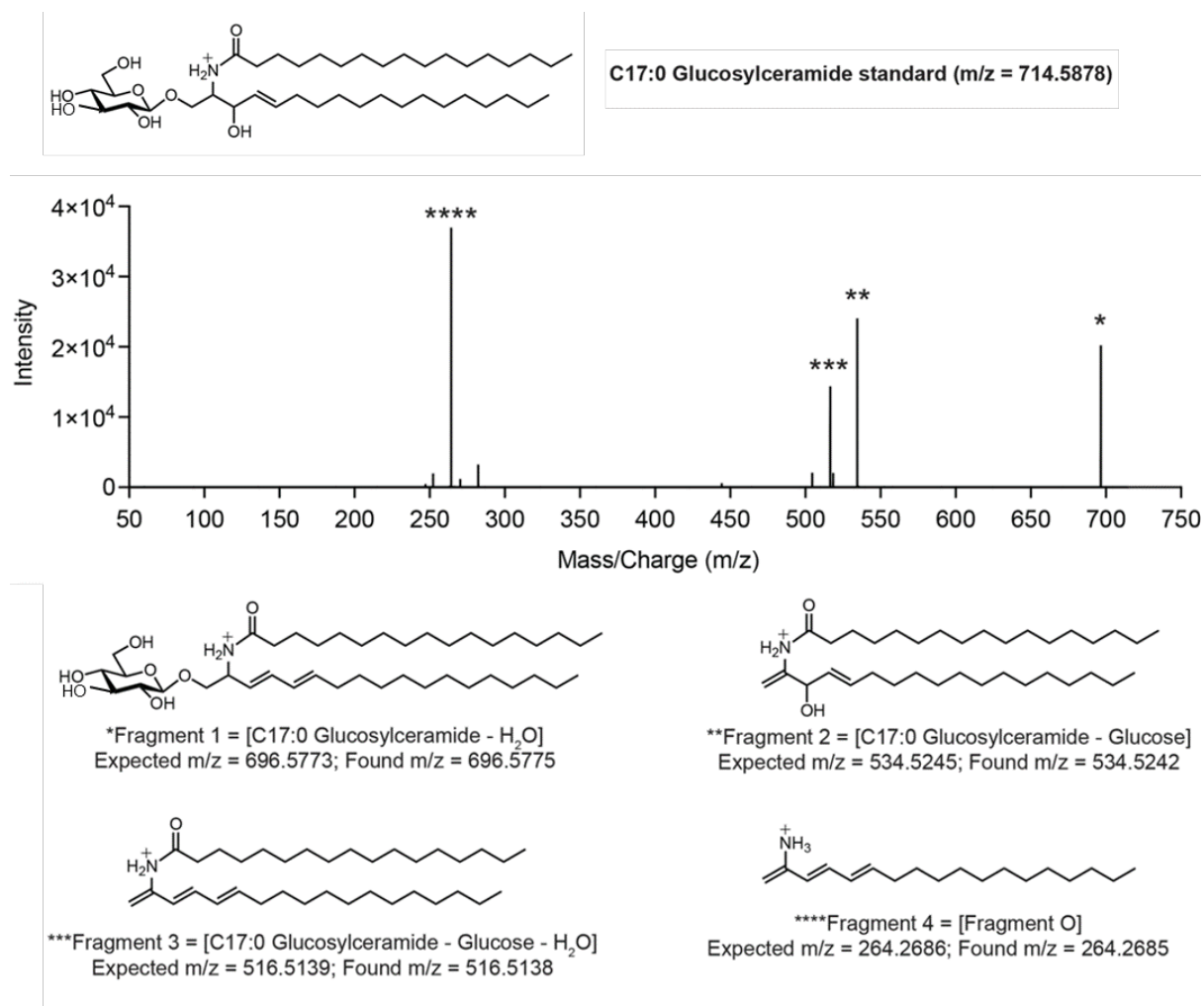
Figure 4.5. MS/MS fragmentation study for C17:0 glucosylceramide. *The four dominant daughter ions generated from the C17:0 glucosylceramide standard from the LC-MS based MS/MS study are marked with different asterisks and their chemical structures are described below the displayed MS/MS spectrum. This experiment was done thrice with reproducible results each time. Complete details of the MS parameters can be found in Table MS1.*

Leveraging established protocols [109,118,119], I extracted lipids from EP and LP preparations, and analyzed the glucosylceramide levels on them using the above described LC-MS based MRM-HR method for absolute quantitation of this class of sphingolipids. I found from this quantitative LC-MS analysis, that like ceramides, the glucosylceramides were significantly enriched on LPs (~ 5-fold) relative to EPs (Figure 4.6). I also found that while the magnitude of the fold-change (~ 5-fold) for the enrichment of the ceramides and glucosylceramides on LPs was similar (Figure 4.6), for a particular ceramide species (e.g. C24:0 ceramide), the concentration of the corresponding glucosylceramide (e.g. C24:0 glucosylceramide) was ~ 5-fold higher on both EP and LP, suggesting that glucosylceramide might indeed be the stable end sphingolipid product during phagosomal maturation. Interestingly, I also observed that, concomitant to VLC chain containing ceramides, VLC containing glucosylceramides were found to increase most profoundly (Figure 4.6), suggesting that these are likely biosynthesized from ceramide precursors on LPs.
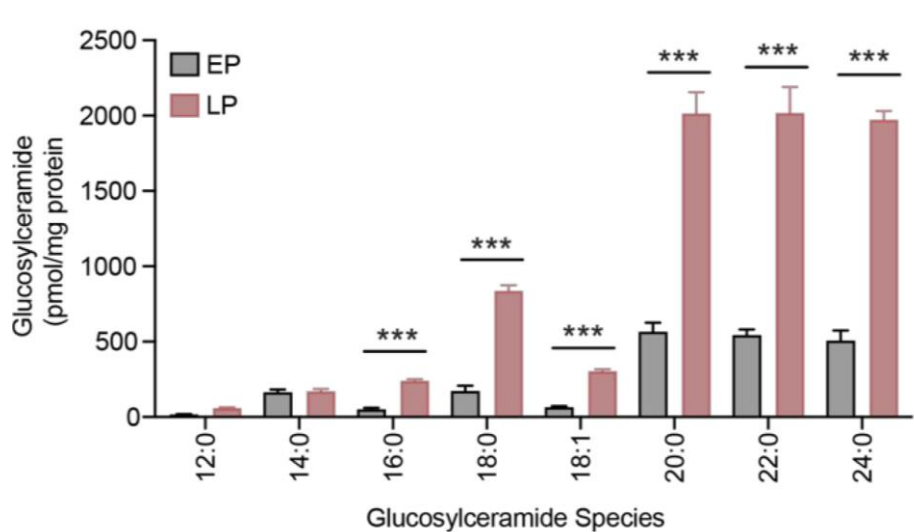
Figure 4.6. Glucosylceramide concentrations on EPs and LPs. *The bar plots represent data as mean ± standard deviation from three biological replicates per experimental group. ***p < 0.001 by Student's t-test for the two groups compared.*

Late phagosomes have higher glucosylceramide synthase activity. Intrigued by the enrichment of glucosylceramides on LPs during phagocytosis (Figure 4.6), I next wanted to assess if phagosomes also possess the enzymatic activities to make glucosylceramides (via glucosylceramide synthase) [139–141] and/or break glucosylceramides (via glucosylceramidase) [139 142,143] and if so, how do these biochemical activities change or enrich as a function of

phagosomal maturation (Figure 4.7A). Like the ceramidase assays, I decided to perform the glucosylceramide synthase and the glucosylceramidase activity assays at pH 4.5 and 7 on both EP and LP preparations. From these substrate assays, I found that relative to the glucosylceramide synthase activity, the glucosylceramidase activity was negligible (~ 40-fold lower) for both EPs and LPs (Figure 4.7B). Next, corroborating the increased glucosylceramide levels on LPs, I found that LP preparations (specific rate: 2.0 ± 0.3 nmol/mg/min at pH 4.5, and 2.2 ± 0.2 nmol/mg/min at pH 7) had significantly more (~ 4-fold) glucosylceramide synthase activity compared to EPs (specific rate: 0.5 ± 0.1 nmol/mg/min at pH 4.5, and 0.5 ± 0.1 nmol/mg/min at pH 7), and that pH did not have much effect on this activity (Figure 4.7B).

In mammals, the enzyme glucosylceramide synthase (GCS) is responsible for the biosynthesis of glucosylceramides [140,141], while the non-lysosomal glucosylceramidase (GBA2) [139,144,145] was likely involved in the degradation of glucosylceramides during phagosomal maturation, and I wanted to determine the relative levels of these enzymes on EPs and LPs. Like I did for the ceramidases, here, I also screened several commercially antibodies, and found again, that none of them were selective enough to robustly report on the abundance of either enzyme from phagosomal preparations. Hence, I again resorted to our targeted proteomics approach, and found from this LC-MS experiment, that consistent with the increased glucosylceramide synthase activity compared to EPs (Figure 4.7B), the protein levels of GCS were significantly higher on LPs (~ 5-fold), when normalized to the control protein β-actin (Figure 4.7C). From this LC-MS based targeted proteomics experiment, I also found that the protein levels of GBA2 did not significantly change between EP and LP preparations (Figure 4.7D), consistent with the glucosylceramidase activity profile observed by us (Figure 4.6B). Taken together, the results from the biochemical assays, and targeted proteomics experiments suggest that compared to EPs, LPs have greater amounts of the glucosylceramide synthase GCS, that makes glucosylceramides from ceramides using UDP-glucose as the glucose donor, and this activity eventually results in the heightened levels of glucosylceramides on LPs.
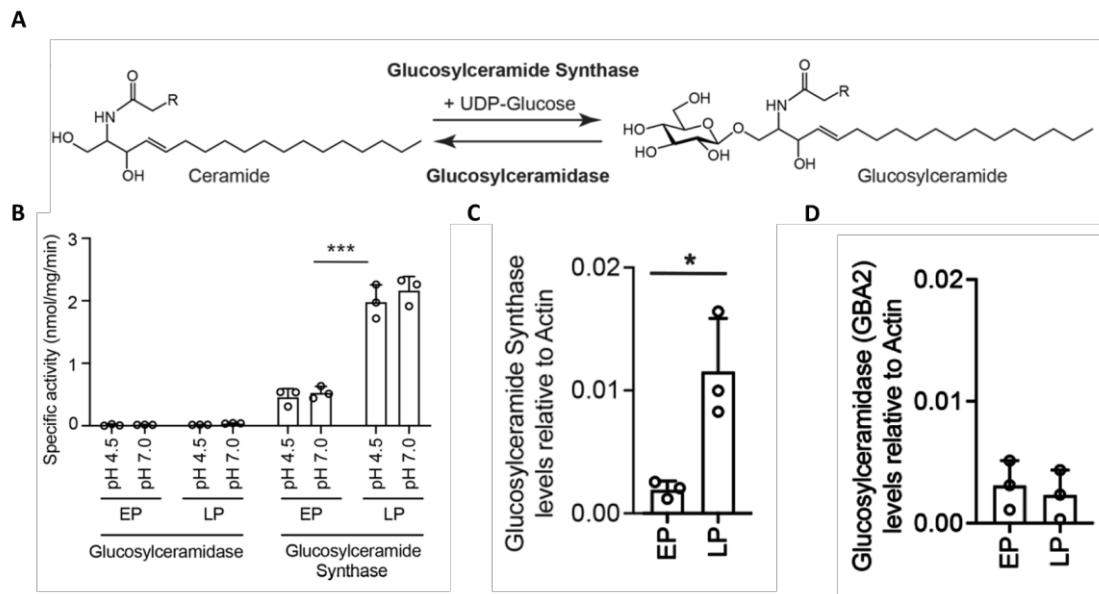
Figure 4.7. LPs have greater glucosylceramide synthase activity. (A) The biochemical reaction catalyzed by the enzymes glucosylceramide synthase and glucosylceramidase towards making and breaking glucosylceramides respectively. (B) The specific glucosylceramidase and glucosylceramide synthase activity of EPs and LPs at neutral (pH 7) and acidic (pH 4.5) conditions. (C, D) Relative protein levels of the enzymes (C) glucosylceramide synthase (GCS) and (D) glucosylceramidase (GBA2) on EP versus LP as determined by targeted proteomics relative to the control protein. For (B), (C) and (D), the bar plots represent data as mean ± standard deviation from three biological replicates per experimental group. *p < 0.05, and ***p < 0.001 by Student's t-test for the two groups compared.

Discussion

Sphingolipids are an essential class of lipids that regulate several important biological functions in all organisms [111]. In mammals, including humans, ceramide forms the central node of sphingolipid metabolism, and metabolically fluxes into various other sphingolipids (e.g. sphingomyelins, ceramide phosphates, glucosylceramides), by the action of dedicated enzymes [111–117] (Figure 4.1). Given its conical shape and ability to complementarily partition with cholesterol, ceramide has many important physiological functions in mammals, including humans. It facilitates the tighter packing membrane bilayers, stabilizes negative membrane curvatures and in doing so, imparts rigidity to other plastic cellular membrane bilayers[38,99,146–149]. Together with cholesterol, ceramides and its sphingolipid derivatives are also thought to form ordered lipid microdomains on membranes, called lipid rafts [99,146–151]. The formation of

these lipid rafts has important implications in phagocytosis, as these rigid membrane structures on LPs are where the dynein motor proteins have been shown to cluster, and collectively produce enough unidirectional force, to transport the maturing phagosome on the underlying cellular microtubule network towards the lysosome for eventual degradation [83]. Given the role of lipids in phagocytosis, my colleagues and I recently performed a rigorous comparative lipidomics analysis on EPs and LPs, and found that as phagosomes mature, concomitant to their increased cholesterol content, the concentration of ceramides, particularly VLC lipid containing ceramides, also significantly increases [109]. Upon further characterization, we found that this accumulation of ceramides on LPs was orchestrated by the enzyme CerS2, and the pharmacological inhibition of CerS2 by fumonisin (a general ceramide synthase inhibitor), resulted in hampered (and/or delayed) phagosomal maturation [109]. Interestingly, and paradoxically, I found from this study that even though the ceramides were enriched on LPs, the protein levels and enzymatic activity of CerS2 was more on EPs, and we attributed this to an anticipatory mechanism of CerS2, where by ceramides are found on LPs during the maturation process.

Following up on our lipidomics study, I first wanted to understand the biochemical basis for the accumulation of ceramides on LPs, and determine if there exists a physiological balance between ceramide synthase (CerS2) and ceramidase activities that eventually leads to the differential ceramide content as phagosomes mature. Using biochemical assays, I show that EPs have significantly more ceramidase activity compared to LPs (~ 4-fold) (Figure 4.2), and that the relative ceramidase activity on EPs is greater than the biosynthetic ceramidase synthase (CerS2) activity (Figure 4.2). Together, the data implies that even though biosynthesis of ceramides is greater on EPs, so is its degradation, and therefore an interplay between the ceramide synthase (CerS2) and ceramidase activities eventually result in increased ceramides on LPs. Though not commensurate with the magnitude of the changes seen in the activity assays, possibly because of reasons such as effect of posttranslational modifications of ASAH2 on activity, or the need for co-factors and/or cellular protein complexes for optimal enzymatic activity, we strongly think that the enrichment neutral ceramidase ASAH2 is possibly the key enzyme responsible for the degradation of ceramides on EPs (Figure 4.3).

I have previously shown that during phagosomal maturation, concentrations of sphingomyelins and ceramide 1-phosphates don't change [109], but I had not investigated other sphingolipids such as DHC or glucosylceramides during this process. I found from lipidomics experiments reported in this study that the levels of DHC do not change during phagosomal maturation

(Figure 4.4), and given the lack of DHC saturase activity (and presence of the enzyme), it appears that de novo ceramide synthesis via this biochemical route contributes little (if any) to the accumulation of ceramides of LPs. I could not find a reliable LC-MS MRM-HR method for quantitatively assessing glucosylceramides, and hence developed one for our studies (Figure 4.5). Performing quantitative lipidomics using this aforementioned method, I found that concomitant to ceramides, glucosylceramides increased profoundly on LPs (Figure 4.6). Interestingly, I found that VLC lipid containing glucosylceramides, exactly similar to their ceramide counterparts, most notably increased and were most abundant in terms of absolute concentrations on LPs (Figure 4.6), leading us to speculate that these glucosylceramides are possibly biosynthesized from precursor ceramides by the activity of GCS [140,141]. Indeed, using biochemical assays, and LC-MS based targeted proteomics approaches, I found that LPs had significantly more GCS activity and concentration of this enzyme compared to EPs, and that both EPs and LPs had negligible counter glucosylceramidase activities and the amounts of the corresponding enzyme, GBA2 (Figure 4.7). Even though the functions of glucosylceramides are not well understood in cell biology, like ceramides, they also form lipid rafts by partitioning with cholesterol and serve as stable and rigid platforms for localization of protein and even enrichment of receptors. Recent reports have suggested that glucosylceramides are essential for the localization and functioning of vATPases [152,153], and publicly available proteomics studies show that presence of vATPases on LPs [105,106]. Therefore, we think that the accumulation of glucosylceramides on LPs possibly results in the formation of rigid lipid rafts (together with cholesterol and ceramides), which facilitate the recruitment and localization of vATPases, that are eventually responsible for the hyperacidification of the phagosomes during the maturation process (Figure 4.8).
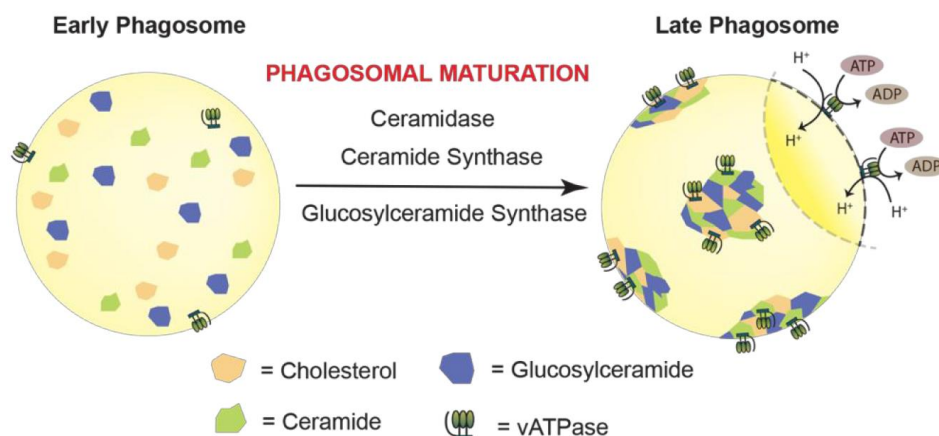
Figure 4.8. Model for sphingolipid changes during phagosomal maturation*. A summary of the sphingolipid changes during the maturation of phagosomes by the interplay of various enzymes that regulate their metabolism. As per the model, the formation of ordered lipid rafts (or microdomains) because of accumulation of ceramide and glucosylceramides along with cholesterol on LPs, causes the recruitment of vATPases, that acidify maturing phagosomes.*

Projecting ahead, the accumulation of glucosylceramides on ageing phagosomes opens up several new questions and research directions. For instance, it would be interesting to figure out, whether glucosylceramides (and perhaps even ceramides) are indeed needed for the formation of stable lipid rafts (microdomains) on LPs, and effects of depletion of this sphingolipid on the recruitment of important proteins that promote phagocytosis (e.g. dynein mediated unidirectional motion of LPs to lysosomes [83], or acidification by vATPases [153,154]). However, to the best of our knowledge, there are no specific inhibitors described in literature or available commercially for GCS, and to probe specific effects of glucosylceramides during phagocytosis (and other cellular processes), it would be beneficial to develop specific cell active GCS inhibitors and/or pharmacological tools (e.g. multifunctional glucosylceramide chemical probes) that besides lipidomics, might also enable complementary proteomics and cellular imaging studies. I also found from my studies that several commercially available antibodies for enzymes involved in the sphingolipid metabolism are not very specific and amenable to cellular studies. Therefore, along with pharmacological tools, the development of specific and high-quality antibodies for the enzymes involved in sphingolipid metabolism, particularly those discussed in this study, along with the lipids themselves (ceramides, glucosylceramides), would greatly facilitate cell biology studies, and expand our understanding of the spatiotemporal regulation of sphingolipids and their synergy with cholesterol during phagocytosis.

Conclusion

Through comparative lipidomics analysis between EPs and LPs, I showed that ceramides are enriched on the LPs by the activity of ceramide synthase 2. However, the rate of ceramide synthesis was higher on EPs. Following up on this study, using biochemical assays, I find that EPs also have increased ceramidase activity - that significantly contributes to the accumulation of ceramides on LPs. Lipidomics analysis revealed that de novo ceramide synthesis does not significantly contribute to the ceramide accumulation on LPs, while concomitant to increased ceramides, glucosylceramides are substantially elevated on LPs. I validated this interesting finding using biochemical assays, and show that LPs indeed have heightened glucosylceramide synthase activity. Taken together, these studies provide a comprehensive picture and possible new roles of sphingolipid metabolism during phagosomal maturation.

CHAPTER V
SUMMARY AND CONCLUSION

Lipid signaling is one of the cornerstones of cellular health. Lipids not only act as messengers for signals but also serve as structural platforms for cellular events. Dysregulated lipid metabolism has been associated with several metabolic diseases. This highlights the need for understanding the biochemistry underlying lipid metabolism.

Presence of oxidized phospholipids draws our attention to the idea that the membrane phospholipids act as a sink for damaging effects of ROS species. Whilst they have borne the brunt of oxidative damage, clearing them from cellular systems is necessary to prevent relaying the damage to other molecules. Thus far lipases capable of hydrolyzing oxidized phosphatidylcholines have been discovered, however, there were no reports describing oxidized PS hydrolyzing lipases. It was hypothesized that cells must have such lipase to hydrolyze oxidized PS, as oxidized PS can be misread as an untimely apoptotic signal.

Towards finding as oxidized PS lipase, firstly we wanted to induce oxidative stress into cells, thereby increasing the probability of detecting oxidized PS in cellular systems. This was to be followed by performing a chemical genetic screen with a library of serine hydrolase inhibitors, to fish out for the candidate lipases. I established a reproducible method to generate intracellular ROS with the help of a probe (MGR1), which specifically elevates ROS within cells. Building upon this, I sequentially inhibited serine hydrolases using the inhibitor library. The principle behind this screen was that, the inhibited candidate oxidized PS lipase will not hydrolyze the resultant elevation in oxidized PS levels, thereby giving us a phenotype of a more pronounced increase in levels of oxidized PS. From this chemical genetic screen, I was able to pick out a few candidate enzymes, of which my colleagues demonstrated ABHD12 to have a robust oxidized PS lipase activity. (Figure 5.1). This methodology described in my thesis could serve as an excellent strategy to expand our knowledge of more lipases able to hydrolyze oxidized lipids of other classes as well.

To further study lipid pathways in macrophages, I explored the biochemistry of sphingolipids in the process of phagosomal maturation, an important subset of phagocytosis. Phagocytes cast internalized particles as membrane bound organelles called phagosomes, which then fuse with lysosomes for hydrolyzing their cargo. The phagosomes have to mature from an early phagosome (EP) stage to a mature Late phagosome (LP) stage before this fusion. The process entails progressive luminal acidification among other changes. The proteomic changes augmenting the maturation process are better understood than the underlying lipidomic changes. Hence I perfomed targeted lipidomic analyses of maturing phagosomes and found

that cholesterol (as reported in litersture), along with ceramides are enriched on phagosomes with a concomitant decrease in sphingosine. This enrichment of ceramide was attributed to the activity of ceramide synthase 2, a necessary step during the maturation process. I further found that the flux of ceramides ias also controlled by the activity of pH dependant cermidases, thus an interplay between the activities of ceramide synthase 2 and (neutral) ceramidase resulted in and increased flux of ceramides on LPs. Furthermore, I found that the ceramides on LPs are fluxed into glucosylceramides by the activity of glucosylceramide synthase. The enrichment of cholesterol on LPs, and rafts formed by their clustering, serve as a platforms for attachment of dyenins for transport of the phagosome towards lysosomes. Cermamides are thought to stabilize such rafts, and thus their enrichment only supports their integrity. Glucosylceramides however have an unclear function in cells. They also have a propensity for forming rafts, with a few reports suggesting that these rafts help recruit vacuolar ATPase (vATPase). By connecting the dots, I put forth a previously unknown role for glucosylceramides in the process of phagosomal maturation, whereby glucosylceramide rafts help recruit vATPase to facilitate phagosomal luminal acidification. Thus, from my research, I find that sphingolipid metabolism is consequential over maturing phagosomes (Figure 5.1).
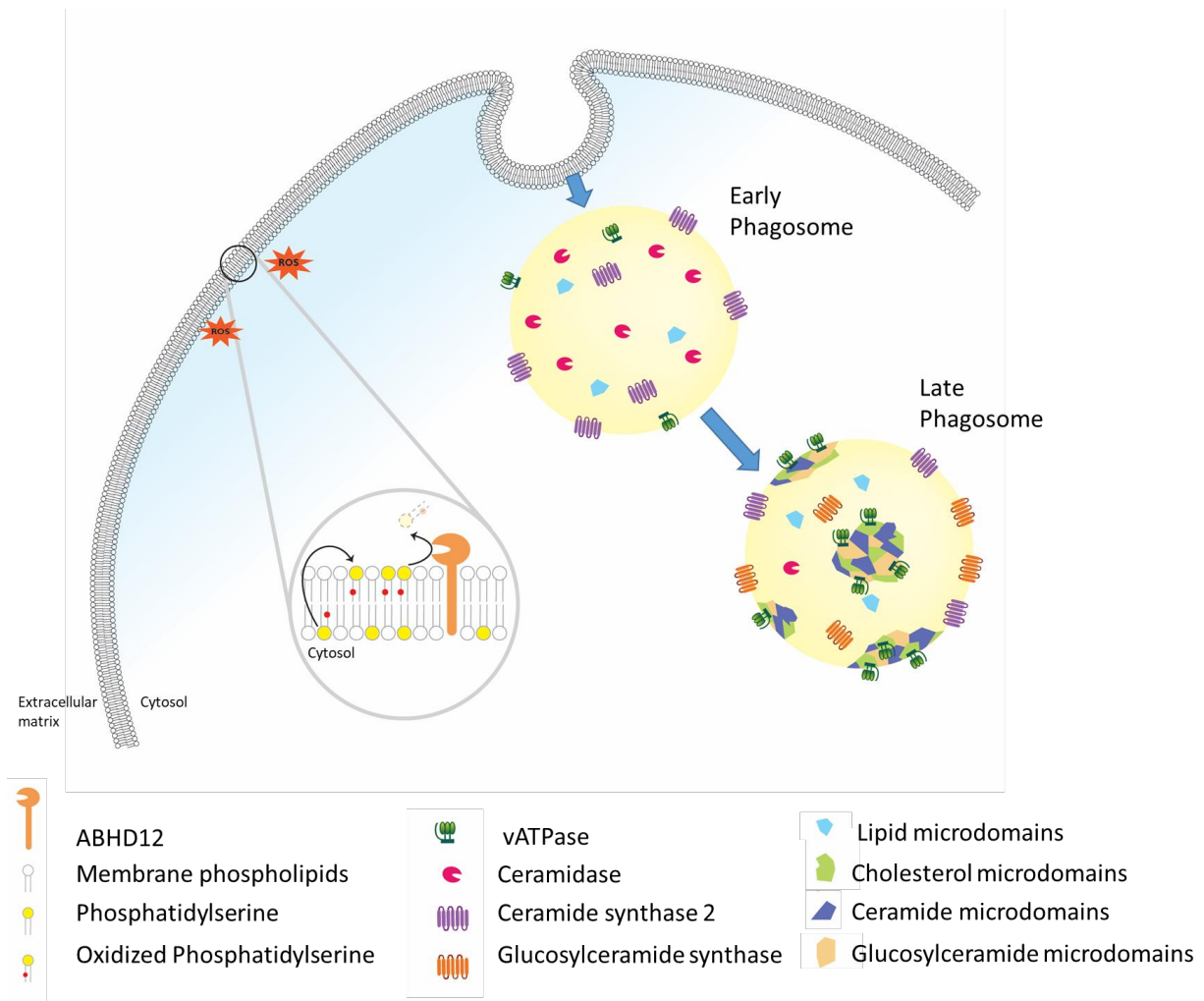
Figure 5.1. Graphical summary. *This figure is an illustration of the summary of my doctoral research on pathways of lipid metabolism in macrophages. I studied the metabolism of oxidized PS, and through a chemical genetic screen, was able to help identify the extracellularly oriented ABHD12 as a lipase capable of hydrolyzing it. Further, I studied the biochemistry of sphingolipids on maturing phagosomes and found that ceramides and glucosylceramides get enriched along the process along with cholesterol. This I was able to attribute to an interplay of the activities of ceramide synthase 2, (neutral) cermidase, and glucosylceramide synthase.*

TABLES FOR MASS SPECTROMETRY

Table 1: Quantification of oxidized PS in the chemical genetic screen. *The table shows oxidized PS levels of RAW264.7 cells treated with serine hydrolase inhibitors and control (highlighted in green) in presence of elevated ROS. The 'hit' compounds have been highlighted in yellow.*

Treatment	Compound (10 µM)	Probe (5 µM)	Relative oxidized PS levels		
			Mean	SEM	N
DMSO	–	–	0.23	0.04	12
DMSO	–	MGR2	0.24	0.03	3
DMSO	–	MGR1	1.00	0.09	15
–	Bromoenol lactone (BEL)	MGR1	0.71	0.05	3
–	JJH251	MGR1	0.71	0.03	3
–	JJH254	MGR1	0.71	0.02	3
–	AS115	MGR1	0.74	0.05	3
–	JW480	MGR1	0.75	0.11	3
–	ABC5	MGR1	0.75	0.09	3
–	WWL153	MGR1	0.76	0.03	3
–	KC02	MGR1	0.77	0.10	3
–	RHC80267	MGR1	0.78	0.08	3
–	ABC16	MGR1	0.79	0.09	3
–	ABC34	MGR1	0.79	0.06	3
–	ABC47	MGR1	0.79	0.17	3
–	JJH221	MGR1	0.81	0.14	3
–	WWL222	MGR1	0.81	0.07	3
–	JJH250	MGR1	0.82	0.12	3
–	ABC45	MGR1	0.82	0.05	3
–	XEN445	MGR1	0.85	0.02	3
–	PF7845	MGR1	0.85	0.01	3
–	DO34	MGR1	0.86	0.12	3

Treatment	Compound (10 μM)	Probe (5 μM)	Relative oxidized PS levels		
			Mean	SEM	N
–	WWL151	MGR1	0.86	0.13	3
–	JJH260	MGR1	0.86	0.07	3
–	KT195	MGR1	0.87	0.08	3
–	KC01	MGR1	0.87	0.07	3
–	WWL92	MGR1	0.89	0.07	3
–	Atglistatin	MGR1	0.90	0.05	3
–	Sitagliptin	MGR1	0.90	0.02	3
–	Palmostatin-M	MGR1	0.90	0.02	3
–	Pyrrophenone	MGR1	0.91	0.07	3
–	Emetine. HCl	MGR1	0.91	0.05	3
–	WWL113	MGR1	0.91	0.11	3
–	KT172	MGR1	0.91	0.14	3
–	KT109	MGR1	0.91	0.03	3
–	DO53	MGR1	0.92	0.18	3
–	JZL184	MGR1	0.92	0.09	3
–	ABC51	MGR1	0.93	0.06	3
–	GSK264220A	MGR1	0.94	0.07	3
–	trans-5c	MGR1	0.96	0.05	3
–	WWL229	MGR1	0.96	0.09	3
–	BAY	MGR1	0.98	0.08	3
–	P11	MGR1	0.98	0.05	3
–	MJN110	MGR1	1.00	0.07	3
–	Palmostatin-B	MGR1	1.01	0.07	3
–	URB597	MGR1	1.02	0.12	3
–	KLH40	MGR1	1.03	0.02	3
–	WWL70	MGR1	1.03	0.06	3
–	Ebdrup-3f	MGR1	1.05	0.06	3

Treatment	Compound (10 μM)	Probe (5 μM)	Relative oxidized PS levels		
			Mean	SEM	N
–	Cay10499	MGR1	1.05	0.03	3
–	KLH45b	MGR1	1.08	0.12	3
–	Cay10502	MGR1	1.09	0.04	3
–	ABL127	MGR1	1.09	0.21	3
–	Darapladib	MGR1	1.27	0.10	3
–	N-arachidonyl maleimide (NAM)	MGR1	1.36	0.06	3
–	Phenylmethylsulfonylfluoride (PMSF)	MGR1	1.39	0.07	3
–	JMN4	MGR1	1.55	0.18	3
–	Methylarachidonyl fluophosphonate (MAFP)	MGR1	**1.89**	**0.23**	**3**
–	Tetrahydrolipstatin (THL)	MGR1	**2.29**	**0.34**	**3**
–	FP-Alkyne	MGR1	**2.70**	**0.26**	**3**

Table MS1: Details for mass transitions for targeted lipidomics analyses. *Species denoted in red are unnatural internal standards used in quantitation of the respective lipid class*

Lipid Class	Species targeted	Accurate Exact masses	Accurate product ion mass	DP	EP	CE (V)	Collision Exit Potential	Ionization Mode	Adduct (if any)
Sterols	Cholesterol	404.3887	369.3516	50	10	15	15	Positive	$[M+NH_4]^+$
	Stigmasterol	430.4043	395.3672	50	10	15	15	Positive	$[M+NH_4]^+$
	Sitosterol	432.4200	397.3829	50	10	15	15	Positive	$[M+NH_4]^+$
	Cholesterol d7 (IS)	411.4326	376.3955	50	10	15	15	Positive	$[M+NH_4]^+$
Sphingolipids	Sphingosine	300.2897	282.2791	45	10	18	10	Positive	N/A
	Sphinganine	302.3054	284.2948	45	10	18	10	Positive	N/A
	17:1 Sphingosine (IS)	286.2741	268.2635	45	10	18	10	Positive	N/A
	Sphingosine 1-phosphate (S1P)	378.2415	78.9591	-90	-10	-60	-10	Negative	N/A
	17:1 S1P (IS)	364.2258	78.9591	-90	-10	-60	-10	Negative	N/A
Triacylglycerols (TAG)	16:0/32:0	824.7704	551.5034	150	10	35	10	Positive	$[M+NH_4]^+$
	16:0/34:1	850.7858	577.5190	150	10	35	10	Positive	$[M+NH_4]^+$
	16:0/34:0	852.8015	579.5347	150	10	35	10	Positive	$[M+NH_4]^+$
	16:0/36:2	876.8015	603.5347	150	10	35	10	Positive	$[M+NH_4]^+$
	16:0/36:1	878.8171	605.5503	150	10	35	10	Positive	$[M+NH_4]^+$
	16:0/36:0	880.8328	607.5660	150	10	35	10	Positive	$[M+NH_4]^+$
	16:0/36:4	872.7702	599.5034	150	10	35	10	Positive	$[M+NH_4]^+$
	16:0/38:4	900.8015	627.5347	150	10	35	10	Positive	$[M+NH_4]^+$
	18:0/32:0	852.8015	551.5034	150	10	35	10	Positive	$[M+NH_4]^+$
	18:0/34:1	878.8171	577.5190	150	10	35	10	Positive	$[M+NH_4]^+$
	18:0/34:0	880.8328	579.5347	150	10	35	10	Positive	$[M+NH_4]^+$
	18:0/36:2	904.8328	603.5347	150	10	35	10	Positive	$[M+NH_4]^+$
	18:0/36:1	906.8484	605.5503	150	10	35	10	Positive	$[M+NH_4]^+$
	18:0/36:0	908.8641	607.5660	150	10	35	10	Positive	$[M+NH_4]^+$
	18:0/36:4	900.8015	599.5034	150	10	35	10	Positive	$[M+NH_4]^+$
	18:0/38:4	928.8325	627.5344	150	10	35	10	Positive	$[M+NH_4]^+$
	18:1/32:0	850.7878	551.5054	150	10	35	10	Positive	$[M+NH_4]^+$
	18:1/34:1	876.8015	577.5191	150	10	35	10	Positive	$[M+NH_4]^+$
	18:1/34:0	878.8171	579.5347	150	10	35	10	Positive	$[M+NH_4]^+$
	18:1/36:2	902.8171	603.5347	150	10	35	10	Positive	$[M+NH_4]^+$
	18:1/36:1	904.8328	605.5504	150	10	35	10	Positive	$[M+NH_4]^+$
	18:1/36:0	906.8484	607.5660	150	10	35	10	Positive	$[M+NH_4]^+$
	18:1/36:4	898.7858	599.5034	150	10	35	10	Positive	$[M+NH_4]^+$
	18:1/38:4	926.8171	627.5347	150	10	35	10	Positive	$[M+NH_4]^+$
	18:2/34:2	872.7702	575.5035	150	10	35	10	Positive	$[M+NH_4]^+$
	17:0/34:1 (IS)	864.8015	577.5190	150	10	35	10	Positive	$[M+NH_4]^+$

Lipid Class	Species targeted	Accurate Exact masses	Accurate product ion mass	DP	EP	CE (V)	Collision Exit Potential	Ionization Mode	Adduct (if any)
Ceramides	16:0	538.5194	520.5088	180	10	20	10	Positive	N/A
	18:1	564.5350	546.5244	180	10	20	10	Positive	N/A
	18:0	566.5507	548.5401	180	10	20	10	Positive	N/A
	20:1	592.5633	574.5527	180	10	20	10	Positive	N/A
	20:4	586.5194	568.5088	180	10	20	10	Positive	N/A
	22:6	610.5194	592.5088	180	10	20	10	Positive	N/A
	25:0 (IS)	664.6602	646.6496	180	10	20	10	Positive	N/A
	16:0	538.5194	520.5088	180	10	20	10	Positive	N/A
	12:0	482.4568	464.3552	180	10	20	10	Positive	N/A
	14:0	510.4881	492.3865	180	10	20	10	Positive	N/A
	18:2	562.5194	544.4178	180	10	20	10	Positive	N/A
	20:0	594.5820	576.4804	180	10	20	10	Positive	N/A
	22:0	622.6133	604.5117	180	10	20	10	Positive	N/A
	22:1	620.5976	602.4960	180	10	20	10	Positive	N/A
	22:4	615.5507	597.4491	180	10	20	10	Positive	N/A
	24:0	650.6446	632.5430	180	10	20	10	Positive	N/A
	24:1	648.6289	630.5273	180	10	20	10	Positive	N/A
Sphingomyelins	12:0	647.5123	184.0733	150	10	55	12	Positive	N/A
	14:0	675.5436	184.0733	150	10	55	12	Positive	N/A
	18:2	727.5749	184.0733	150	10	55	12	Positive	N/A
	20:0	759.6375	184.0733	150	10	55	12	Positive	N/A
	22:0	787.6688	184.0733	150	10	55	12	Positive	N/A
	22:1	785.6531	184.0733	150	10	55	12	Positive	N/A
	22:4	779.6062	184.0733	150	10	55	12	Positive	N/A
	24:0	815.7001	184.0733	150	10	55	12	Positive	N/A
	24:1	813.6844	184.0733	150	10	55	12	Positive	N/A
	16:0	703.5749	184.0733	150	10	55	12	Positive	N/A
	18:1	729.5905	184.0733	150	10	55	12	Positive	N/A
	18:0	731.6062	184.0733	150	10	55	12	Positive	N/A
	20:1	757.6218	184.0733	150	10	55	12	Positive	N/A
	20:4	751.5749	184.0733	150	10	55	12	Positive	N/A
	22:6	775.5749	184.0733	150	10	55	12	Positive	N/A
	12:0 (IS)	647.5123	184.0733	150	10	55	12	Positive	N/A
Free fatty acids	16:0	255.2330	255.2330	-100	-10	-15	-10	Negative	N/A
	18:1	281.2486	281.2486	-100	-10	-15	-10	Negative	N/A
	18:0	283.2643	283.2643	-100	-10	-15	-10	Negative	N/A
	20:1	309.2799	309.2799	-100	-10	-15	-10	Negative	N/A
	20:4	303.2330	303.2330	-100	-10	-15	-10	Negative	N/A
	22:6	327.2330	327.2330	-100	-10	-15	-10	Negative	N/A
	17:1 (IS)	267.2330	267.2330	-100	-10	-15	-10	Negative	N/A
	12:0	199.1704	199.1704	-100	-10	-15	-10	Negative	N/A
	14:0	227.2017	227.2017	-100	-10	-15	-10	Negative	N/A
	18:2	279.2330	279.2330	-100	-10	-15	-10	Negative	N/A
	20:0	311.2956	311.2956	-100	-10	-15	-10	Negative	N/A
	22:0	339.3267	339.3267	-100	-10	-15	-10	Negative	N/A
	22:1	337.3112	337.3112	-100	-10	-15	-10	Negative	N/A
	22:4	331.2643	331.2643	-100	-10	-15	-10	Negative	N/A
	24:0	367.3582	367.3582	-100	-10	-15	-10	Negative	N/A

Lipid Class	Species targeted	Accurate Exact masses	Accurate product ion mass	DP	EP	CE (V)	Collision Exit Potential	Ionization Mode	Adduct (if any)
Free fatty acids	24:1	365.3425	365.3425	-100	-10	-15	-10	Negative	N/A
Monoacyl glycerols (MAG)	16:0	331.2843	239.2369	80	10	25	10	Positive	N/A
	18:1	357.2999	265.2526	80	10	25	10	Positive	N/A
	18:0	359.3156	267.2682	80	10	25	10	Positive	N/A
	20:1	385.3312	293.2839	80	10	25	10	Positive	N/A
	20:4	379.2843	287.2369	80	10	25	10	Positive	N/A
	22:6	403.2843	311.2369	80	10	25	10	Positive	N/A
	20:4 (d5-glycerol) IS	384.3157	287.2369	80	10	25	10	Positive	N/A
	12:0	275.2217	183.1810	80	10	25	10	Positive	N/A
	14:0	303.2530	211.2123	80	10	25	10	Positive	N/A
	18:2	355.2843	263.2436	80	10	25	10	Positive	N/A
	20:0	387.3469	295.3062	80	10	25	10	Positive	N/A
	22:0	415.3782	323.3375	80	10	25	10	Positive	N/A
	22:1	413.3625	321.3218	80	10	25	10	Positive	N/A
	22:4	407.3156	315.2749	80	10	25	10	Positive	N/A
	24:0	443.4095	351.3688	80	10	25	10	Positive	N/A
	24:1	441.3938	349.3531	80	10	25	10	Positive	N/A
Cholesterol esters	16:0	625.5918	369.3516	110	10	35	7	Positive	N/A
	18:1	651.6075	369.3516	110	10	35	7	Positive	N/A
	18:0	653.6231	369.3516	110	10	35	7	Positive	N/A
	20:1	679.6388	369.3516	110	10	35	7	Positive	N/A
	20:4	673.5918	369.3516	110	10	35	7	Positive	N/A
	22:6	697.5918	369.3516	110	10	35	7	Positive	N/A
	19:0 (IS)	667.6388	369.3516	110	10	35	7	Positive	N/A
	12:0	569.5292	369.3516	110	10	35	7	Positive	N/A
	14:0	597.5605	369.3516	110	10	35	7	Positive	N/A
	18:2	649.5918	369.3516	110	10	35	7	Positive	N/A
	20:0	681.6544	369.3516	110	10	35	7	Positive	N/A
	22:0	709.6857	369.3516	110	10	35	7	Positive	N/A
	22:1	707.6701	369.3516	110	10	35	7	Positive	N/A
	22:4	701.6231	369.3516	110	10	35	7	Positive	N/A
	24:0	737.7170	369.3516	110	10	35	7	Positive	N/A
	24:1	735.7014	369.3516	110	10	35	7	Positive	N/A
Ceramide 1-phosphates	16:0	616.4711	78.9591	-100	-10	-105	-12	Negative	N/A
	18:1	642.4868	78.9591	-100	-10	-105	-12	Negative	N/A
	18:0	644.5024	78.9591	-100	-10	-105	-12	Negative	N/A
	20:1	670.5181	78.9591	-100	-10	-105	-12	Negative	N/A
	20:4	664.4711	78.9591	-100	-10	-105	-12	Negative	N/A
	22:6	688.4711	78.9591	-100	-10	-105	-12	Negative	N/A
	12:0 (IS)	560.4085	78.9591	-100	-10	-105	-12	Negative	N/A

Lipid Class	Species targeted	Accurate Exact masses	Accurate product ion mass	DP	EP	CE (V)	Collision Exit Potential	Ionization Mode	Adduct (if any)
Ceramide 1-phosphates	12:0	560.4085	78.9591	-100	-10	-105	-12	Negative	N/A
	14:0	588.4398	78.9591	-100	-10	-105	-12	Negative	N/A
	18:2	640.4711	78.9591	-100	-10	-105	-12	Negative	N/A
	20:0	672.5337	78.9591	-100	-10	-105	-12	Negative	N/A
	22:0	700.5650	78.9591	-100	-10	-105	-12	Negative	N/A
	22:1	698.5494	78.9591	-100	-10	-105	-12	Negative	N/A
	22:4	692.5024	78.9591	-100	-10	-105	-12	Negative	N/A
	24:0	728.5963	78.9591	-100	-10	-105	-12	Negative	N/A
	24:1	726.5807	78.9591	-100	-10	-105	-12	Negative	N/A
Phosphatidylcholines (PC)	32:0	734.5694	184.0733	170	10	45	15	Positive	N/A
	32:1	732.5538	184.0733	170	10	45	15	Positive	N/A
	34:0	762.6007	184.0733	170	10	45	15	Positive	N/A
	34:1	760.5851	184.0733	170	10	45	15	Positive	N/A
	34:2	758.5694	184.0733	170	10	45	15	Positive	N/A
	36:0	790.6320	184.0733	170	10	45	15	Positive	N/A
	36:1	788.6164	184.0733	170	10	45	15	Positive	N/A
	36:2	786.6007	184.0733	170	10	45	15	Positive	N/A
	36:4	782.5684	184.0733	170	10	45	15	Positive	N/A
	38:4	810.6007	184.0733	170	10	45	15	Positive	N/A
	40:6	834.6007	184.0733	170	10	45	15	Positive	N/A
	37:4 (IS)	796.5851	184.0733	170	10	45	15	Positive	N/A
Phosphatidylethanolamine (PE)	32:0	692.5225	551.5034	150	10	50	10	Positive	N/A
	32:1	690.5068	549.4877	150	10	50	10	Positive	N/A
	34:0	720.5538	579.5347	150	10	50	10	Positive	N/A
	34:1	718.5381	577.5190	150	10	50	10	Positive	N/A
	34:2	716.5225	575.5034	150	10	50	10	Positive	N/A
	36:0	748.5851	607.5660	150	10	50	10	Positive	N/A
	36:1	746.5694	605.5503	150	10	50	10	Positive	N/A
	36:2	744.5538	603.5347	150	10	50	10	Positive	N/A
	36:4	740.5225	599.5034	150	10	50	10	Positive	N/A
	38:4	768.5538	627.5347	150	10	50	10	Positive	N/A
	40:6	792.5538	651.5347	150	10	50	10	Positive	N/A
	37:4 (IS)	754.5381	613.5190	150	10	50	10	Positive	N/A
Phosphatidic acid (PA)	32:0	647.4657	255.2330	-65	-10	-45	-10	Negative	N/A
	32:1	645.4501	255.2330	-65	-10	-45	-10	Negative	N/A
	34:0	675.4970	255.2330	-65	-10	-45	-10	Negative	N/A
	34:1	673.4814	255.2330	-65	-10	-45	-10	Negative	N/A
	34:2	671.4657	255.2330	-65	-10	-45	-10	Negative	N/A
	36:0	703.5283	283.2643	-65	-10	-45	-10	Negative	N/A
	36:1	701.5127	283.2643	-65	-10	-45	-10	Negative	N/A

Lipid Class	Species targeted	Accurate Exact masses	Accurate product ion mass	DP	EP	CE (V)	Collision Exit Potential	Ionization Mode	Adduct (if any)
Phosphatidic acid (PA)	36:2	699.4740	281.2486	-65	-10	-45	-10	Negative	N/A
	36:4	695.4657	255.2330	-65	-10	-45	-10	Negative	N/A
	38:4	723.4970	283.2643	-65	-10	-45	-10	Negative	N/A
	40:6	747.4970	283.2643	-65	-10	-45	-10	Negative	N/A
	37:4 (IS)	709.4814	269.2486	-65	-10	-45	-10	Negative	N/A
Phosphatidylglycerol (PG)	32:0	721.5025	255.2330	-120	-10	-50	-12	Negative	N/A
	32:1	719.4869	255.2330	-120	-10	-50	-12	Negative	N/A
	34:0	749.5338	255.2330	-120	-10	-50	-12	Negative	N/A
	34:1	747.5182	255.2330	-120	-10	-50	-12	Negative	N/A
	34:2	745.5025	255.2330	-120	-10	-50	-12	Negative	N/A
	36:0	777.5615	283.2643	-120	-10	-50	-12	Negative	N/A
	36:1	775.5495	283.2643	-120	-10	-50	-12	Negative	N/A
	36:2	773.5338	281.2486	-120	-10	-50	-12	Negative	N/A
	36:4	769.5025	255.2330	-120	-10	-50	-12	Negative	N/A
	38:4	797.5338	283.2643	-120	-10	-50	-12	Negative	N/A
	40:6	821.5338	283.2643	-120	-10	-50	-12	Negative	N/A
	37:4 (IS)	783.5182	269.2486	-120	-10	-50	-12	Negative	N/A
Phosphatidylserine (PS)	16:0/18:2	758.5	255.3	-120	-10	-52	-11	Negative	N/A
	16:0/ 18:1	760.5	255.3	-120	-10	-52	-11	Negative	N/A
	16:0/ 18:0	762.5	255.3	-120	-10	-52	-11	Negative	N/A
	16:0/20:4	782.5	255.3	-120	-10	-52	-11	Negative	N/A
	18:1/18:2	784.5	281.2	-120	-10	-52	-11	Negative	N/A
	18:1/ 18:1	786.5	281.3	-120	-10	-52	-11	Negative	N/A
	18:0/18:2	786.5	283.3	-120	-10	-52	-11	Negative	N/A
	18:0/ 18:1	788.5	283.3	-120	-10	-52	-11	Negative	N/A
	17:0/ 20:4 (Internal Standard) (1 nmol)	796.5	269.3	-120	-10	-52	-11	Negative	N/A
	16:0/22:6	806.5	255.3	-120	-10	-52	-11	Negative	N/A
	18:1/ 20:4	808.5	281.3	-120	-10	-52	-11	Negative	N/A
	18:0/ 20:4	810.5	283.3	-120	-10	-52	-11	Negative	N/A
	20:0/18:2	814.6	311.3	-120	-10	-52	-11	Negative	N/A
	18:1/ 20:1	814.6	281.3	-120	-10	-52	-11	Negative	N/A
	18:0/ 20:1	816.6	283.3	-120	-10	-52	-11	Negative	N/A
	18:1/ 20:0	816.6	281.3	-120	-10	-52	-11	Negative	N/A
	18:0/ 20:0	818.6	283.3	-120	-10	-52	-11	Negative	N/A
	18:1/ 22:6	832.8	281.3	-120	-10	-52	-11	Negative	N/A
	18:0/ 22:6	834.8	283.3	-120	-10	-52	-11	Negative	N/A
	20:1/ 20:4	836.6	309.3	-120	-10	-52	-11	Negative	N/A
	20:0/ 20:4	838.6	311.3	-120	-10	-52	-11	Negative	N/A
	18:0/ 22:4	838.6	283.3	-120	-10	-52	-11	Negative	N/A
	18:1/ 22:1	842.6	281.2	-120	-10	-52	-11	Negative	N/A
	18:0/ 22:1	844.6	283.3	-120	-10	-52	-11	Negative	N/A
	18:1/ 22:0	844.6	281.2	-120	-10	-52	-11	Negative	N/A
	18:0/ 22:0	846.6	283.3	-120	-10	-52	-11	Negative	N/A

Lipid Class	Species targeted	Accurate Exact masses	Accurate product ion mass	DP	EP	CE (V)	Collision Exit Potential	Ionization Mode	Adduct (if any)
Phosphatidylserine (PS)	20:1/ 22:6	860.8	309.3	-120	-10	-52	-11	Negative	N/A
	20:0/ 22:6	862.8	311.3	-120	-10	-52	-11	Negative	N/A
	22:1/ 20:4	864.6	337.3	-120	-10	-52	-11	Negative	N/A
	22:0/ 20:4	866.6	339.3	-120	-10	-52	-11	Negative	N/A
	18:1/ 24:1	870.6	281.3	-120	-10	-52	-11	Negative	N/A
	18:0/ 24:1	872.6	283.3	-120	-10	-52	-11	Negative	N/A
	18:1/ 24:0	872.6	281.2	-120	-10	-52	-11	Negative	N/A
	18:0/ 24:0	874.7	283.3	-120	-10	-52	-11	Negative	N/A
	22:0/ 22:6	888.8	339.3	-120	-10	-52	-11	Negative	N/A
	20:0/ 24:1	890.8	311.3	-120	-10	-52	-11	Negative	N/A
	24:1/ 20:4	892.6	365.3	-120	-10	-52	-11	Negative	N/A
	24:0/ 20:4	894.6	367.4	-120	-10	-52	-11	Negative	N/A
	20:1/ 24:1	898.7	309.3	-120	-10	-52	-11	Negative	N/A
	22:1/ 22:6	900.7	337.3	-120	-10	-52	-11	Negative	N/A
	20:0/ 24:1	900.7	311.3	-120	-10	-52	-11	Negative	N/A
	20:0/ 24:0	902.7	311.3	-120	-10	-52	-11	Negative	N/A
	24:1/ 22:6	916.9	365.3	-120	-10	-52	-11	Negative	N/A
	24:0/ 22:6	918.9	367.4	-120	-10	-52	-11	Negative	N/A
Oxidized Phophatidylserine **'hy'=hydroxy** **'ox'=epoxy**	hy-16:0/18:1	778.5	255.3	-95	-10	-40	-12	Negative	N/A
	hy-16:0/18:2	776.5	255.3	-95	-10	-40	-12	Negative	N/A
	hy-16:0/20:4	800.5	255.3	-95	-10	-40	-12	Negative	N/A
	hy-16:0/22:6	825.5	255.3	-95	-10	-40	-12	Negative	N/A
	hy-18:0/18:1	806.6	283.3	-95	-10	-40	-12	Negative	N/A
	hy-18:0/18:2	804.5	283.3	-95	-10	-40	-12	Negative	N/A
	hy-18:0/20:4	828.5	283.3	-95	-10	-40	-12	Negative	N/A
	hy-18:0/22:6	853.5	283.3	-95	-10	-40	-12	Negative	N/A
	hy-18:1/18:1	804.5	281.3	-95	-10	-40	-12	Negative	N/A
	hy-18:1/18:2	802.5	281.3	-95	-10	-40	-12	Negative	N/A
	hy-18:1/20:4	826.5	281.3	-95	-10	-40	-12	Negative	N/A
	hy-18:1/22:6	851.5	281.3	-95	-10	-40	-12	Negative	N/A
	hy-20:0/18:1	834.6	311.3	-95	-10	-40	-12	Negative	N/A
	hy-20:0/18:2	832.6	311.3	-95	-10	-40	-12	Negative	N/A
	hy-20:0/20:4	856.6	311.3	-95	-10	-40	-12	Negative	N/A
	hy-20:0/22:6	881.6	311.3	-95	-10	-40	-12	Negative	N/A
	ox-16:0/18:1	776.5	255.3	-95	-10	-40	-12	Negative	N/A
	ox-16:0/18:2	774.5	255.3	-95	-10	-40	-12	Negative	N/A
	ox-16:0/20:4	798.5	255.3	-95	-10	-40	-12	Negative	N/A
	ox-16:0/22:6	823.5	255.3	-95	-10	-40	-12	Negative	N/A
	ox-18:0/18:1	804.5	283.3	-95	-10	-40	-12	Negative	N/A
	ox-18:0/18:2	802.5	283.3	-95	-10	-40	-12	Negative	N/A
	ox-18:0/20:4	826.5	283.3	-95	-10	-40	-12	Negative	N/A
	ox-18:0/22:6	851.5	283.3	-95	-10	-40	-12	Negative	N/A
	ox-18:1/18:1	802.5	281.3	-95	-10	-40	-12	Negative	N/A
	ox-18:1/18:2	800.5	281.3	-95	-10	-40	-12	Negative	N/A
	ox-18:1/20:4	824.5	281.3	-95	-10	-40	-12	Negative	N/A

Lipid Class	Species targeted	Accurate Exact masses	Accurate product ion mass	DP	EP	CE (V)	Collision Exit Potential	Ionization Mode	Adduct (if any)
Oxidized Phophatidylserine 'hy'=hydroxy 'ox'=epoxy	ox-18:1/22:6	849.5	281.3	-95	-10	-40	-12	Negative	N/A
	ox-20:0/18:1	832.6	311.3	-95	-10	-40	-12	Negative	N/A
	ox-20:0/18:2	830.6	311.3	-95	-10	-40	-12	Negative	N/A
	ox-20:0/20:4	854.6	311.3	-95	-10	-40	-12	Negative	N/A
	ox-20:0/22:6	879.6	311.3	-95	-10	-40	-12	Negative	N/A
	C12:0/13:0 (Internal Standard) (50 pmol)	636.4	199.2	-95	-10	-40	-12	Negative	N/A
Phosphatidylinositol (PI)	32:0	809.5186	255.2330	-40	-10	-70	-11	Negative	N/A
	32:1	807.5029	255.2330	-40	-10	-70	-11	Negative	N/A
	34:0	837.5499	255.2330	-40	-10	-70	-11	Negative	N/A
	34:1	835.5342	255.2330	-40	-10	-70	-11	Negative	N/A
	34:2	833.5186	255.2330	-40	-10	-70	-11	Negative	N/A
	36:0	865.5812	283.2643	-40	-10	-70	-11	Negative	N/A
	36:1	863.5655	283.2643	-40	-10	-70	-11	Negative	N/A
	36:2	861.5499	281.2486	-40	-10	-70	-11	Negative	N/A
	36:4	857.5186	255.2330	-40	-10	-70	-11	Negative	N/A
	38:4	885.5499	283.2643	-40	-10	-70	-11	Negative	N/A
	40:6	909.5499	283.2643	-40	-10	-70	-11	Negative	N/A
	37:4 (IS)	871.5342	269.2486	-40	-10	-70	-11	Negative	N/A
Diacylglycerols (DAG)	32:0	586.5405	313.2737	50	10	25	10	Positive	[M+NH4]+
	32:1	584.5249	313.2737	50	10	25	10	Positive	[M+NH4]+
	34:0	614.5718	313.2737	50	10	25	10	Positive	[M+NH4]+
	34:1	612.5562	313.2737	50	10	25	10	Positive	[M+NH4]+
	34:2	610.5405	313.2737	50	10	25	10	Positive	[M+NH4]+
	36:0	642.6031	341.3050	50	10	25	10	Positive	[M+NH4]+
	36:1	640.5875	341.3050	50	10	25	10	Positive	[M+NH4]+
	36:2	638.5718	341.3050	50	10	25	10	Positive	[M+NH4]+
	36:4	634.5405	313.2737	50	10	25	10	Positive	[M+NH4]+
	38:4	662.5718	341.3050	50	10	25	10	Positive	[M+NH4]+
	40:6	686.5718	341.3050	50	10	25	10	Positive	[M+NH4]+
	32:0 (d5-glycerol) (IS)	591.5719	318.3051	50	10	25	10	Positive	[M+NH4]+
Lyso-PC	16:0	496.3398	184.0733	130	10	40	12	Positive	N/A
	18:1	522.3554	184.0733	130	10	40	12	Positive	N/A
	18:0	524.3711	184.0733	130	10	40	12	Positive	N/A
	20:1	550.3867	184.0733	130	10	40	12	Positive	N/A
	20:4	544.3398	184.0733	130	10	40	12	Positive	N/A
	22:6	568.3398	184.0733	130	10	40	12	Positive	N/A
	17:1 (IS)	508.3398	184.0733	130	10	40	12	Positive	N/A
	12:0	440.2772	184.0733	130	10	40	12	Positive	N/A
	14:0	468.3085	184.0733	130	10	40	12	Positive	N/A
	18:2	520.3398	184.0733	130	10	40	12	Positive	N/A
	20:0	552.4024	184.0733	130	10	40	12	Positive	N/A

Lipid Class	Species targeted	Accurate Exact masses	Accurate product ion mass	DP	EP	CE (V)	Collision Exit Potential	Ionization Mode	Adduct (if any)
Lyso-PC	22:0	580.4337	184.0733	130	10	40	12	Positive	N/A
	22:1	578.4180	184.0733	130	10	40	12	Positive	N/A
	22:4	572.3711	184.0733	130	10	40	12	Positive	N/A
	24:0	608.4650	184.0733	130	10	40	12	Positive	N/A
	24:1	606.4493	184.0733	130	10	40	12	Positive	N/A
Lyso-PE	16:0	454.2928	313.2737	125	10	45	15	Positive	N/A
	18:1	480.3085	339.2894	125	10	45	15	Positive	N/A
	18:0	482.3241	341.3050	125	10	45	15	Positive	N/A
	20:1	508.3398	367.3207	125	10	45	15	Positive	N/A
	20:4	502.2928	361.2737	125	10	45	15	Positive	N/A
	22:6	526.2928	385.2737	125	10	45	15	Positive	N/A
	17:1 (IS)	466.2928	325.2737	125	10	45	15	Positive	N/A
	12:0	398.3202	257.3011	125	10	45	15	Positive	N/A
	14:0	426.2615	285.2424	125	10	45	15	Positive	N/A
	18:2	478.2928	337.2737	125	10	45	15	Positive	N/A
	20:0	510.3554	369.3363	125	10	45	15	Positive	N/A
	22:0	538.3867	397.3676	125	10	45	15	Positive	N/A
	22:1	536.3711	395.3520	125	10	45	15	Positive	N/A
	22:4	530.3241	389.3050	125	10	45	15	Positive	N/A
	24:0	566.4180	425.3989	125	10	45	15	Positive	N/A
	24:1	564.4024	423.3833	125	10	45	15	Positive	N/A
Lyso-PA	16:0	409.2361	78.9591	-80	-10	-115	-10	Negative	N/A
	18:1	435.2517	78.9591	-80	-10	-115	-10	Negative	N/A
	18:0	437.2674	78.9591	-80	-10	-115	-10	Negative	N/A
	20:1	463.2830	78.9591	-80	-10	-115	-10	Negative	N/A
	20:4	457.2361	78.9591	-80	-10	-115	-10	Negative	N/A
	22:6	481.2361	78.9591	-80	-10	-115	-10	Negative	N/A
	17:1 (IS)	421.2361	78.9591	-80	-10	-115	-10	Negative	N/A
	12:0	353.1735	78.9591	-80	-10	-115	-10	Negative	N/A
	14:0	381.2048	78.9591	-80	-10	-115	-10	Negative	N/A
	18:2	433.2361	78.9591	-80	-10	-115	-10	Negative	N/A
	20:0	465.2987	78.9591	-80	-10	-115	-10	Negative	N/A
	22:0	493.3300	78.9591	-80	-10	-115	-10	Negative	N/A
	22:1	491.3143	78.9591	-80	-10	-115	-10	Negative	N/A
	22:4	485.2674	78.9591	-80	-10	-115	-10	Negative	N/A
	24:0	521.3613	78.9591	-80	-10	-115	-10	Negative	N/A

Lipid Class	Species targeted	Accurate Exact masses	Accurate product ion mass	DP	EP	CE (V)	Collision Exit Potential	Ionization Mode	Adduct (if any)
Lyso-PA	24:1	519.3456	78.9591	-80	-10	-115	-10	Negative	N/A
Lyso-PG	16:0	483.2728	152.9958	-100	-10	-45	-12	Negative	N/A
	18:1	509.2885	152.9958	-100	-10	-45	-12	Negative	N/A
	18:0	511.3041	152.9958	-100	-10	-45	-12	Negative	N/A
	20:1	537.3198	152.9958	-100	-10	-45	-12	Negative	N/A
	20:4	531.2728	152.9958	-100	-10	-45	-12	Negative	N/A
	22:6	555.2728	152.9958	-100	-10	-45	-12	Negative	N/A
	17:1 (IS)	495.2728	152.9958	-100	-10	-45	-12	Negative	N/A
	12:0	427.2102	152.9958	-100	-10	-45	-12	Negative	N/A
	14:0	455.2415	152.9958	-100	-10	-45	-12	Negative	N/A
	18:2	507.2728	152.9958	-100	-10	-45	-12	Negative	N/A
	20:0	539.3354	152.9958	-100	-10	-45	-12	Negative	N/A
	22:0	567.3667	152.9958	-100	-10	-45	-12	Negative	N/A
	22:1	565.3511	152.9958	-100	-10	-45	-12	Negative	N/A
	22:4	559.3041	152.9958	-100	-10	-45	-12	Negative	N/A
	24:0	595.3980	152.9958	-100	-10	-45	-12	Negative	N/A
	24:1	597.3824	152.9958	-100	-10	-45	-12	Negative	N/A
Lyso-PS	16:0	496.2681	152.9958	-70	-10	-30	-15	Negative	N/A
	18:1	522.2837	152.9958	-70	-10	-30	-15	Negative	N/A
	18:0	524.2994	152.9958	-70	-10	-30	-15	Negative	N/A
	20:1	550.3150	152.9958	-70	-10	-30	-15	Negative	N/A
	20:4	544.2681	152.9958	-70	-10	-30	-15	Negative	N/A
	22:6	568.2681	152.9958	-70	-10	-30	-15	Negative	N/A
	17:1 (IS)	508.2681	152.9958	-70	-10	-30	-15	Negative	N/A
	12:0	440.2055	152.9958	-70	-10	-30	-15	Negative	N/A
	14:0	468.2368	152.9958	-70	-10	-30	-15	Negative	N/A
	18:2	520.2681	152.9958	-70	-10	-30	-15	Negative	N/A
	20:0	552.3307	152.9958	-70	-10	-30	-15	Negative	N/A
	22:0	580.3620	152.9958	-70	-10	-30	-15	Negative	N/A
	22:1	578.3463	152.9958	-70	-10	-30	-15	Negative	N/A
	22:4	572.2994	152.9958	-70	-10	-30	-15	Negative	N/A
	24:0	608.3933	152.9958	-70	-10	-30	-15	Negative	N/A
	24:1	606.3776	152.9958	-70	-10	-30	-15	Negative	N/A
Lyso-PI	16:0	571.2889	259.0224	-50	-10	-60	-11	Negative	N/A
	18:1	597.3045	259.0224	-50	-10	-60	-11	Negative	N/A
	18:0	599.3202	259.0224	-50	-10	-60	-11	Negative	N/A
	20:1	625.3358	259.0224	-50	-10	-60	-11	Negative	N/A
	20:4	619.2889	259.0224	-50	-10	-60	-11	Negative	N/A
	22:6	643.2889	259.0224	-50	-10	-60	-11	Negative	N/A
	17:1 (IS)	583.2889	259.0224	-50	-10	-60	-11	Negative	N/A
	12:0	515.2263	259.0224	-50	-10	-60	-11	Negative	N/A
	14:0	543.2576	259.0224	-50	-10	-60	-11	Negative	N/A
	18:2	595.2889	259.0224	-50	-10	-60	-11	Negative	N/A
	20:0	627.3515	259.0224	-50	-10	-60	-11	Negative	N/A
	22:0	655.3828	259.0224	-50	-10	-60	-11	Negative	N/A

Lipid Class	Species targeted	Accurate Exact masses	Accurate product ion mass	DP	EP	CE (V)	Collision Exit Potential	Ionization Mode	Adduct (if any)
Lyso-PI	22:1	653.3671	259.0224	-50	-10	-60	-11	Negative	N/A
	22:4	647.3202	259.0224	-50	-10	-60	-11	Negative	N/A
	24:0	683.4141	259.0224	-50	-10	-60	-11	Negative	N/A
	24:1	681.3984	259.0224	-50	-10	-60	-11	Negative	N/A
GlucosylCeramides	8:0	588.4470	570.3454, 264.2686	180	10	40	10	Positive	N/A
	10:0	616.4783	598.3767, 264.2686	180	10	40	10	Positive	N/A
	12:0	644.5096	626.408, 264.2686	180	10	40	10	Positive	N/A
	14:0	672.5409	654.4393, 264.2686	180	10	40	10	Positive	N/A
	16:0	700.5722	682.4706, 264.2686	180	10	40	10	Positive	N/A
	18:0	728.6035	710.5019, 264.2686	180	10	40	10	Positive	N/A
	18:1	726.5878	708.4862, 264.2686	180	10	40	10	Positive	N/A
	18:2	724.5722	706.4706, 264.2686	180	10	40	10	Positive	N/A
	20:0	756.6348	738.5332, 264.2686	180	10	40	10	Positive	N/A
	20:1	754.6191	736.5175, 264.2686	180	10	40	10	Positive	N/A
	20:4	748.5722	730.4706, 264.2686	180	10	40	10	Positive	N/A
	22:0	784.6661	766.5645, 264.2686	180	10	40	10	Positive	N/A
	22:1	782.6504	764.5488, 264.2686	180	10	40	10	Positive	N/A
	22:4	776.6035	758.5019, 264.2686	180	10	40	10	Positive	N/A
	22:6	772.5722	754.4706, 264.2686	180	10	40	10	Positive	N/A
	24:0	812.6974	794.5958, 264.2686	180	10	40	10	Positive	N/A
	24:1	810.6817	792.5801, 264.2686	180	10	40	10	Positive	N/A
	17:0 (IS)	714.5878	696.4862, 264.2686	180	10	40	10	Positive	N/A
Dihydro Ceramide	16:0	540.535	522.5244	180	10	20	10	Positive	N/A
	18:1	566.5507	548.5401	180	10	20	10	Positive	N/A
	18:0	568.5663	550.5557	180	10	20	10	Positive	N/A
	20:1	594.5789	576.5683	180	10	20	10	Positive	N/A
	20:4	588.535	570.5244	180	10	20	10	Positive	N/A
	22:6	612.535	594.5244	180	10	20	10	Positive	N/A
	25:0 (IS)	666.6758	648.6652	180	10	20	10	Positive	N/A
	16:0	540.535	522.5244	180	10	20	10	Positive	N/A
	12:0	484.4724	466.4618	180	10	20	10	Positive	N/A
	14:0	512.5037	494.4931	180	10	20	10	Positive	N/A
	18:2	564.535	546.5244	180	10	20	10	Positive	N/A
	20:0	596.5976	578.5870	180	10	20	10	Positive	N/A

Lipid Class	Species targeted	Accurate Exact masses	Accurate product ion mass	DP	EP	CE (V)	Collision Exit Potential	Ionization Mode	Adduct (if any)
Dihydro Ceramide	22:0	624.6289	606.6183	180	10	20	10	Positive	N/A
	22:1	622.6132	604.6026	180	10	20	10	Positive	N/A
	22:4	617.5663	599.5557	180	10	20	10	Positive	N/A
	24:0	652.6602	634.6496	180	10	20	10	Positive	N/A
	24:1	650.6445	632.6339	180	10	20	10	Positive	N/A

Table MS2: Details for mass transitions for proteomics analyses.

Sr.No.	Name of enzyme	Accession number from UniprotKB	Peptide Sequence	Precursor m/z	Product m/z
1	ASAH1	Q9WV54	LTVFTTLMDVTK	684.88	1055.54
2	ASAH2	Q9JHE3	GNVANVQINR	542.80	814.45
3	GCS	O88693	VGLVHGLPYVADR	465.93	460.25
4	GCS	O88693	QGFAATLEQVYFGTSHPR	670.33	272.17
5	GBA (GLCM)	P17439	WAEVVLSDPEAAK	707.86	515.28
6	GBA2	Q69ZF3	ISAWQNPVLDDR	707.36	201.12
7	Actin	P63260	VAPEEHPVLLTEAPLNPK	652.03	892.48

REFERENCES

1. Sunshine, H. & Iruela-Arispe, M. L. Membrane lipids and cell signaling. *Current Opinion in Lipidology* vol. 28 408–413 (2017).
2. Fahy, E., Sud, M., Cotter, D. & Subramaniam, S. LIPID MAPS online tools for lipid research. *Nucleic Acids Res.* **35**, W606 (2007).
3. Fahy, E. *et al.* Update of the LIPID MAPS comprehensive classification system for lipids. *Journal of Lipid Research* vol. 50 S9 (2009).
4. Menendez, J. A. & Lupu, R. Fatty acid synthase and the lipogenic phenotype in cancer pathogenesis. *Nature Reviews Cancer* vol. 7 763–777 (2007).
5. Reddy, J. K. & Hashimoto, T. Peroxisomal β-oxidation and peroxisome proliferator - Activated receptor α: An adaptive metabolic system. *Annual Review of Nutrition* vol. 21 193–230 (2001).
6. Bell, R. M. & Coleman, R. A. Enzymes of glycerolipid synthesis in eukaryotes. *Annual review of biochemistry* vol. 49 459–487 (1980).
7. Vance, J. E. Phospholipid Synthesis and Transport in Mammalian Cells. *Traffic* vol. 16 1–18 (2015).
8. Futerman, A. H. & Hannun, Y. A. The complex life of simple sphingolipids. *EMBO Reports* vol. 5 777–782 (2004).
9. Yang, Y., Lee, M. & Fairn, G. D. Phospholipid subcellular localization and dynamics. *J. Biol. Chem.* **293**, 6230–6240 (2018).
10. Tarling, E. J., Vallim, T. Q. d. A. & Edwards, P. A. Role of ABC transporters in lipid transport and human disease. *Trends in Endocrinology and Metabolism* vol. 24 342–350 (2013).
11. Segawa, K. & Nagata, S. An Apoptotic 'Eat Me' Signal: Phosphatidylserine Exposure. *Trends in Cell Biology* vol. 25 639–650 (2015).
12. Hanada, K. Discovery of the molecular machinery CERT for endoplasmic reticulum-to-Golgi trafficking of ceramide. *Molecular and Cellular Biochemistry* vol. 286 23–31 (2006).
13. Albeituni, S. & Stiban, J. Roles of Ceramides and Other Sphingolipids in Immune Cell Function and Inflammation. in *Advances in Experimental Medicine and Biology* vol. 1161 169–191 (Springer New York LLC, 2019).
14. Casas-Godoy, L. *et al.* Lipases: An overview. in *Methods in Molecular Biology* vol. 1835 3–38 (Humana Press Inc., 2018).
15. Yin, H., Xu, L. & Porter, N. A. Free radical lipid peroxidation: Mechanisms and analysis. *Chemical Reviews* vol. 111 5944–5972 (2011).
16. Abe, A., Hiraoka, M., Ohguro, H., Tesmer, J. J. & Shayman, J. A. Preferential hydrolysis of truncated oxidized glycerophospholipids by lysosomal phospholipase A2. *J. Lipid Res.* **58**, 339–349 (2017).
17. Balakrishna, M. *et al.* Hydrolysis of oxidized phosphatidylcholines by crude enzymes from chicken, pork and beef muscles. *Food Chem.* **313**, (2020).
18. Avela, H. F. & Sirén, H. Advances in lipidomics. *Clinica Chimica Acta* vol. 510 123–141 (2020).
19. Holmström, K. M. & Finkel, T. Cellular mechanisms and physiological consequences of redox-dependent signalling. *Nat. Rev. Mol. Cell Biol.* **15**, 411–21 (2014).
20. Winterbourn, C. C. Reconciling the chemistry and biology of reactive oxygen species. *Nature Chemical Biology* vol. 4 278–286 (2008).
21. Valavanidis, A., Vlachogianni, T. & Fiotakis, C. 8-Hydroxy-2′ -deoxyguanosine (8-OHdG): A critical biomarker of oxidative stress and carcinogenesis. *J. Environ. Sci. Heal. - Part C Environ. Carcinog. Ecotoxicol. Rev.* **27**, 120–139 (2009).
22. Spickett, C. M. & Pitt, A. R. Protein oxidation: Role in signalling and detection by mass spectrometry. in *Amino Acids* vol. 42 5–21 (Springer, 2012).
23. Reuter, S., Gupta, S. C., Chaturvedi, M. M. & Aggarwal, B. B. Oxidative stress, inflammation, and cancer: How are they linked? *Free Radical Biology and Medicine* vol. 49 1603–1616 (2010).

24. Huang, W. J., Zhang, X. & Chen, W. W. Role of oxidative stress in Alzheimer's disease (review). *Biomedical Reports* vol. 4 519–522 (2016).

25. Rani, V., Deep, G., Singh, R. K., Palle, K. & Yadav, U. C. S. Oxidative stress and metabolic disorders: Pathogenesis and therapeutic strategies. *Life Sciences* vol. 148 183–193 (2016).

26. Catala, A. The Ability of Melatonin to Counteract Lipid Peroxidation in Biological Membranes. *Curr. Mol. Med.* **7**, 638–649 (2007).

27. Greenberg, M. E. *et al.* The Lipid Whisker Model of the Structure of Oxidized Cell Membranes. *J. Biol. Chem.* **283**, 2385–2396 (2008).

28. Kay, J. G., Koivusalo, M., Ma, X., Wohland, T. & Grinstein, S. Phosphatidylserine dynamics in cellular membranes. *Mol. Biol. Cell* **23**, 2198–2212 (2012).

29. Tyurina, Y. Y. *et al.* Oxidation of phosphatidylserine: A mechanism for plasma membrane phospholipid scrambling during apoptosis? *Biochem. Biophys. Res. Commun.* **324**, 1059–1064 (2004).

30. Solati, Z., Edel, A. L., Shang, Y., Karmin, O. & Ravandi, A. Oxidized phosphatidylcholines are produced in renal ischemia reperfusion injury. *PLoS One* **13**, e0195172 (2018).

31. McIntyre, T. M., Prescott, S. M. & Stafforini, D. M. The emerging roles of PAF acetylhydrolase. *J. Lipid Res.* **50 Suppl**, S255-9 (2009).

32. Levental, K. R. *et al.* Lipidomic and biophysical homeostasis of mammalian membranes counteracts dietary lipid perturbations to maintain cellular fitness. *Nat. Commun.* **11**, 1–13 (2020).

33. Ellinger, I. & Pietschmann, P. Endocytosis in health and disease—a thematic issue dedicated to Renate Fuchs. *Wiener Medizinische Wochenschrift* vol. 166 193–195 (2016).

34. Tauber, A. I. Metchnikoff and the phagocytosis theory. *Nature Reviews Molecular Cell Biology* vol. 4 897–901 (2003).

35. Schmid, S. L., Sorkin, A. & Zerial, M. Endocytosis: Past, Present, And future. *Cold Spring Harb. Perspect. Biol.* **6**, a022509 (2014).

36. Flannagan, R. S., Jaumouillé, V. & Grinstein, S. The cell biology of phagocytosis. *Annual Review of Pathology: Mechanisms of Disease* vol. 7 61–98 (2012).

37. Levin, R., Grinstein, S. & Canton, J. The life cycle of phagosomes: formation, maturation, and resolution. *Immunological Reviews* (2016) doi:10.1111/imr.12439.

38. Lee, B. Greasing the receptor. *Nature Microbiology* (2018) doi:10.1038/s41564-018-0251-2.

39. Messner, M. C. & Cabot, M. C. Glucosylceramide in humans. *Adv. Exp. Med. Biol.* **688**, 156–164 (2010).

40. Alessenko, A. V. & Albi, E. Exploring Sphingolipid Implications in Neurodegeneration. *Frontiers in Neurology* vol. 11 (2020).

41. Stirnemann, J. Ô. *et al.* A review of gaucher disease pathophysiology, clinical presentation and treatments. *International Journal of Molecular Sciences* vol. 18 (2017).

42. Aruoma, O. I. Free radicals, oxidative stress, and antioxidants in human health and disease. *JAOCS, J. Am. Oil Chem. Soc.* **75**, 199–212 (1998).

43. Hybertson, B. M., Gao, B., Bose, S. K. & McCord, J. M. Oxidative stress in health and disease: The therapeutic potential of Nrf2 activation. *Mol. Aspects Med.* **32**, 234–246 (2011).

44. Niedzielska, E. *et al.* Oxidative Stress in Neurodegenerative Diseases. *Molecular Neurobiology* vol. 53 4094–4125 (2016).

45. Finkel, T. & Holbrook, N. J. Oxidants, oxidative stress and the biology of ageing. *Nature* vol. 408 239–247 (2000).

46. Liou, G. Y. & Storz, P. Reactive oxygen species in cancer. *Free Radical Research* vol. 44 479–496 (2010).

47. Imlay, J. A. Cellular defenses against superoxide and hydrogen peroxide. *Annual Review of Biochemistry* vol. 77 755–776 (2008).

48. Imlay, J. A. The molecular mechanisms and physiological consequences of oxidative stress: Lessons from a model bacterium. *Nature Reviews Microbiology* vol. 11 443–454 (2013).

49. Brown, H. A. & Murphy, R. C. Working towards an exegesis for lipids in biology. *Nature Chemical Biology* vol. 5 602–606 (2009).

50. Fahy, E. *et al.* A comprehensive classification system for lipids. *J. Lipid Res.* **46**, 839–861 (2005).

51. Porter, N. A. A perspective on free radical autoxidation: The physical organic chemistry of polyunsaturated fatty acid and sterol peroxidation. *Journal of Organic Chemistry* vol. 78 3511–3524 (2013).

52. Spickett, C. M. & Pitt, A. R. Oxidative lipidomics coming of age: Advances in analysis of oxidized phospholipids in physiology and pathology. *Antioxidants and Redox Signaling* vol. 22 1646–1666 (2015).

53. Smith, W. L. & Murphy, R. C. Oxidized lipids formed non-enzymatically by reactive oxygen species. *Journal of Biological Chemistry* vol. 283 15513–15514 (2008).

54. Vance, J. E. & Tasseva, G. Formation and function of phosphatidylserine and phosphatidylethanolamine in mammalian cells. *Biochimica et Biophysica Acta - Molecular and Cell Biology of Lipids* vol. 1831 543–554 (2013).

55. Leventis, P. A. & Grinstein, S. The distribution and function of phosphatidylserine in cellular membranes. *Annual Review of Biophysics* vol. 39 407–427 (2010).

56. Hazen, S. L. Oxidized phospholipids as endogenous pattern recognition ligands in innate immunity. *Journal of Biological Chemistry* vol. 283 15527–15531 (2008).

57. Greenberg, M. E. *et al.* Oxidized phosphatidylserine-CD36 interactions play an essential role in macrophage-dependent phagocytosis of apoptotic cells. *J. Exp. Med.* **203**, 2613–2625 (2006).

58. Kagan, V. E. *et al.* A Role for Oxidative Stress in Apoptosis: Oxidation and Externalization of Phosphatidylserine Is Required for Macrophage Clearance of Cells Undergoing Fas-Mediated Apoptosis. *J. Immunol.* **169**, 487–499 (2002).

59. Blankman, J. L., Long, J. Z., Trauger, S. A., Siuzdak, G. & Cravatt, B. F. ABHD12 controls brain lysophosphatidylserine pathways that are deregulated in a murine model of the neurodegenerative disease PHARC. *Proc. Natl. Acad. Sci. U. S. A.* **110**, 1500–1505 (2013).

60. Borrull, A., López-Martínez, G., Poblet, M., Cordero-Otero, R. & Rozès, N. A simple method for the separation and quantification of neutral lipid species using GC-MS. *Eur. J. Lipid Sci. Technol.* **117**, 274–280 (2015).

61. FOLCH, J., LEES, M. & SLOANE STANLEY, G. H. A simple method for the isolation and purification of total lipides from animal tissues. *J. Biol. Chem.* (1957) doi:10.1016/s0021-9258(18)64849-5.

62. Dharmaraja, A. T. & Chakrapani, H. A small molecule for controlled generation of reactive oxygen species (ROS). *Org. Lett.* **16**, 398–401 (2014).

63. Long, J. Z. *et al.* Metabolomics annotates ABHD3 as a physiologic regulator of medium-chain phospholipids. *Nat. Chem. Biol.* **7**, 763–765 (2011).

64. Dharmaraja, A. T., Alvala, M., Sriram, D., Yogeeswari, P. & Chakrapani, H. Design, synthesis and evaluation of small molecule reactive oxygen species generators as selective mycobacterium tuberculosis inhibitors. *Chem. Commun.* **48**, 10325–10327 (2012).

65. McCormack, D. & McFadden, D. A review of pterostilbene antioxidant activity and disease modification. *Oxidative Medicine and Cellular Longevity* vol. 2013 (2013).

66. Kerksick, C. & Willoughby, D. The Antioxidant Role of Glutathione and N-Acetyl-Cysteine Supplements and Exercise-Induced Oxidative Stress. *J. Int. Soc. Sports Nutr.* **2**, (2005).

67. Kamat, S. S. *et al.* Immunomodulatory lysophosphatidylserines are regulated by ABHD16A and ABHD12 interplay. *Nat. Chem. Biol.* **11**, 164–171 (2015).

68. Long, J. Z. & Cravatt, B. F. The metabolic serine hydrolases and their functions in mammalian physiology and disease. *Chemical Reviews* vol. 111 6022–6063 (2011).

69. Nomura, D. K. & Casida, J. E. Lipases and their inhibitors in health and disease. *Chem. Biol. Interact.* **259**, 211–222 (2016).

70. Wu, C., Jin, X., Tsueng, G., Afrasiabi, C. & Su, A. I. BioGPS: Building your own mash-up of gene annotations and expression profiles. *Nucleic Acids Res.* **44**, D313–D316 (2016).

71. Hoover, H. S., Blankman, J. L., Niessen, S. & Cravatt, B. F. Selectivity of inhibitors of endocannabinoid biosynthesis evaluated by activity-based protein profiling. *Bioorganic Med. Chem. Lett.* **18**, 5838–5841 (2008).

72. Shimanaka, Y. *et al.* Omega-3 fatty acid epoxides are autocrine mediators that control the magnitude of IgE-mediated mast cell activation. *Nat. Med.* **23**, 1287–1297 (2017).

73. Matsura, T. *et al.* The presence of oxidized phosphatidylserine on Fas-mediated apoptotic cell

surface. *Biochim. Biophys. Acta - Mol. Cell Biol. Lipids* **1736**, 181–188 (2005).

74. Niphakis, M. J. & Cravatt, B. F. Enzyme inhibitor discovery by activity-based protein profiling. *Annual Review of Biochemistry* vol. 83 341–377 (2014).

75. Simon, G. M. & Cravatt, B. F. Activity-based proteomics of enzyme superfamilies: Serine hydrolases as a case study. *Journal of Biological Chemistry* vol. 285 11051–11055 (2010).

76. Hsu, K. L. *et al.* DAGLβ inhibition perturbs a lipid network involved in macrophage inflammatory responses. *Nat. Chem. Biol.* **8**, 999–1007 (2012).

77. Inloes, J. M. *et al.* The hereditary spastic paraplegia-related enzyme DDHD2 is a principal brain triglyceride lipase. *Proc. Natl. Acad. Sci. U. S. A.* **111**, 14924–14929 (2014).

78. Vieira, O. V., Botelho, R. J. & Grinstein, S. Phagosome maturation: Aging gracefully. *Biochemical Journal* (2002) doi:10.1042/BJ20020691.

79. Kinchen, J. M. & Ravichandran, K. S. Phagosome maturation: Going through the acid test. *Nature Reviews Molecular Cell Biology* (2008) doi:10.1038/nrm2515.

80. Rai, A. K., Rai, A., Ramaiya, A. J., Jha, R. & Mallik, R. Molecular adaptations allow dynein to generate large collective forces inside cells. *Cell* (2013) doi:10.1016/j.cell.2012.11.044.

81. Steinberg, B. E. & Grinstein, S. Pathogen destruction versus intracellular survival: The role of lipids as phagosomal fate determinants. *Journal of Clinical Investigation* vol. 118 2002–2011 (2008).

82. Yeung, T. & Grinstein, S. Lipid signaling and the modulation of surface charge during phagocytosis. *Immunological Reviews* vol. 219 17–36 (2007).

83. Rai, A. *et al.* Dynein Clusters into Lipid Microdomains on Phagosomes to Drive Rapid Transport toward Lysosomes. *Cell* (2016) doi:10.1016/j.cell.2015.12.054.

84. Dermine, J. F. *et al.* Flotillin-1-enriched Lipid Raft Domains Accumulate on Maturing Phagosomes. *J. Biol. Chem.* (2001) doi:10.1074/jbc.M101113200.

85. Huynh, K. K., Gershenzon, E. & Grinstein, S. Cholesterol accumulation by macrophages impairs phagosome maturation. *J. Biol. Chem.* **283**, 35745–35755 (2008).

86. Kory, N. *et al.* Mice lacking lipid droplet-Associated hydrolase, a gene linked to human prostate cancer, have normal cholesterol ester metabolism. *J. Lipid Res.* **58**, 226–235 (2017).

87. Spassieva, S. *et al.* Necessary role for the Lag1p motif in (Dihydro)ceramide synthase activity. *J. Biol. Chem.* (2006) doi:10.1074/jbc.M608092200.

88. Rai, P. *et al.* Kinesin-dependent mechanism for controlling triglyceride secretion from the liver. *Proc. Natl. Acad. Sci. U. S. A.* **114**, 12958–12963 (2017).

89. Merrill, A. H., Dennis, E. A., McDonald, J. G. & Fahy, E. Lipidomics technologies at the end of the first decade and the beginning of the next. *Adv. Nutr.* **4**, 565–567 (2013).

90. Brügger, B. Lipidomics: Analysis of the lipid composition of cells and Subcellular organelles by Electrospray ionization mass spectrometry. *Annual Review of Biochemistry* vol. 83 79–98 (2014).

91. Levy, M. & Futerman, A. H. Mammalian ceramide synthases. *IUBMB Life* vol. 62 347–356 (2010).

92. Halasiddappa, L. M., Koefeler, H., Futerman, A. H. & Hermetter, A. Oxidized Phospholipids Induce Ceramide Accumulation in RAW 264.7 Macrophages: Role of Ceramide Synthases. *PLoS One* **8**, 70002 (2013).

93. Laviad, E. L. *et al.* Characterization of ceramide synthase 2: Tissue distribution, substrate specificity, and inhibition by sphingosine 1-phosphate. *J. Biol. Chem.* **283**, 5677–5684 (2008).

94. Pewzner-Jung, Y. *et al.* A critical role for ceramide synthase 2 in liver homeostasis: I. alterations in lipid metabolic pathways. *J. Biol. Chem.* **285**, 10902–10910 (2010).

95. Yoo, H. S., Norred, W. P., Wang, E., Merrill, A. H. & Riley, R. T. Fumonisin inhibition of de Novo sphingolipid biosynthesis and cytotoxicity are correlated in LLC-PK1 cells. *Toxicol. Appl. Pharmacol.* **114**, 9–15 (1992).

96. Spassieva, S. *et al.* Necessary role for the Lag1p motif in (Dihydro)ceramide synthase activity. *J. Biol. Chem.* **281**, 33931–33938 (2006).

97. Ogura, Y., Parsons, W. H., Kamat, S. S. & Cravatt, B. F. A calcium-dependent acyltransferase that produces N-Acyl phosphatidylethanolamines. *Nat. Chem. Biol.* **12**, 669–671 (2016).

98. Pathak, D. & Mallik, R. Lipid - Motor Interactions: Soap Opera or Symphony? *Current Opinion in Cell Biology* vol. 44 79–85 (2017).

99.   Megha & London, E. Ceramide selectively displaces cholesterol from ordered lipid domains (rafts): Implications for lipid raft structure and function. *J. Biol. Chem.* **279**, 9997–10004 (2004).

100.   Murray, P. J. & Wynn, T. A. Protective and pathogenic functions of macrophage subsets. *Nature Reviews Immunology* vol. 11 723–737 (2011).

101.   Storrie, B. & Desjardins, M. The biogenesis of lysosomes: Is it a kiss and run, continuous fusion and fission process? *BioEssays* vol. 18 895–903 (1996).

102.   Desjardins, M. Biogenesis of phagolysosomes: the 'kiss and run' hypothesis. *Trends Cell Biol.* **5**, 183–186 (1995).

103.   Guo, M. *et al.* High-resolution quantitative proteome analysis reveals substantial differences between phagosomes of RAW 264.7 and bone marrow derived macrophages. *Proteomics* (2015) doi:10.1002/pmic.201400431.

104.   Shui, W. *et al.* Membrane proteomics of phagosomes suggests a connection to autophagy. *Proc. Natl. Acad. Sci. U. S. A.* (2008) doi:10.1073/pnas.0809218105.

105.   Boulais, J. *et al.* Molecular characterization of the evolution of phagosomes. *Mol. Syst. Biol.* (2010) doi:10.1038/msb.2010.80.

106.   Pauwels, A. M., Trost, M., Beyaert, R. & Hoffmann, E. Patterns, Receptors, and Signals: Regulation of Phagosome Maturation. *Trends in Immunology* (2017) doi:10.1016/j.it.2017.03.006.

107.   Bohdanowicz, M. & Grinstein, S. Vesicular Traffic: A Rab SANDwich. *Current Biology* (2010) doi:10.1016/j.cub.2010.02.030.

108.   Vieira, O. V. *et al.* Modulation of Rab5 and Rab7 Recruitment to Phagosomes by Phosphatidylinositol 3-Kinase. *Mol. Cell. Biol.* (2003) doi:10.1128/mcb.23.7.2501-2514.2003.

109.   Pathak, D., Mehendale, N., Singh, S., Mallik, R. & Kamat, S. S. Lipidomics Suggests a New Role for Ceramide Synthase in Phagocytosis. *ACS Chem. Biol.* (2018) doi:10.1021/acschembio.8b00438.

110.   Pewzner-Jung, Y. *et al.* A critical role for ceramide synthase 2 in liver homeostasis II. Insights into molecular changes leading to hepatopathy. *J. Biol. Chem.* **285**, 10911–10923 (2010).

111.   Gault, C. R., Obeid, L. M. & Hannun, Y. A. An overview of sphingolipid metabolism: From synthesis to breakdown. *Advances in Experimental Medicine and Biology* vol. 688 1–23 (2010).

112.   Kitatani, K., Idkowiak-Baldys, J. & Hannun, Y. A. The sphingolipid salvage pathway in ceramide metabolism and signaling. *Cellular Signalling* vol. 20 1010–1018 (2008).

113.   Ogretmen, B. Sphingolipid metabolism in cancer signalling and therapy. *Nature Reviews Cancer* vol. 18 33–50 (2017).

114.   Petrache, I. & Berdyshev, E. V. Ceramide Signaling and Metabolism in Pathophysiological States of the Lung. *Annual Review of Physiology* vol. 78 463–480 (2016).

115.   Bikman, B. T. & Summers, S. A. Ceramides as modulators of cellular and whole-body metabolism. *Journal of Clinical Investigation* vol. 121 4222–4230 (2011).

116.   Billich, A. & Baumruker, T. Sphingolipid metabolizing enzymes as novel therapeutic targets. *Subcell. Biochem.* **49**, 487–522 (2008).

117.   Mullen, T. D., Hannun, Y. A. & Obeid, L. M. Ceramide synthases at the centre of sphingolipid metabolism and biology. *Biochemical Journal* vol. 441 789–802 (2012).

118.   Kelkar, D. S. *et al.* A chemical–genetic screen identifies ABHD12 as an oxidized-phosphatidylserine lipase. *Nat. Chem. Biol.* **15**, 169–178 (2019).

119.   Abhyankar, V., Kaduskar, B., Kamat, S. S., Deobagkar, D. & Ratnaparkhi, G. S. Drosophila DNA/RNA methyltransferase contributes to robust host defense in aging animals by regulating sphingolipid metabolism. *J. Exp. Biol.* **221**, (2018).

120.   Bedia, C., Camacho, L., Abad, J. L., Fabriàs, G. & Levade, T. A simple fluorogenic method for determination of acid ceramidase activity and diagnosis of Farber disease. *J. Lipid Res.* **51**, 3542–3547 (2010).

121.   Karatas, M. *et al.* Enzyme kinetics and inhibition parameters of human leukocyte glucosylceramidase. *Heliyon* (2020) doi:10.1016/j.heliyon.2020.e05191.

122.   Fu, Z. *et al.* Development of a label-free LC-MS/MS-based glucosylceramide synthase assay and its application to inhibitors screening for ceramide-related diseases. *Biomol. Ther.* **27**,

193–200 (2019).

123. Kumar, K., Mhetre, A., Ratnaparkhi, G. S. & Kamat, S. S. A Superfamily-wide Activity Atlas of Serine Hydrolases in Drosophila melanogaster. *Biochemistry* **60**, 1312–1324 (2021).

124. Rappsilber, J., Mann, M. & Ishihama, Y. Protocol for micro-purification, enrichment, pre-fractionation and storage of peptides for proteomics using StageTips. *Nat. Protoc. 2007 28* **2**, 1896–1906 (2007).

125. MacLean, B. *et al.* Skyline: An open source document editor for creating and analyzing targeted proteomics experiments. *Bioinformatics* (2010) doi:10.1093/bioinformatics/btq054.

126. Atak, A. *et al.* Targeted Proteomics Workshop and International Symposium (IIT Bombay, Mumbai, India): An Accelerator for Global Proteomics. in *OMICS A Journal of Integrative Biology* vol. 20 199–201 (Mary Ann Liebert Inc., 2016).

127. Carr, S. A. *et al.* Targeted peptide measurements in biology and medicine: Best practices for mass spectrometry-based assay development using a fit-for-purpose approach. *Mol. Cell. Proteomics* **13**, 907–917 (2014).

128. Liebler, D. C. & Zimmerman, L. J. Targeted quantitation of proteins by mass spectrometry. *Biochemistry* **52**, 3797–3806 (2013).

129. Picotti, P. & Aebersold, R. Selected reaction monitoring-based proteomics: Workflows, potential, pitfalls and future directions. *Nature Methods* vol. 9 555–566 (2012).

130. Lange, V., Picotti, P., Domon, B. & Aebersold, R. Selected reaction monitoring for quantitative proteomics: A tutorial. *Molecular Systems Biology* vol. 4 222 (2008).

131. Song, E. *et al.* Targeted proteomic assays for quantitation of proteins identified by proteogenomic analysis of ovarian cancer. *Sci. Data* **4**, 1–13 (2017).

132. Parveen, F. *et al.* Role of Ceramidases in Sphingolipid Metabolism and Human Diseases. *Cells* vol. 8 (2019).

133. Coant, N., Sakamoto, W., Mao, C. & Hannun, Y. A. Ceramidases, roles in sphingolipid metabolism and in health and disease. *Advances in Biological Regulation* vol. 63 122–131 (2017).

134. Kulkarni, A. *et al.* Chemoproteomics of an indole-based quinone epoxide identifies druggable vulnerabilities in vancomycin-resistant staphylococcus aureus. *J. Med. Chem.* **62**, 6785–6795 (2019).

135. Rodriguez-Cuenca, S., Barbarroja, N. & Vidal-Puig, A. Dihydroceramide desaturase 1, the gatekeeper of ceramide induced lipotoxicity. *Biochimica et Biophysica Acta - Molecular and Cell Biology of Lipids* vol. 1851 40–50 (2015).

136. Fabrias, G. *et al.* Dihydroceramide desaturase and dihydrosphingolipids: Debutant players in the sphingolipid arena. *Progress in Lipid Research* vol. 51 82–94 (2012).

137. Hsu, F. F. & Turk, J. Characterization of ceramides by low energy collisional-activated dissociation tandem mass spectrometry with negative-ion electrospray ionization. *J. Am. Soc. Mass Spectrom.* **13**, 558–570 (2002).

138. Liebisch, G. *et al.* Quantitative measurement of different ceramide species from crude cellular extracts by electrospray ionization tandem mass spectrometry (ESI- MS/MS). *J. Lipid Res.* **40**, 1539–1546 (1999).

139. Ishibashi, Y., Kohyama-Koganeya, A. & Hirabayashi, Y. New insights on glucosylated lipids: Metabolism and functions. *Biochimica et Biophysica Acta - Molecular and Cell Biology of Lipids* vol. 1831 1475–1485 (2013).

140. Leipelt, M. *et al.* Glucosylceramide Synthases, a Gene Family Responsible for the Biosynthesis of Glucosphingolipids in Animals, Plants, and Fungi*. (2001) doi:10.1074/jbc.M104952200.

141. Ichikawa, S. & Hirabayashi, Y. Glucosylceramide synthase and glycosphingolipid synthesis. *Trends in Cell Biology* vol. 8 198–202 (1998).

142. Elleder, M. Glucosylceramide transfer from lysosomes - The missing link in molecular pathology of glucosylceramidase deficiency: A hypothesis based on existing data. *J. Inherit. Metab. Dis.* **29**, 707–715 (2006).

143. Gegg, M. E. & Schapira, A. H. V. The role of glucocerebrosidase in Parkinson disease pathogenesis. *FEBS Journal* vol. 285 3591–3603 (2018).

144. Woeste, M. A. & Wachten, D. The enigmatic role of GBA2 in controlling locomotor function.

Frontiers in Molecular Neuroscience vol. 10 (2017).

145. Martin, E. *et al.* Loss of function of glucocerebrosidase GBA2 is responsible for motor neuron defects in hereditary spastic paraplegia. *Am. J. Hum. Genet.* **92**, 238–244 (2013).

146. Zhang, Y., Li, X., Becker, K. A. & Gulbins, E. Ceramide-enriched membrane domains-Structure and function. *Biochimica et Biophysica Acta - Biomembranes* vol. 1788 178–183 (2009).

147. Silva, L. C., De Almeida, R. F. M., Castro, B. M., Fedorov, A. & Prieto, M. Ceramide-domain formation and collapse in lipid rafts: Membrane reorganization by an apoptotic lipid. *Biophys. J.* **92**, 502–516 (2007).

148. Grassmé, H., Riethmüller, J. & Gulbins, E. Biological aspects of ceramide-enriched membrane domains. *Progress in Lipid Research* vol. 46 161–170 (2007).

149. Bollinger, C. R., Teichgräber, V. & Gulbins, E. Ceramide-enriched membrane domains. *Biochimica et Biophysica Acta - Molecular Cell Research* vol. 1746 284–294 (2005).

150. Mayor, S. & Rao, M. Rafts: Scale-dependent, active lipid organization at the cell surface. *Traffic* vol. 5 231–240 (2004).

151. Bieberich, E. Sphingolipids and lipid rafts: Novel concepts and methods of analysis. *Chemistry and Physics of Lipids* vol. 216 114–131 (2018).

152. van der Poel, S. *et al.* Hyperacidification of trans-golgi network and endo/lysosomes in melanocytes by glucosylceramide-dependent V-ATPase activity. *Traffic* **12**, 1634–1647 (2011).

153. Yamaguchi, M. & Kasamo, K. Modulation in the activity of purified tonoplast H+-ATPase by tonoplast glycolipids prepared from cultured rice (Oryza sativa L. var. Boro) cells. *Plant Cell Physiol.* **42**, 516–523 (2001).

154. van der Poel, S. *et al.* Hyperacidification of trans-golgi network and endo/lysosomes in melanocytes by glucosylceramide-dependent V-ATPase activity. *Traffic* (2011) doi:10.1111/j.1600-0854.2011.01263.x.

PUBLICATIONS

1) Malik S.A., Acharya J.D., Mehendale N., Kamat S., Ghaskadbi S.: Pterostilbene reverses palmitic acid mediated insulin resistance in HepG2 cells by reducing oxidative stress and triglyceride accumulation. Free Radical Research. 2019 Jul;53(7):815-827.

2) Kelkar DS*., Ravikumar G*., Mehendale N*., Singh S*., Joshi A., Abinaya R., Mhetre A., Harinath Chakrapani H., Kamat SS. A Chemical Genetic Screen Identifies ABHD12 as an Oxidized Phosphatidylserine Lipase. Nature Chemical Biology, 2019 ;15(2):169-178. DOI: 10.1038/s41589- 018-0195-0 (*= Equal Contribution)

3) Pathak D*., Mehendale N*., Singh S., Mallik R., Kamat SS. Lipidomics suggests a new role for ceramide synthase in phagocytosis. ACS Chemical Biology, 2018; 13 (8), pp 2280–2287. DOI: 10.1021/acschembio.8b00438. (*= Equal Contribution). *The paper featured on the cover of the issue which was designed and executed by Neelay Mehendale.*

4) Mehendale N., Mallik R.*, Kamat SS. Mapping sphingolipid metabolism pathways during phagosomal maturation. (Manuscript under review)

PERMISSIONS

Permission for reuse of:

Kelkar DS*., Ravikumar G*., Mehendale N*., Singh S*., Joshi A., Abinaya R., Mhetre A., Harinath Chakrapani H., Kamat SS. A Chemical Genetic Screen Identifies ABHD12 as an Oxidized Phosphatidylserine Lipase. Nature Chemical Biology, 2019 ;15(2):169-178. DOI: 10.1038/s41589- 018-0195-0

SPRINGER NATURE

A chemical–genetic screen identifies ABHD12 as an oxidized-phosphatidylserine lipase

Author: Dhanashree S. Kelkar et al
Publication: Nature Chemical Biology
Publisher: Springer Nature
Date: Jan 14, 2019

Copyright © 2019, The Author(s), under exclusive licence to Springer Nature America, Inc.

Permission for reuse of:

Pathak D*., Mehendale N*., Singh S., Mallik R., Kamat SS. Lipidomics suggests a new role for ceramide synthase in phagocytosis. ACS Chemical Biology, 2018; 13 (8), pp 2280–2287. DOI: 10.1021/acschembio.8b00438.

VITA

Name: Neelay Mehendale

Address: Department of Biology,

                        IISER-Pune, Dr. Homi Bhabha Road,

                        Pashan,

                        Pune, Maharashtra – 411008.

Email address: mehendale.neelay@students.iiserpune.ac.in

Education: M.Sc. Biotechnology, Institute of Bioinformatics and Biotechnology - Savitribai Phule Pune University, 2015

                        Ph.D., Biological Sciences, IISER-Pune, 2021